






TRICOT

Calculations of Boiling Two-Phase Flow Using a Porous Media Model

Authors: Ville Hovi

Confidentiality: Public

Report's title Calculations of Boiling Two-Phase Flow Using a Porous Media Model		
Customer, contact person, address VYR, VTT	Order reference -	
Project name Tridimensional core transient analysis methods	Project number/Short name 23857 / TRICOT	
Author Ville Hovi	Pages 112	
Keywords Thermal-hydraulics, two-phase flow, 5-equation model, porous media model, the SIMPLE algorithm	Report identification code VTT-R-04858-08	
<p>Summary</p> <p>This is a Master's Thesis conducted at VTT Technical Research Centre of Finland between 18.6.2007 and 14.5.2008. The work was started in REATU project and continued in TRICOT.</p> <p>Boiling two-phase flow and the equations governing the motion of fluid in two-phase flows are discussed in this thesis. Disposition of the governing equations in three-dimensional complex geometries is considered from the perspective of the porous medium concept. The equations governing motion in two-phase flows were formulated, discretized and implemented in a subroutine for pressure-velocity solution utilizing the SIMPLE algorithm modified for two-phase flow. The subroutine was included in PORFLO, which is a three-dimensional 5-equation porous media model developed at VTT by Jaakko Miettinen. The development of two-phase flow and the resulting void fraction distribution was predicted in a geometry resembling a section of BWR fuel bundle in a couple of test cases using PORFLO.</p>		
Confidentiality	Public	
Espoo 28.5.2008		
Signatures 	Signatures 	Signatures 
Written by Ville Hovi Trainee Research Scientist	Reviewed by Elina Syrjälähti Project Manager	Accepted by Timo Vanttola Technology Manager
VTT's contact address VTT, P.O.B. 1000, FI-02044 VTT, Finland		
Distribution (customer and VTT) In pdf-form: SAFIR 2010 reference group 3, Rätty, Syrjälähti, TK5015		
<p><i>The use of the name of the VTT Technical Research Centre of Finland (VTT) in advertising or publication in part of this report is only permissible with written authorisation from the VTT Technical Research Centre of Finland.</i></p>		



Faculty of Technology
Department of Energy and Environmental Technology
Energy Technology
Nuclear Engineering

CALCULATIONS OF BOILING TWO-PHASE FLOW USING A POROUS MEDIA MODEL

MASTER'S THESIS

Examiners Professor Dr.Sc.(Tech.) Riitta Kyrki-Rajamäki
Senior Research Scientist Lic.Sc.(Tech.) Mikko Ilvonen

Supervisor Senior Research Scientist Lic.Sc.(Tech.) Jaakko Miettinen

Ville Hovi
Puistokaari 15 B 24
00200 Helsinki
tel. +358 50 3477882

ABSTRACT

Lappeenranta University of Technology
Faculty of Technology
Energy Technology

Ville Hovi

Calculations of Boiling Two-Phase Flow Using a Porous Media Model

Master's thesis

2008

112 pages, 26 figures, 4 tables and 2 appendices

Examiners: Professor Dr.Sc.(Tech.) Riitta Kyrki-Rajamäki
Senior Research Scientist Lic.Sc.(Tech.) Mikko Ilvonen

Keywords: Thermal-hydraulics, two-phase flow, 5-equation model, porous media model, the SIMPLE algorithm.

Boiling two-phase flow and the equations governing the motion of fluid in two-phase flows are discussed in this thesis. Disposition of the governing equations in three-dimensional complex geometries is considered from the perspective of the porous medium concept. The equations governing motion in two-phase flows were formulated, discretized and implemented in a subroutine for pressure-velocity solution utilizing the SIMPLE algorithm modified for two-phase flow. The subroutine was included in PORFLO, which is a three-dimensional 5-equation porous media model developed at VTT by Jaakko Miettinen. The development of two-phase flow and the resulting void fraction distribution was predicted in a geometry resembling a section of BWR fuel bundle in a couple of test cases using PORFLO.

TIIVISTELMÄ

Lappeenrannan teknillinen yliopisto
Teknillinen tiedekunta
Energiatekniikka

Ville Hovi

Porositeettimallin käyttö kiehuvan kaksifaasivirtauksen laskennassa

Diplomityö

2008

112 sivua, 26 kuvaa, 4 taulukkoa ja 2 liitettä

Tarkastajat: Professori TkT Riitta Kyrki-Rajamäki
Erikoistutkija TkL Mikko Ilvonen

Hakusanat: Termohydrauliikka, kaksifaasivirtaus, 5-yhtälömalli, porositeettimalli, SIMPLE-algoritmi

Tässä työssä tarkastellaan kiehuvaa kaksifaasivirtausta, sitä hallitsevia yhtälöitä ja niiden asettelua kolmiulotteisessa laskenta-alueessa porositeettimallin kannalta. Kaksifaasivirtauksen paineen ja nopeuden ratkaisuun vaadittavat yhtälöt formuloitiin ja diskretoitiin, minkä jälkeen SIMPLE-algoritmiin perustuva paine- ja nopeuskentän ratkaiseva aliohjelma ohjelmoitiin ja liitettiin PORFLO-ohjelmaan. Testitapauksissa kaksifaasivirtauksen syntyä ja kehittymistä simuloitiin kiehutusvesireaktorin polttoainepun osaa vastaavassa geometriassa PORFLO-ohjelmalla. PORFLO on Jaakko Miettisen VTT:llä kehittämä kolmiulotteinen viisisäilymsyhtälöinen porositeettimalli.

TABLE OF CONTENTS

1	Introduction	6
2	Basic approaches in modeling two-phase flow	8
3	Physics of Boiling.....	10
3.1	Flow patterns	11
3.2	Heat transfer	12
4	PORFLO Two-phase solution code.....	15
4.1	Structure of PORFLO	15
4.2	Conservation equations	18
4.2.1	Conservation of mass	18
4.2.2	Conservation of momentum.....	19
4.2.3	Conservation of energy.....	23
4.3	Phase separation by drift-flux model	24
4.4	Correlations	25
4.4.1	Heat transfer correlations.....	26
4.4.2	Critical heat flux.....	29
4.4.3	Friction factor.....	30
5	Discussion of pressure-velocity coupling	31
6	Discretization of the governing equations	33
6.1	Basic principles used in discretization	33
6.2	Notations used in discretization.....	35
6.3	Discretization for the iterative methods in PORFLO	38
6.3.1	Discretization of the mass conservation equations	39
6.3.2	Discretization of the volume conservation equations.....	44
6.3.3	Discretization of the momentum equations for SIMPLE	47
6.4	Discretization for the direct method in PORFLO.....	52
6.4.1	Discretized forms of the volume conservation equations.....	53
6.4.2	Discretized forms of the momentum equations	54
6.4.3	Combining the volume conservation and momentum equations	56
6.5	Discretization of the energy conservation equations	59

7	The SIMPLE family of algorithms.....	64
7.1	The SIMPLE algorithm	65
7.2	The SIMPLER algorithm.....	71
7.3	The SIMPLEC algorithm.....	75
7.4	Pressure and velocity under-relaxation.....	78
8	Development of the code.....	80
8.1	Basis for the pressure correction equation.....	80
8.2	Diagonal dominance of the pressure correction equations	83
8.3	Increasing the implicitness of the overall solution.....	87
9	BWR Full-size Fine-mesh Bundle Tests	90
9.1	Description of the test facility	90
9.2	Void fraction measurement	93
10	Simulations	95
10.1	Variations of the under-relaxation factors	96
10.1.1	Variations of the under-relaxation factors in SIMPLE	97
10.1.2	Variations of the under-relaxation factors in SIMPLEC.....	98
10.2	Transient simulation	99
10.3	Steady-state results	102
11	Discussion of simulation results	105
12	Conclusions.....	109
	REFERENCES	111

Appendices

Appendix A Discussion of viscous forces

Appendix B Discretized forms of the momentum equations for SIMPLE

NOMENCLATURE

Latin symbols

A	flow or surface area	$[m^2]$
\mathbf{A}	square matrix, whose dimensions $n \times n$	$[-]$
a	coefficient of velocities in momentum equations	$[kg/s]$
b	coefficient of pressures and pressure corrections	$[ms]$
\bar{b}	solution vector	$[-]$
\mathbf{B}	square matrix, whose dimensions $r \times r$	$[-]$
C_V	specific heat capacity in constant volume	$[J/kgK]$
c	source term in momentum equations	$[kgm/s^2]$ or $[N]$
\mathbf{C}	vector, whose components (C_1, C_2, C_3)	$[-]$
d	source term in pressure and pressure correction eqs.	$[kg/s]$
d_e	equivalent diameter	$[m]$
F	mixture mass flow rate	$[kg/s]$
F_x	force in x-direction	$[N]$
F_y	force in y-direction	$[N]$
F_z	force in z-direction	$[N]$
\mathbf{F}	square matrix, whose dimensions $(n-r) \times (n-r)$	$[-]$
G	vapour mass flow rate	$[kg/s]$
f	frictional coefficient	$[-]$
\mathbf{f}	sum vector of body forces per volume	$[N/m^3]$
g	acceleration due to gravity	$[m/s^2]$
h	specific enthalpy	$[J/kg]$
h''	heat transfer coefficient	$[W/m^2K]$
h'''	volumetric heat transfer coefficient	$[W/m^3K]$
h_{fg}	specific latent heat of vaporization	$[J/kg]$
\bar{i}	unit vector in x-direction	$[-]$
J	volumetric flow rate	$[m^3/s]$
\bar{j}	area averaged velocity	$[m/s]$
\bar{j}	unit vector in y-direction	$[-]$
k	thermal conductivity	$[W/mK]$
\bar{k}	unit vector in z-direction	$[-]$
M	mass	$[kg]$
n	arbitrary positive integer	$[-]$
\bar{n}	surface normal vector	$[-]$
P	power generated inside the control volume	
	per unit volume	$[W/m^3]$
p	pressure	$[Pa]$
Q	heat rate into the control volume per unit volume	$[W/m^3]$
r	arbitrary positive integer	$[-]$
q''	surface heat flux	$[W/m^2]$
q'''	volumetric heat flux	$[W/m^3]$
T	temperature	$[^\circ C]$ or $[K]$
\mathbf{T}	surface force tensor	$[N/m^2]$
t	time	$[s]$
u	specific internal energy	$[J/kg]$

u	velocity in x-direction	[m/s]
\mathbf{u}	velocity vector, whose components (u, v, w)	[m/s]
V	volume	[m ³]
V_{gj}	drift-flux velocity	[m/s]
v	velocity in y-direction	[m/s]
v	specific volume	[m ³ /kg]
W	liquid mass flow rate	[kg/s]
w	velocity in z-direction	[m/s]
x, y, z	3D Cartesian coordinates	[m]
\bar{x}	unknown vector	[-]

Greek symbols

α	void fraction (vapour fraction of fluid volume)	[-]
α_p	under-relaxation factor for pressures	[-]
α_u	under-relaxation factor for velocities	[-]
β	coefficient	[-]
Γ	mass transfer rate	[kg/s]
γ	volumetric mass transfer rate	[kg/m ³ s]
Δ	difference	[-]
$\delta x, \delta y, \delta z$	dimensions of the smallest fluid element whose macroscopic properties are not influenced by individual molecules	[-]
ε	porosity (fluid fraction of total volume)	[-]
λ	second viscosity	[Ns/m ²]
μ	dynamic viscosity	[Ns/m ²]
ρ	density	[kg/m ³]
τ	surface stress	[N/m ²]
φ	general variable (velocity, temperature etc.)	
ω	weighting factor for mass error correction	[-]

Subscripts

con	convection
CHF	critical heat flux
d	(down) bottom face of the node
e	east face of the node
f	fluid
fluid	fluid
g	(gas) vapour
I, J, K	refers to the center of the node
i, j, k	refers to the boundary of the node
l	liquid
lg	liquid to vapour
m	mixture
me	mass error
n	north face of the node
nb	neighbour
nb	nucleate boiling

s	south face of the node
sat	saturation
u	upper face of the node
w	west face of the node
wall	heat transfer surface
wl	wall to liquid
wg	wall to vapour
xx, xy, xz, \dots	viscous stress components, where the first index denotes the face the component is located on (x: the face perpendicular to x-axis) and the second index denotes the direction of the force.

Superscripts

<i>i</i>	x-direction
<i>j</i>	y-direction
<i>k</i>	z-direction
<i>n</i>	timestep
o	(old), value of the previous converged state
*	guessed or known value
**	improved value
'	correction

Abbreviations

BFBT	B WR F ull-size F ine-mesh B undle T ests
BWR	B oiling W ater R eactor
CFD	C omputational F luid D ynamics
CFL	C ourant- F riedrichs- L evy (number)
CHF	C ritical H eat F lux
CPU	C entral P rocessing U nit
CT	C omputerized T omography
NUPEC	N uclear P ower E ngineering C orporation
SIMPLE	S emi- I mplicit M ethod for P ressure L inked E quations
SIMPLEC	SIMPLE-Consistent
SIMPLER	SIMPLE-Revised
UDS	U pwind D ifferencing S cheme
VOF	V olume of F luid

1 INTRODUCTION

The thermal-hydraulics of BWR core and various heat exchangers for vapour generation on the shell side is to a large extent concerned with two-phase flows and heat transfer, since the coolant is mostly composed of both the liquid and vapour phases of water. Boiling two-phase flows in narrow channels, such as the flow channels of a BWR fuel bundle, exhibit different flow patterns, depending on the local flow conditions and void fraction distributions. The prediction of void fraction distribution is crucial when equipment design and operational and safety procedures are considered, since void fraction distribution is a necessary input for the prediction of fission power distribution, flow patterns, mass inventories of the phases, mixture densities, and most importantly: heat transfer from the fuel rod or tube bundle to the boiling fluid and dryout prediction. High local values of void fraction on the heat transfer surface indicate impending crisis of heat transfer and dryout. Void fraction distribution is vital in both BWRs and steam generators in order to produce high vapour quality steam without jeopardizing the safety margins. In addition to increasing the efficiency of the turbine assembly by reducing the fraction of liquid in the steam, in both BWRs and steam generators, contamination of the steam lines and turbine assemblies in BWRs is reduced as well.

Understanding of steady-state and transient behaviour of entire nuclear processes, or its parts, has been a challenge in process simulation since the 1960s. In the earliest models one-dimensional (1D) numerical equations were solved for the loop thermal-hydraulics, and the results were used as boundary values for the neutronics for calculating the core power dynamics. By the end of 1960s the first three-dimensional (3D) models were developed for steady-state calculations, in which the neutronics were solved for each fuel element and the thermal-hydraulics were solved for a group of parallel 1D channels. Since then the models have been expanded to transient simulation as well. Together with the CFD model development the present thermal-hydraulic models are capable of 3D simulation of single process components with a resolution of centimeter or millimeter class.

The main objectives of this thesis are: (1) to present the equations that govern the boiling two-phase flow in three-dimensional domains, in Chapters 4 and 6, (2) to briefly present

the structure of the older solution procedure in the computer program PORFLO, in Chapter 4 and section 6.4, (3) to present the model developed for pressure-velocity solution in transient 3D two-phase flow during this thesis, in section 6.3 and Chapters 7 and 8, and (4) to simulate a couple of test cases with the new model in a geometry resembling a portion of a BWR fuel bundle, in Chapter 10.

PORFLO is a three-dimensional 5-equation porosity model, developed for transient calculations of two-phase flow in complex geometries. Most of the PORFLO code has been developed by Jaakko Miettinen at VTT. The contribution of Mikko Ilvonen to the development of PORFLO is mainly related to grid generation and iterative solution of linear systems of equations.

Due to historical reasons, some aspects of the pressure-velocity solution, the handling of momentum convection terms for instance, have been simplified in the older solution procedure of PORFLO, to facilitate the use of a direct method in pressure-velocity solution. Partially due to these simplifications, the code was not ready for the simulation of a BWR fuel bundle. It was decided that an iterative method for pressure-velocity solution, based on the SIMPLE algorithm modified for two-phase flow, is developed during this thesis, therefore most of this thesis is focused on the formulation of equations used in SIMPLE and the special aspects of two-phase flow that need to be considered, when implementing the SIMPLE algorithm for two-phase flow.

As a part of this thesis, a subroutine implementing the SIMPLE algorithm was coded and included in PORFLO, and some test cases were simulated using the newly developed subroutine. In addition to the general progress in the development of PORFLO, which also benefited the development of the subroutine that implements the SIMPLE algorithm, substantial help on coding the subroutine, in particular, was received from Jaakko Miettinen.

2 BASIC APPROACHES IN MODELING TWO-PHASE FLOW

A brief comparison of the basic approaches available in two-phase flow calculations is presented in this chapter. The different types of two-phase flow models are explored briefly and the differences between the porous media approach and the more common approaches in CFD are explained.

Many different types of models have been developed for two-phase flow with a different number of conservation equations depending on the application, such as the homogenous equilibrium model (HEM) developed mainly for safety analysis for predicting the critical mass flow rates at blowdown. Other widely used models include the 5-equation and 6-equation models, named after the number of conservation equations used to describe the two-phase flow.

A complete description of the two-phase flow (6-equation model), both for 1D, 2D and 3D domains alike, involves six equations: conservation of mass, momentum and energy equations written for both phases. The momentum equations of both phases in 6-equation models include terms that describe the interactions between the two phases, the interphasial shear term for instance, which are hard to define experimentally.

Another widely used model is the 5-equation model, which has conservation of mass and energy equations for both phases and a momentum equation for the mixture. Interaction between the two phases, phase separation, is defined by an empirical correlation, such as the Zuber-Findlay drift-flux model originally developed by Zuber and Findlay (1965).

The 5-equation models have a certain advantage over the 6-equations models, since experimentally measured void fraction distributions can be developed further into drift-flux model parameters using the total mixture flow rate, vapour flow rate and pressure measured during the experiments. EPRI made an extensive work collecting the phase separation data measured all over the world by that time and developed a full-range drift-flux correlation for vertical flows, (Chexal & Lellouche 1986), against the comprehensive data set. On the other hand it must be said that 5-equation models always depend on an

empirical correlation to govern the phase separation, since the underlying physics affecting the interaction between the phases are absent.

In 6-equation models the separate momentum equations for each phase provide a way to introduce terms that account for various types of interactions between the phases; so in principle, the mechanisms affecting phase separation can be modeled; instead of replicating the results of the measurements by using an empirical correlation. These terms, the interfacial shear or lift force, are however hard to be determined experimentally and, in addition, depend strongly on structure of the interface that separates the two phases. Advanced methods, such as front tracking and volume of the fluid (VOF), have been developed to track and reconstruct the interfaces between the phases during the simulation. The potential gained by introducing the interphasial terms in 6-equation models is best realized in methods like VOF; otherwise approximations have to be made about the structure of the interfaces to obtain an estimate of the terms in question. One of such approximations, widely used in 6-equation models, is to assume that vapour is only present as bubbles with a fixed diameter. Due to the difficulties in estimating the interphasial terms, many 6-equation models have developed the terms directly from the drift-flux correlation, and thus provided some experimental basis for the estimates. An example of such a procedure is the 1D safety code RELAP5.

Despite all the difficulties, the 6-equation models are considered to have more potential in the development of future codes than the 5-equation models.

The typical approach in CFD codes is to generate the calculation grid so that it follows the interfaces between the structure and fluid according to the geometry that is being modeled. The grid that is resulted from such a procedure is called either unstructured or body-fitted. Another approach, which is called the concept of porous medium, is to divide the geometry, usually orthogonally, regardless of the interfaces. The calculation nodes are divided between the structure and the two phases. Porosity ε is used to define the fraction of the fluid from the volume of the node, $V_{\text{fluid}} = \varepsilon V$, and void fraction α is used to divide the fluid volume between the two phases, $V_{\text{fluid}} = V_g + V_l = \alpha V_{\text{fluid}} + (1 - \alpha) V_{\text{fluid}}$.

3 PHYSICS OF BOILING

Perhaps the most profound difficulty in modeling of two-phase flow, as far as realistic results are concerned, is the prediction of the flow regime and the related heat transfer mode between the heat transfer surface and fluid. These two are closely interlinked; on the other hand geometry of the flow defines the heat transfer and, at the same time, the heat transfer affects the flow geometry and may cause an onset of a different flow pattern. In addition, heat transfer rates between the two phases are distinctively different depending on the prevailing flow pattern, due to differences in the interfacial area density. Distribution of the phases is therefore an important part of the solution of the flow field, without which any other parameters of importance in engineering applications, heat transfer and two-phase pressure drop for instance, cannot be evaluated accurately. (Lahey & Moody 1993, Section 5.2: pp. 224-242)

Heat transfer modes between the heat transfer surface and fluid are divided into two categories: wetted wall heat transfer and post-dryout heat transfer. In the wetted wall heat transfer liquid is in contact with the walls, while vapour is flowing as a dispersed phase, as bubbles, slugs or a vapour core, inside the liquid annulus. In the post-dryout heat transfer only vapour is contacting the walls and liquid is flowing inside the vapour as droplets or a liquid core.

In BWR applications void fraction distributions in different subchannels along the heated length of the fuel bundle and at the outlet are of particular interest, since the local void fraction affects the performance, and later properties, of the fuel bundle, not to mention the behavior of the whole reactor due to feedback effects on pressure and fission power generation. The thermal-hydraulic state of each fuel bundle is traditionally described in present neutronics models with a single radial node, where as dryout prediction requires at least one node in the radial direction for each subchannel, since dryout can be a quite localized phenomenon. A collection of subchannel codes have been developed for dryout prediction for a single fuel pin, in particular.

Though flow patterns and heat transfer modes have mostly been studied in circular conduits, tubes, most of the results may still be considered useful in more intricate

geometries, like the flow channel of a BWR fuel bundle. Flow patterns and corresponding heat transfer regions of boiling two-phase flow in a vertical tube are presented in Figure 3.1.

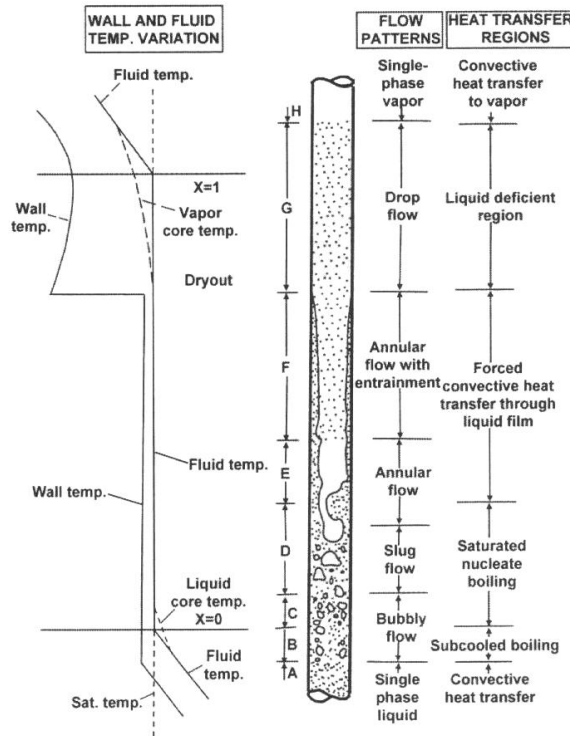


Figure 3.1: Flow patterns and heat transfer regions in a vertical tube. (Collier & Thome 1996)

3.1 Flow patterns

Typically the flow patterns are divided into five categories: bubble flow, slug flow, churn flow, annular flow, and wispy annular flow. Though some authors choose define the flow patterns using more categories, for the scope of this thesis, these five presented below (Collier & Thome 1996, pp. 10-13) and in Figure 3.2 are sufficient for BWR flow channel in nominal operating conditions.

- 1) **Bubble flow:** The gas phase is dispersed as discrete bubbles in the continuous liquid phase. The bubbles are smaller than the diameter of the tube.
- 2) **Slug (or plug) flow:** As void fraction increases the bubbles coalesce and form larger bubbles, similar to the diameter of the tube. These bubbles are called Taylor bubbles. The consecutive Taylor bubbles are separated by a liquid region, slugs, which may or may not contain smaller bubbles. A liquid film separates the tube wall and the Taylor bubble.

- 3) **Churn flow:** When the flow is increased, the Taylor bubbles break up and liquid is displaced more towards the tube walls.
- 4) **Annular flow:** The bulk of the liquid flows on the tube walls, as a continuous gas phase flows, usually significantly faster, through the center of the tube. Some liquid may be entrained in the continuous gas phase as droplets and there may be some gas in the form of bubbles inside the liquid film. As the gas flow rate increases ripples start to form on the liquid film, which increases the entrainment of droplets.
- 5) **Wispy annular flow:** If the liquid flow rate is increased (compared to annular flow), the amount of liquid in the gas core increases. Increasing amount of liquid droplets in the gas core increases the coalescence of droplets into larger lumps of liquid, or wisps.

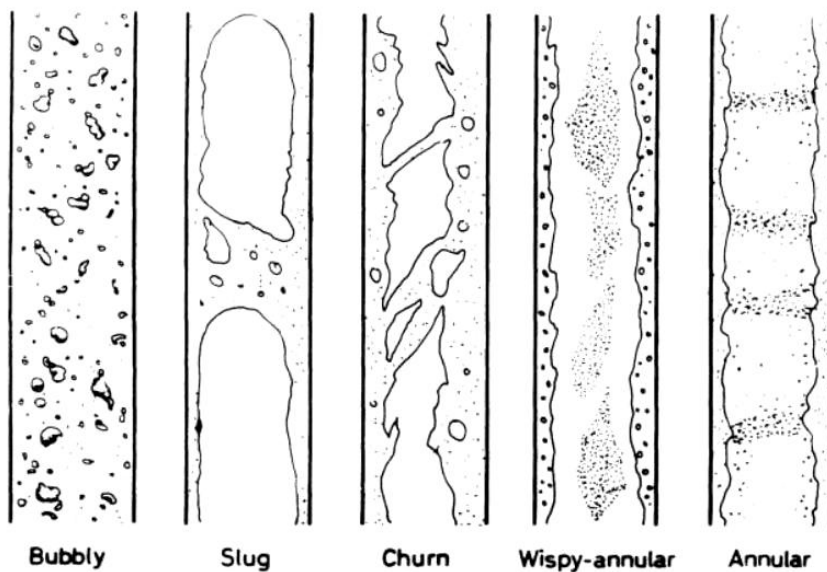


Figure 3.2: Flow patterns in vertical tubes. (Collier & Thome 1996, p. 11)

In addition to the flow these five flow patterns there is, of course, others, such as the inverted annular flow occurring during reflooding, in which a liquid core or dispersed drops flow in the center separated from the channel walls by a thin vapour layer. However, as this thesis is more related to simulation of the wetted wall conditions, these unusual conditions have been left out of the discussion.

3.2 Heat transfer

As was mentioned above, flow patterns, or flow regimes, have a substantial effect on heat transfer. Most 1D models rely solely on correlations to provide the heat transfer coefficients, since they contain no information about the radial distribution of the phases. Usually separate correlations are formulated for the heat transfer coefficients depending on

the prevailing flow regime as one of the parameters, so that the heat transfer coefficient changes together with the flow regime along the length of the conduit, or alternatively the correlation can be applicable to more than one flow regimes or the formulation can be made independent of the flow pattern. In any case, one of the parameters used in the correlation usually has a set range, either a certain flow pattern or a set range in some dimensional number or combination of dimensional numbers, which defines the applicability of the correlation in question.

Flow regime at any given axial position can be deciphered from flow pattern maps, which are commonly given as a function of flow rates of the two phases. An example of a flow pattern map is presented in Figure 3.3 for low-pressure air-water mixture in small diameter (1-3 cm) vertical tubes. The axes represent the superficial momentum fluxes of the liquid ($\rho_l j_l^2$) and vapour ($\rho_g j_g^2$) phases respectively.

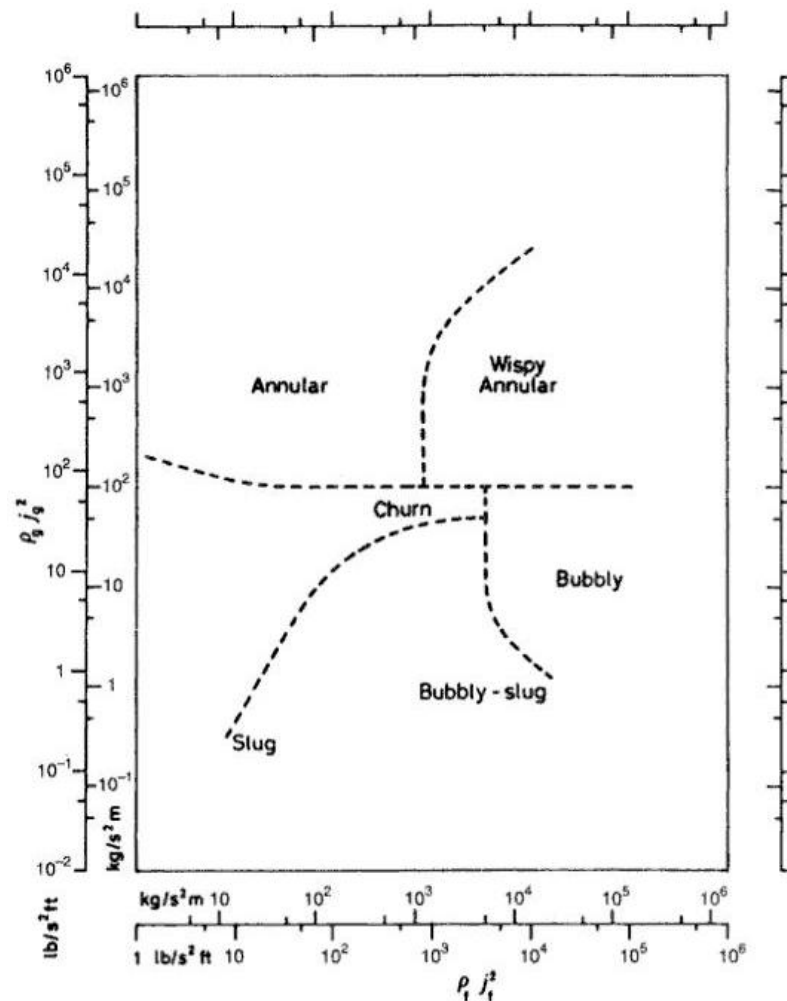


Figure 3.3: Flow pattern map for vertical air-water flow (Collier & Thome 1996, p. 19).

Once a suitable correlation for the heat transfer coefficient has been selected, the heat transfer coefficient can be calculated. In addition to the value of the heat transfer coefficient, the temperature relations are important as well. Three essential temperatures exist: fluid temperature, structure temperature and saturation temperature. Once the three temperatures and the heat transfer coefficient are known, the heat flux from structure to the surrounding fluid is given.

Codes that use correlations that depend on the prevailing flow regime are not particularly suitable as general purpose codes, since the development of flow regimes and heat transfer coefficients depend strongly on fluid properties and geometry of the flow channel and the correlations have set ranges for fluid properties and flow conditions, outside of which they no longer apply and extrapolation has proven to be difficult. However, in order to model convective or boiling heat transfer, whose length scales are far beyond the resolution of the typical meshes used in engineering applications, one has to resort to the use of some heat transfer correlations. (Lahey & Moody 1993, Section 5.2: pp. 224-242)

As correlations are, in essence, nothing more than the best fit to a certain set of experimental data, the best way to ensure accurate results on a given geometry and flow conditions would be to produce the data set by specific experiments. However, this is often time consuming, expensive and impractical. A wide range of correlations, often fitted to vast sets of data, can be found in literature, but the restrictions discussed above should be kept in mind. Special care needs to be taken when applying a code to different flow conditions than the code was originally intended for.

2D and 3D codes have an advantage over 1D codes, since they contain information about the distribution of the two phases. Velocities and fluid properties near the heat transfer interfaces could be used to obtain the heat transfer coefficients from suitable correlations, and local void fractions could be used together with the preset geometrical data to approximate the area of the heat transfer interfaces.

4 PORFLO TWO-PHASE SOLUTION CODE

Boiling two-phase flow calculations were performed with a porous media model called PORFLO. The code has recently been modified to better suit the BFBT benchmark problem by, among other things, introducing iterative solvers as an alternative for the direct matrix solver in order to facilitate solution of bigger meshes.

In a porous media model the grid is not necessarily generated to follow the boundaries between structures and fluid; instead, porosity is used to define the fractions of the control volumes filled with fluid. A separate module is used to generate a non-uniform orthogonal grid at the beginning of the simulation.

In PORFLO, the 3-dimensional two-phase flow problem is solved using a 5-equation model, which has two equations for conservation of mass and energy, one for each phase, and a conservation of momentum equation for the mixture. The interactions between the two phases, phase separation, are defined by the Zuber-Findlay drift-flux model.

4.1 Structure of PORFLO

The main program is split into separate cases optimized for different applications: particle bed, isolation condenser and BWR fuel bundle for example. The main strategies to solve the flow problem remain the same for all applications, but initialization and fine tuning of some parameters are case specific.

There are two distinctively different strategies to solve the pressure and velocity fields: direct methods that combine the momentum and mass conservation equations to yield a single system of equations for pressure, which is the older approach in PORFLO, and iterative methods (SIMPLE), which couple the momentum and mass conservation equations through pressure corrections. The choice between the two strategies is made in the input file. Though these two branches differ significantly, the rest of the solution procedure advances in a similar manner, hence most subroutines can be used in both cases. The sequence of operations in PORFLO solution procedure is shown in Figure 4.1.

The solution procedure starts with reading the input file tailored for a specific application, after which the grid is generated according to the geometrical data given in the input file. Then, the process and flow parameters are initialized. If the simulation is to be continued from a previously simulated state, the restart file is read after initialization. The restart file contains only dynamic data, such as pressure, mixture density, void fraction, and volumetric flow distributions, as function of location.

The transient calculation loop starts with advancing forward in time. After that, the interfacial and structure heat transfer are solved in separate subroutines. These subroutines are not very sophisticated at present, since most of the coding effort so far has been focused on improving the stability of the solution. However, improvement here is relatively easy once the stability issues are resolved first.

After the heat transfer is solved, pressure and velocity fields need to be considered. Since pressure and velocity distributions are strongly interlinked, they have to be solved simultaneously. At present, four different subroutines are dedicated to implement the different solution methods, which result in volumetric flow rates for mixture in each direction and the corresponding pressure field. The bulk of the coding effort so far has been spent on improving the solution of pressure and volumetric flow distributions.

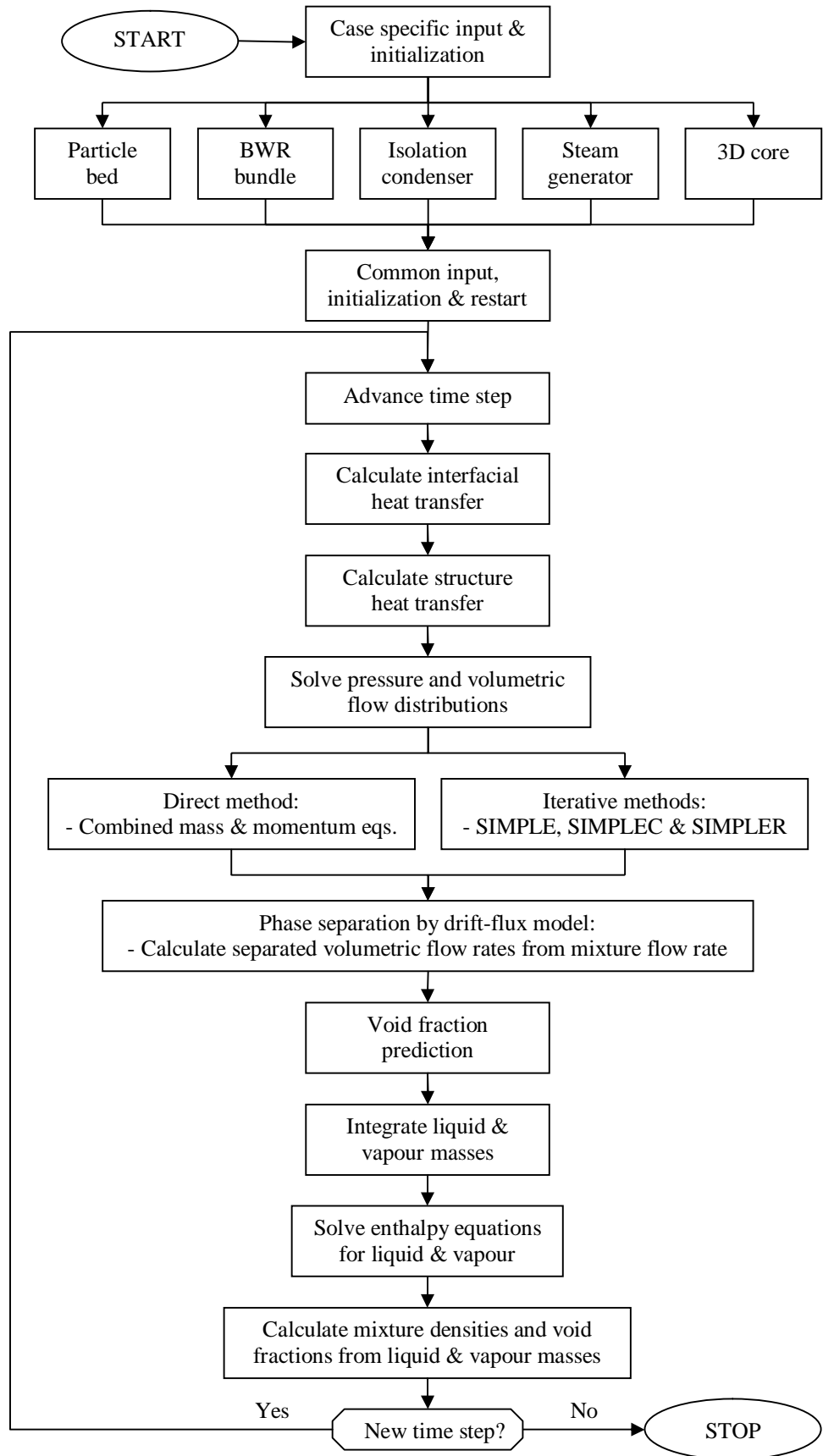


Figure 4.1: PORFLO solution procedure.

Phase separation is defined by the Zuber-Findlay drift-flux model. The drift-flux model is, in essence, used to divide the mixture flow rates over each face into separate flow rates for liquid and vapour, according to the local void fraction. The next step is to predict the void fraction distribution at the end of the time step. This is done by implementing the volumetric vapour flow rates, given by the drift-flux model, in a conservation equation for vapour phase mass, which results in a system of equations, where each equation contains the void fractions of the central and neighboring nodes. Void fractions at the end of the time step are obtained by solving this system of equations implicitly.

After the void fraction distribution is predicted and the volumetric flow rates for each phase are known, the mass flow rates of the two phases at each interface are also given. The mass flow rates are used to solve the enthalpy equations for each phase to obtain the temperatures and the mass conservation equations to obtain the vapour and liquid masses at the end of the time step. In the final step the mixture densities and the true void fraction distributions can be calculated from the vapour and liquid masses.

4.2 Conservation equations

The conservation equations used in PORFLO for solving momentum originate from Navier-Stokes equations, which are an application of Newton's second law. Navier-Stokes equations consist of three time-dependent conservation of momentum equations; one for each direction. In 5-equation models the momentum equations are formed for the mixture of phases, whereas continuity equations for conservation of mass and energy are formulated for each phase. The velocities of the separate phases are obtained from the mixture velocity using the drift-flux model.

4.2.1 Conservation of mass

The continuity equation for conservation of mass in its most general form is given through (White 2006, p. 61):

$$\frac{\partial \rho}{\partial t} + \nabla \cdot (\rho \mathbf{u}) = 0. \quad (4.1)$$

where

ρ	density [kg/m ³]
t	time [s]
\mathbf{u}	velocity vector (u, v, w) [m/s]

Using partial derivatives the continuity equation for conservation of vapour phase mass can be expressed as follows:

$$\frac{\partial(\alpha\rho_g)}{\partial t} + \frac{\partial(\alpha\rho_g u_g)}{\partial x} + \frac{\partial(\alpha\rho_g v_g)}{\partial y} + \frac{\partial(\alpha\rho_g w_g)}{\partial z} = +\gamma \quad (4.2)$$

where

α	void fraction [-]
ρ_g	gas density [kg/m ³]
γ	mass transfer from liquid to vapour phase [kg/m ³ s]
(u_g, v_g, w_g)	gas velocity in x, y and z-directions respectively [m/s]
(x, y, z)	3-dimensional Cartesian coordinates [m].

The first term (1) on the left-hand side of equation (4.2) expresses the time rate of change of gas mass inside an infinitesimally small control volume. The second (2), third (3) and fourth (4) terms on the left-hand side represent the changes in control volume mass due to the difference between inflow and outflow; the net outflow of mass in x, y and z-directions respectively. The fifth term (5) accounts for the mass transfer between the two phases.

A similar equation can be formulated for the liquid phase as well:

$$\frac{\partial[(1-\alpha)\rho_l]}{\partial t} + \frac{\partial[(1-\alpha)\rho_l u_l]}{\partial x} + \frac{\partial[(1-\alpha)\rho_l v_l]}{\partial y} + \frac{\partial[(1-\alpha)\rho_l w_l]}{\partial z} = -\gamma \quad (4.3)$$

where

ρ_l	liquid density [kg/m ³]
(u_l, v_l, w_l)	liquid velocity in x, y and z-directions respectively [m/s]

The terms in the equation account for the same effects, as in the gas phase above, with the exception that liquid mass is expressed as a fraction $(1 - \alpha)$ of the total mass and the mass transfer from gas to liquid equals $-\gamma$.

4.2.2 Conservation of momentum

The equations governing motion of the flow in PORFLO are based on the famous Navier-Stokes equations. The representation by White (2006, p. 68) can be written a bit differently using the vector differential operator del, represented by the nabla symbol. A general form of the conservation of momentum equation can be expressed through:

$$\frac{\partial(\rho\mathbf{u})}{\partial t} + \nabla \cdot [(\rho\mathbf{u}) \otimes \mathbf{u}] = -\nabla p + \nabla \cdot \mathbf{T} + \mathbf{f} \quad (4.4)$$

where	\mathbf{f}	sum vector of body forces [N/m ³]
	p	pressure [Pa]
	\mathbf{T}	surface force tensor (of rank 2) [N/m ²], $[\nabla \cdot \mathbf{T}] = \text{N/m}^3$
	\mathbf{u}	velocity vector (u, v, w) [m/s]
	\otimes	outer product.

The left-hand side of equation (4.4) defines the inertia of the flow and consists of unsteady acceleration (1), which measures the time rate of change of momentum of the fluid inside the control volume, and convective acceleration (2), which measures the net outflow of momentum due to differences in the velocity field near the control volume. The momentum is conveyed into, or out of, the control volume by the mass flows at the node faces. Unsteady acceleration represents the changes in the velocity field and therefore equals zero in stationary flow, where as convective acceleration represents the acceleration of a fluid particle in fixed coordinates, and doesn't necessarily equal zero in stationary flow. The right-hand side of the equation represents the forces acting on the fluid: pressure gradient (3), surface forces (viscosity) (4) and body forces (friction and gravity) (5).

If the outer product of momentum and velocity and the components of the surface force tensor are presented, equation (4.4) can be written as follows:

$$\frac{\partial(\rho\mathbf{u})}{\partial t} + \nabla \cdot \left[\begin{pmatrix} \rho u \\ \rho v \\ \rho w \end{pmatrix} \otimes \begin{pmatrix} u & v & w \end{pmatrix} \right] = -\nabla p + \nabla \cdot \begin{bmatrix} \tau_{xx} & \tau_{yx} & \tau_{zx} \\ \tau_{xy} & \tau_{yy} & \tau_{zy} \\ \tau_{xz} & \tau_{yz} & \tau_{zz} \end{bmatrix} + \mathbf{f} \quad (4.5)$$

where τ surface stress [N/m²].

Equation (4.5) can also be presented using partial derivatives, in which case the separate effects of each vector component, for instance each velocity component, are presented in its own term. The net outflow of u-momentum, momentum in x-direction, is simply the divergence of x-directional momentum ($\rho_m u_m$), the first row of the tensor obtained by calculating the outer product of momentum and velocity. First, the left-hand side of the momentum equation is considered separately. Inertia of the flow in x-direction is defined by the following terms:

$$\frac{\partial(\rho_m u_m)}{\partial t} + \frac{\partial(\rho_m u_m u_m)}{\partial x} + \frac{\partial(\rho_m u_m v_m)}{\partial y} + \frac{\partial(\rho_m u_m w_m)}{\partial z} = \sum \frac{F_x}{V} \quad (4.6)$$

where ρ_m mixture density [kg/m³]
 F_x force in x-direction [N]
 (u_m, v_m, w_m) mixture velocity in x, y and z-directions respectively [m/s]
 V (control) volume [m³].

Equation (4.6) is called a conservative form of the momentum equation. The first term (1) is the time rate of change of mixture u-momentum, momentum in x-direction, inside the control volume. The second (2), third (3) and fourth (4) terms represent the net fluxes of u-momentum out of the control volume in x, y and z-directions respectively.

Using the product rule on equation (4.6) leads to the following form:

$$\rho_m \frac{\partial u_m}{\partial t} + \rho_m u_m \frac{\partial u_m}{\partial x} + \rho_m v_m \frac{\partial u_m}{\partial y} + \rho_m w_m \frac{\partial u_m}{\partial z} + u_m \frac{\partial \rho_m}{\partial t} + u_m \frac{\partial(\rho_m u_m)}{\partial x} + u_m \frac{\partial(\rho_m v_m)}{\partial y} + u_m \frac{\partial(\rho_m w_m)}{\partial z} = \sum \frac{F_x}{V} \quad (4.7)$$

Conservation of mass equation $\times u_m$

The iterative methods in PORFLO use the conservative forms of the momentum equations to obtain the discretized equations, whereas the direct method, the older method in PORFLO, uses the non-conservative, or primitive, forms of the momentum equations. The non-conservative form of u-momentum, momentum in x-direction, results from equation (4.7) when the conservation of mass equation times u_m , the last four terms on the left-hand side of the equation (4.7), is reduced from the momentum equation. This is simply because the flow has to satisfy the continuity equation, therefore the terms mentioned equal zero. The non-conservative form of the momentum equation for x-direction is given through

$$\rho_m \frac{\partial u_m}{\partial t} + \rho_m u_m \frac{\partial u_m}{\partial x} + \rho_m v_m \frac{\partial u_m}{\partial y} + \rho_m w_m \frac{\partial u_m}{\partial z} = \sum \frac{F_x}{V}. \quad (4.8)$$

Now that the left-hand side of the momentum equation is complete, the forces on the right-hand side can be discussed. The forces acting in x-direction are presented below:

$$\sum \frac{F_x}{V} = -\frac{\partial p}{\partial x} + \frac{\partial}{\partial x} \left(\mu \frac{\partial u}{\partial x} \right) + \frac{\partial}{\partial y} \left(\mu \frac{\partial u}{\partial y} \right) + \frac{\partial}{\partial z} \left(\mu \frac{\partial u}{\partial z} \right) - 0,5 \times \frac{f}{d_e} \rho_m u_m |u_m|, \quad (4.9)$$

where d_e equivalent diameter [m]
 f frictional coefficient
 p pressure [Pa]
 μ dynamic viscosity [Ns/m²].

The net force, in equation (4.9), is comprised of the pressure gradient (1), viscosity (2) and the pressure loss due to friction (3). The surface stress components that appear in equation (4.5) are not very useful, but with some approximations, presented in appendix A, the surface stresses, in this case viscous stresses, are developed to relate the changes in the velocity field to the resulting forces through dynamic viscosity. Combining equations (4.8) and (4.9) leads to the final form of the momentum equation for x-direction:

$$\begin{aligned} & \rho_m \frac{\partial u_m}{\partial t} + \rho_m u_m \frac{\partial u_m}{\partial x} + \rho_m v_m \frac{\partial u_m}{\partial y} + \rho_m w_m \frac{\partial u_m}{\partial z} \\ & = -\frac{\partial p}{\partial x} + \frac{\partial}{\partial x} \left(\mu \frac{\partial u}{\partial x} \right) + \frac{\partial}{\partial y} \left(\mu \frac{\partial u}{\partial y} \right) + \frac{\partial}{\partial z} \left(\mu \frac{\partial u}{\partial z} \right) - 0,5 \times \frac{f}{d_e} \rho_m u_m |u_m| \end{aligned} \quad (4.10)$$

Momentum equations can be written for other directions using the same approach. In vertical direction a term that accounts for gravitation has been added to the equation. The momentum equations for y and z-directions respectively are given through

$$\begin{aligned} & \rho_m \frac{\partial v_m}{\partial t} + \rho_m u_m \frac{\partial v_m}{\partial x} + \rho_m v_m \frac{\partial v_m}{\partial y} + \rho_m w_m \frac{\partial v_m}{\partial z} \\ & = -\frac{\partial p}{\partial y} + \frac{\partial}{\partial x} \left(\mu \frac{\partial v}{\partial x} \right) + \frac{\partial}{\partial y} \left(\mu \frac{\partial v}{\partial y} \right) + \frac{\partial}{\partial z} \left(\mu \frac{\partial v}{\partial z} \right) - 0,5 \times \frac{f}{d_e} \rho_m v_m |v_m| \end{aligned} \quad \text{and} \quad (4.11)$$

$$\begin{aligned} & \rho_m \frac{\partial w_m}{\partial t} + \rho_m u_m \frac{\partial w_m}{\partial x} + \rho_m v_m \frac{\partial w_m}{\partial y} + \rho_m w_m \frac{\partial w_m}{\partial z} \\ & = -\frac{\partial p}{\partial z} + \frac{\partial}{\partial x} \left(\mu \frac{\partial w}{\partial x} \right) + \frac{\partial}{\partial y} \left(\mu \frac{\partial w}{\partial y} \right) + \frac{\partial}{\partial z} \left(\mu \frac{\partial w}{\partial z} \right) - 0,5 \times \frac{f}{d_e} \rho_m w_m |w_m| - \rho_m g \end{aligned} \quad (4.12)$$

where g acceleration due to gravity [m/s²].

4.2.3 Conservation of energy

The conservation equations for energy can contain different terms depending on how accurately the equations need to be solved. In most engineering applications some terms are strongly dominant while the effect of others is relatively small. One approach to derive the energy equations for each phase would be to start from specific enthalpy equations. Total specific enthalpy, in quite general form, can be expressed through

$$h_{TOT} = \underbrace{u}_{1} + \underbrace{pv}_{2} + \underbrace{\frac{1}{2}w^2}_{3} + \underbrace{gz}_{4} + \frac{A\sigma}{m}, \quad (4.13)$$

where	A	surface area of liquid or vapour volume [m ²]
	g	acceleration of gravity [m/s ²]
	h_{TOT}	total specific enthalpy [J/kg]
	m	mass of the liquid or vapour volume [kg]
	p	pressure [Pa]
	u	specific internal energy [J/kg]
	v	specific volume [m ³ /kg]
	w	velocity of the flow [m/s]
	z	vertical distance from an arbitrary level [m]
	σ	surface tension [N/m]

The right-hand side of equation (4.13) consists of specific enthalpy (1), specific kinetic energy (2), specific potential energy (3), and specific surface tension energy (4). Additional terms could be added to the right hand side, if necessary, to account for changes in chemical, or other forms of, energy. However, in a BWR fuel bundle, as well as in all the other applications of PORFLO, the energy content of the flow is properly defined with only the specific enthalpy (Moran & Shapiro 1998, p. 78), which is a function of pressure and temperature, as follows:

$$h = u(T) + pv, \quad (4.14)$$

where h specific enthalpy [J/kg].

Specific enthalpies for vapour and liquid can be obtained from either (material) tables or, more conveniently, functions, which are fitted to the same data as the tables are based on.

Since it was decided that the energy content of the flow is sufficiently defined with specific enthalpy, the energy conservation equations for both gas and liquid phase are derived by

formulating conservation equations for enthalpy. A general form of the enthalpy equations is given through

$$\frac{\partial(\rho h)}{\partial t} + \nabla \cdot (\rho h \mathbf{u}) = Q + P, \quad (4.15)$$

where P power generated in the control volume per unit volume [W/m³]
 Q heat rate into the control volume per unit volume [W/m³]
 \mathbf{u} velocity vector, whose components (u, v, w) [m/s].

The energy conservation equations are presented below for the gas and liquid phase respectively:

$$\frac{\partial(\alpha \rho_g h_g)}{\partial t} + \frac{\partial(\alpha \rho_g h_g u_g)}{\partial x} + \frac{\partial(\alpha \rho_g h_g v_g)}{\partial y} + \frac{\partial(\alpha \rho_g h_g w_g)}{\partial z} = q_{wg}''' + q_{lg}''' \quad (4.16)$$

$$\frac{\partial[(1-\alpha)\rho_l h_l]}{\partial t} + \frac{\partial[(1-\alpha)\rho_l h_l u_l]}{\partial x} + \frac{\partial[(1-\alpha)\rho_l h_l v_l]}{\partial y} + \frac{\partial[(1-\alpha)\rho_l h_l w_l]}{\partial z} = q_{wl}''' - q_{lg}''', \quad (4.17)$$

where h_g gas enthalpy [J/kg]
 h_l liquid enthalpy [J/kg]
 q_{wg}''' heat rate from wall to vapour per unit volume [W/m³]
 q_{lg}''' heat rate from liquid to vapour per unit volume [W/m³]
 q_{wl}''' heat rate from wall to liquid per unit volume [W/m³].

4.3 Phase separation by drift-flux model

Phase separation, the velocity difference between vapour and liquid phase, is described by Zuber-Findlay drift-flux model (Zuber & Findlay 1965). It contains two empirical fitting parameters, the distribution parameter C_0 and the drift-flux velocity V_{gj} , which are defined by the user. The model uses the two parameters to connect the gas phase velocity to the mixture velocity. The velocities j_i are area averaged velocities of phase i across the cross-section of the flow.

$$v_g = C_0 j_m + V_{gj}, \quad (4.18)$$

where v_g real gas phase velocity [m/s]
 j_m area averaged mixture velocity [m/s]
 C_0 distribution parameter
 V_{gj} drift-flux velocity [m/s].

The area averaged velocities can be attained from volumetric flow rates by dividing them with cross-sectional area of the flow. Real velocities are linked to area averaged velocities as follows:

$$j_g = \alpha v_g, \quad (4.19)$$

$$j_l = (1 - \alpha)v_l, \quad (4.20)$$

$$j_m = j_g + j_l, \quad (4.21)$$

where

j_g	area averaged gas velocity [m/s]
j_l	area averaged liquid velocity [m/s]
v_l	real liquid phase velocity [m/s].

Relative velocity between the two phases can be solved using equations (4.18), (4.19), (4.20) and (4.21).

$$\Delta u = v_g - v_l = \frac{[(1 - \alpha)C_0 - 1]j_m + V_{gj}}{(1 - \alpha)} \quad (4.22)$$

The distribution parameter and the drift-flux velocity proposed in the original paper by Zuber and Findlay (1965) for *churn-turbulent bubbly* flow region are given below:

$$C_0 = 1.2 \quad (4.23)$$

$$V_{gj} = 1.53 \left[\frac{g\sigma(\rho_l - \rho_g)}{\rho_l^2} \right]^{0.25} \quad (4.24)$$

where

g	acceleration due to gravity [m/s ²]
ρ_l	liquid density [kg/m ³]
ρ_g	vapour density [kg/m ³]
σ	surface tension [N/m].

4.4 Correlations

The empirical correlations used in PORFLO, relevant for this thesis, are presented in this section. Factors that are functions of both void fraction and porosity have been added to some of the original correlations to account for the changes in heat transfer surface area due to changes in void fraction and porosity.

4.4.1 Heat transfer correlations

Heat transfer inside a BWR fuel bundle comprises different heat transfer modes: convective heat transfer to liquid and vapour, boiling heat transfer, condensation of vapour to liquid when liquid temperature is subcooled and flashing of liquid when liquid is superheated. However, since the current application of PORFLO, and the scope of this thesis, is more concerned with the model development for wetted surface heat transfer, more attention is given to the most important heat transfer modes in BWR nominal conditions: boiling heat transfer and convective heat transfer to liquid and gas, respectively. Flashing and condensation are not discussed, though models for those heat transfer modes are included in PORFLO.

Both the boiling heat transfer and convective heat transfer alike have been extensively studied in single tubular flow channels and annular flow channels around a heated rod. The geometry of a BWR fuel bundle can easily be projected into these two basic geometries piece-wise: a subchannel enclosed by four fuel rods is reminiscent of a tubular flow channel, while the flow around a single fuel rod can be considered as a flow in an annular geometry. This is the argumentation, why the heat transfer correlations developed for tubular and annular flow channels can be applied to BWR fuel bundles.

It is widely established that implementation of heat transfer correlations, originally developed for 1D calculations in steady-state and fully developed flow conditions, to 3D domains and often transient conditions is problematic, to say the least. In the original 1D heat transfer correlations most of the parameters are either averages or otherwise representative values for the whole geometry: it is therefore challenging to define the parameters used in 3D calculations so that the heat transfer rates remain dependent on the local conditions, temperature of the fluid near the heat transfer surface for instance, while changes in the resolution of the grid do not affect the total heat transfer rate.

The equivalent diameter is a fine example of this dilemma: It could be either calculated for a cross-section of the fuel bundle or more locally. An assumption, that the equivalent diameter calculated for the entire cross-section of the fuel bundle is also applicable in the

heat transfer correlations calculated on a node-by-node basis, is used in PORFLO. The equivalent diameter is defined through

$$d_e = \frac{4V_f}{A_{\text{wall}}} \quad (4.25)$$

where A_{wall} heated area (heated rod, solid) [m²]
 d_e equivalent diameter [m]
 V_f fluid volume [m³].

Convective heat transfer from structure to liquid and vapour is based on the Dittus-Boelter turbulent heat transfer correlation (Dittus & Boelter 1930).

$$h''_{\text{con,l}} = 0.023 \frac{k_l}{d_e} \text{Re}_m^{0.8} \text{Pr}^{0.4} \quad (4.26)$$

$$h''_{\text{con,g}} = 0.023 \frac{k_g}{d_e} \text{Re}_m^{0.8} \text{Pr}^{0.4} \quad (4.27)$$

where d_e equivalent diameter [m]
 $h''_{\text{con,g}}$ convective heat transfer coefficient for vapour [W/m²K]
 $h''_{\text{con,l}}$ convective heat transfer coefficient for liquid [W/m²K]
 k_g thermal conductivity of vapour [W/mK]
 k_l thermal conductivity of liquid [W/mK]
 Pr Prandtl number [-]
 Re mixture Reynolds number [-]

The mixture Reynolds number is defined as

$$\text{Re}_m = \frac{\rho_m u_m d_e}{\mu_l} \quad (4.28)$$

Currently only liquid viscosity is used to calculate the Reynolds number, since liquid is the continuous phase throughout most of the BWR flow channel.

The convective heat transfer coefficients, according to Dittus-Boelter, are applied in the following equations for convective heat transfer to vapour and liquid, respectively:

$$q''_{\text{con,wg}} = \frac{A_{\text{wall}}}{V_f} h''_{\text{con,g}} (T_{\text{wall}} - T_g) \alpha \quad (4.29)$$

$$q''_{\text{con, wl}} = \frac{A_{\text{wall}}}{V_f} h''_{\text{con, l}} (T_{\text{wall}} - T_1)(1 - \alpha) \quad (4.30)$$

where	A_{wall}	surface heat transfer area [m ²]
	$q''_{\text{con, wg}}$	volumetric heat transfer rate from wall to vapour due to convection [W/m ³]
	$q''_{\text{con, wl}}$	volumetric heat transfer rate from wall to liquid due to convection [W/m ³]
	T_g	vapour temperature [K or °C]
	T_1	liquid temperature [K or °C]
	T_{wall}	temperature of the heat transfer surface [K or °C]
	V_f	fluid volume [m ³].

Boiling heat transfer only occurs when temperature of the heat transfer surface exceeds the saturation temperature of the liquid. The correlation for boiling heat transfer coefficient is based on Thom's correlation (Hewitt, G. F. & Delhaye, J. M. & Zuber, N. 1986), which is a simplified correlation for the nucleate boiling region and hence very popular option in 1D fuel bundle heat transfer models:

$$(T_{\text{wall}} - T_{\text{sat}}) = 22.52 \left(\frac{q_{\text{nb}}}{10^6} \right)^{0.5} e^{-0.0115 p} \quad (4.31)$$

where	q_{nb}	nucleate boiling heat flux [W/m ²]
	p	pressure [bar]
	T_{sat}	saturation temperature [K or °C].

The boiling heat transfer coefficient can be solved from the previous relation:

$$\Leftrightarrow q_{\text{nb}} = \frac{10^6}{22.52^2} \frac{1}{e^{-0.023 p}} (T_{\text{wall}} - T_{\text{sat}})^2 \quad (4.32)$$

$$\Rightarrow h''_{\text{nb}} \approx 1972 e^{0.023 p} \quad (4.33)$$

where	h''_{nb}	boiling heat transfer coefficient [W/m ² K ²].
-------	-------------------	---

The decrease in boiling heat transfer rate with increasing void fraction has been taken into account by including a factor that is a nonlinear function of void fraction.

$$q''_{\text{nb}} = \frac{A_{\text{wall}}}{V_f} h''_{\text{nb}} [\max(T_{\text{wall}} - T_{\text{sat}}, 0)]^2 (1 - \alpha)^{0.3} \quad (4.34)$$

where	q''_{nb}	volumetric heat transfer rate for boiling [W/m ³]
-------	-------------------	---

Convective heat transfer rate into liquid and boiling heat transfer rate are used to vaporize liquid. The current limit for liquid subcooling is 30 °C; if the subcooling is more than that, the heat transfers are used for heating the liquid. The transition is done with a ramp function.

$$\gamma = \frac{\max[30\text{K} - (T_{\text{sat}} - T_1), 0]}{30\text{K}} \frac{(q_{\text{nb}}'' + q_{\text{wl}}'')}{h_{\text{fg}}}, \quad (4.35)$$

where h_{fg} specific latent heat of vaporization [J/kg].

Since the development of PORFLO is still in the testing stage, the values of the heat transfer coefficients used in the heat transfer correlations are given fixed values for the test runs. These values are listed below in Table 4.1.

Table 4.1: Heat transfer coefficients used in calculations.

Mode	Symbol	Value	Unit
Convective heat transfer to liquid	$h_{\text{con,l}}''$	50,000	W/m ² K
Convective heat transfer to vapour	$h_{\text{con,g}}''$	500	W/m ² K
Boiling heat transfer	h_{nb}''	950,000	W/m ² K ²

4.4.2 Critical heat flux

Several correlations for critical heat flux that exist in the literature include mass flow rate as one of the defining parameters, which is undesirable from the perspective of the current application of PORFLO. Since dryout is a rather local phenomenon, the use of local values instead of averaged values would be preferred in the correlation for critical heat flux. Therefore, a correlation proposed by Griffith, Pearson and Lepkowski (1977) has been selected, since it does not include mass flow rate, which facilitates the use of local values in the correlation.

$$\frac{q_{\text{CHF}}''}{h_{\text{fg}}\rho_g} = 0,131 \left(\frac{\sigma(\rho_l - \rho_g)g}{\rho_g^2} \right)^{0,25} (1 - \alpha) \quad (4.36)$$

where q_{CHF}'' critical heat flux [W/m²]

4.4.3 Friction factor

In the current version of PORFLO friction is assumed to be evenly distributed throughout the 3-dimensional domain. Thus the force exerted on the fluid per unit volume is defined by a relation similar to the pressure drop in one-dimensional tubes, shown for x-direction:

$$\frac{F_{x, \text{fric}}}{V} = -\frac{1}{2} \times \frac{f}{d_e} \rho_m u_m |u_m| \quad (4.37)$$

where d_e hydraulic diameter of the flow channel [m]
 $F_{x, \text{fric}}$ force exerted on the fluid due to friction
 f friction factor [-].

The friction factor could be varied depending on the flow conditions and different values could be used for the flow across the tube bundle, in horizontal flow directions, and vertical direction, but at the moment fixed values are set in the input file for the friction factors (usually between 0.01 - 0.001). Correlations, such as (Blasius 1913), could be used to evaluate the friction factor.

$$f = \frac{0.3165}{\text{Re}_m^{0.25}} \quad (4.38)$$

5 DISCUSSION OF PRESSURE-VELOCITY COUPLING

As was briefly mentioned in the previous chapter, velocity and pressure fields are closely interlinked, and thus have to be solved simultaneously. There are two fundamentally different ways to do this: direct methods and iterative methods.

In direct methods the conservation equations for mixture mass are either combined with the three mixture momentum equations to yield a single system of equations for pressure, or otherwise solved simultaneously. One of the perks of this method is that the amount of calculations needed for solving a problem with one system of equations is much less than a problem with several systems of equations.

Another approach is to couple the pressures and velocities indirectly, which leads to an iterative procedure where the approximations for pressures and velocities are improved with every cycle. SIMPLE, Semi-Implicit Method for Pressure-Linked Equations, algorithm is an example of an iterative method. The SIMPLE algorithm starts with guessed pressure and velocity fields which are first input to the momentum equations to obtain improved values for the velocities. The improved velocities are used in the pressure correction equation, which is obtained by combining the mass and momentum conservation equations. The pressure corrections are used to yield corrected pressures and velocities, which are again used in the momentum equations at the start of the next cycle.

Iterative methods, like SIMPLE, require more calculations, since firstly multiple systems of equations have to be solved during one iteration cycle, the momentum equations and the pressure corrections, and secondly multiple iterations are needed to reach a converged solution. In this perspective it would seem unreasonable to use SIMPLE. However, fully implicit discretization can be applied to formulate the momentum equations and all the terms in the momentum equations, convection, diffusion and even turbulence, can be introduced without significant hardship. The convective terms in the momentum equations can be quite problematic in some direct methods, especially in the direct method implemented in PORFLO.

It is important to recognise that though SIMPLE makes no assumptions about the type of the solver with which the systems of equations are to be solved, being an iterative procedure itself, the intermediate solutions of the iteration cycles do not have to be solved precisely; only the final solution is of importance. Therefore, the use of an iterative solver and careful consideration of the convergence criteria can significantly reduce the amount of calculations needed to perform one time step, and hence the overall computational time is reduced as well.

6 DISCRETIZATION OF THE GOVERNING EQUATIONS

Though thorough discussion of discretization is often dismissed in literature, the importance of consistent discretization procedures can not be denied; consistent implementation of the selected discretization scheme, throughout all the conservation equations, lays the foundation for solving the flow problem. Even though solvability and convergence are not guaranteed with a proper discretization procedure alone, the choices made in the discretization procedure can have quite far-reaching effects.

In this chapter the basic principles and notations used in discretization are presented first. Then, the discretization and coupling of the mass and momentum equations are presented first for the iterative methods and then for the direct method, both of which are implemented in PORFLO.

6.1 Basic principles used in discretization

The conservation equations can not be used in computations in their basic continuous forms, but have to be transformed into the computational grid to yield equations for each node. The grid, shown in Figure 6.1, is generated so that it is composed of cuboids, rectangular boxes, with changing dimensions; in other words: the grid is non-uniform and orthogonal.

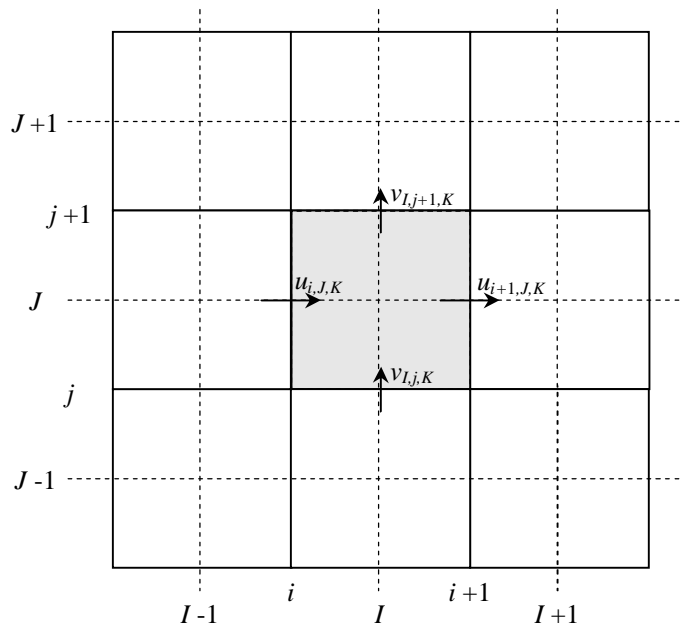


Figure 6.1: A portion of the grid and positions of the velocities.

The shaded area in Figure 6.1 represents the pressure node (I, J, K) . Indexes I, J and K refer to the center point of the control volume and indexes i, j and k refer to the control volume faces where the velocities are located.

Backward staggering has been used to create the velocity grids in order to avoid the *pressure field checkerboard effect* presented by Patankar (1980, pp. 118-120). Each velocity component, $u, v,$ and $w,$ has its own unique grid. In backward staggering, the velocity nodes are located on top of the velocity components; each velocity node is bounded by the centerline of the pressure node with the same indexes as the velocity component, (I, J, K) for velocities $u_{i,J,K}$, and the centerline of the previous pressure node parallel to the velocity component, $(I-1, J, K)$ for velocities $u_{i,J,K}$, hence the expression: backward staggered. The velocity grids are only staggered in the direction parallel to the velocity component in question; the other grid lines remain unchanged compared to the pressure grid. A portion of u-velocity grid, a grid for the x-directional components of velocity, is shown in Figure 6.2. The shaded area in Figure 6.2 is the velocity node or u-control volume (i, J, K) .

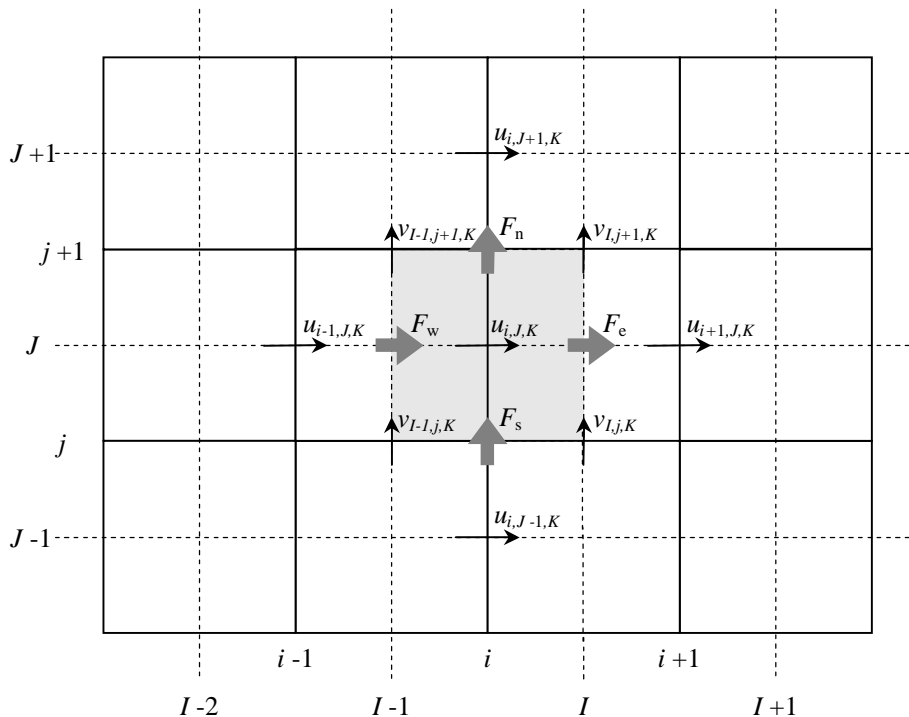


Figure 6.2: A portion of u-velocity grid.

Some variables located on the faces of the control volumes are referred to with a subscript depending on the direction where the face is located compared to the center point of the

node: e (east), w (west), s (south), n (north), u (up) and d (down). These notations are used mainly with flows that cross the faces, for example the mass flow rates (F_e, F_w, \dots) in Figure 6.2. The mass flow rates at each boundary are handled according to *the upwind differencing scheme*, UDS, which means that the densities are taken from the pressure node upstream of the face the flow goes through. Patankar (1980, pp. 83-85) includes a representation of the upwind differencing scheme in his work, though he is not the inventor of the scheme.

6.2 Notations used in discretization

Before proceeding any further some notations and abbreviations are defined that are used throughout this thesis. As the grid is orthogonal, the formulation of the discretized equations is simplified, since the opposite faces of the control volume have the same surface area. The surface areas of the control volume faces are denoted by superscripts according to the axis that goes through the face: $A_{I,J,K}^i$, $A_{I,J,K}^j$ and $A_{I,J,K}^k$. The same notation is used with densities, porosities and dynamic viscosities as well.

During the course of the discretization process it became apparent that a certain average is repeated quite frequently, therefore abbreviations are presented here that significantly reduce the length of the upcoming discretized equations. Pressure, temperature, density, void fraction, porosity and dynamic viscosity are averaged over the control volume and thought to be located at the center point of the pressure node. The values of some of these variables are, nevertheless, needed at the faces of the nodes; hence a proper average is needed to approximate the values at the interfaces.

The densities at interfaces, equations (6.1) through (6.3), are simply volume averaged; the density of the pressure node is weighted with the volume of the pressure node when forming the average over the u-control volume. In this case the weighting of two contiguous nodes is performed with the length of the node, since the other two dimensions do not change over the face of the node. These volume averaged densities are only used with forces acting on the fluid, inertia, gravity and friction, not with flows that cross the interfaces.

$$\rho_{I,J,K}^i = \frac{\varepsilon_{I-1,J,K} \Delta x_{I-1,J,K} \rho_{I-1,J,K} + \varepsilon_{I,J,K} \Delta x_{I,J,K} \rho_{I,J,K}}{\varepsilon_{I-1,J,K} \Delta x_{I-1,J,K} + \varepsilon_{I,J,K} \Delta x_{I,J,K}} \quad (6.1)$$

$$\rho_{I,J,K}^j = \frac{\varepsilon_{I,J-1,K} \Delta y_{I,J-1,K} \rho_{I,J-1,K} + \varepsilon_{I,J,K} \Delta y_{I,J,K} \rho_{I,J,K}}{\varepsilon_{I,J-1,K} \Delta y_{I,J-1,K} + \varepsilon_{I,J,K} \Delta y_{I,J,K}} \quad (6.2)$$

$$\rho_{I,J,K}^k = \frac{\varepsilon_{I,J,K-1} \Delta z_{I,J,K-1} \rho_{I,J,K-1} + \varepsilon_{I,J,K} \Delta z_{I,J,K} \rho_{I,J,K}}{\varepsilon_{I,J,K-1} \Delta z_{I,J,K-1} + \varepsilon_{I,J,K} \Delta z_{I,J,K}} \quad (6.3)$$

where

$\rho_{I,J,K}$	density of node I,J,K
$\varepsilon_{I,J,K}$	porosity of node I,J,K
Δx	length of the node in x-direction
Δy	length of the node in y-direction
Δz	length of the node in z-direction.

In a porous media model an approximation is needed for evaluating the porosities inside the velocity nodes and at the boundaries of the pressure nodes. The problem arises when there is an abrupt change in porosities of the adjoining nodes. As the grid used in PORFLO does not follow the surfaces of the structures, the values of porosity can change quite significantly from one node to the next. In the case of BWR fuel bundle, porosities change smoothly most of the time, since the geometry being modeled is made of round shapes and no sharp edges are present. However, when approaching the fuel rods perpendicularly to the surface of the fuel rod, large differences in porosities can occur while the interface between the two nodes is in reality completely filled with fluid.

This contradiction makes it difficult to formulate the average for porosities at the node faces that can be consistently applied throughout the calculation domain, since the flow area, which is defined as the surface area of the node times the porosity at the node interface, has proven to be one of the most sensitive parameters in PORFLO. Aside from the practical point of view, there is a more fundamental issue on how the porosities at the interfaces should be defined: on the other hand one of the axioms, and most definitely one of the substantial strengths, of porosity modeling is that the true geometry can be disregarded, but at the same time the true geometry ceases to exist and the information about the interfaces is blurred. Provided that there is more detailed information about the geometry of the structural interfaces than the porosities at each pressure node would imply,

should this information be used in the formulation of the surface flow areas in the first place?

It would be quite straightforward to use the more detailed information about the geometry, if available, to calculate the flow surface areas, but then again other effects of this choice should be considered, the center point of the fluid volume for instance. Most averaging procedures require information about the location of the center point of the fluid volume, the point where the values averaged over the pressure nodes are thought to be located; if the true geometry is used, the center points of the fluid volumes near the structural interfaces, where porosity is $\varepsilon > 0$, should be shifted away from the structure, as opposed to the porosity approach where the center of the fluid volume would always be located in the center point of the node; hence all the averaging procedures would be affected. If the effects on the true center point of the fluid volume are modeled, the formulation becomes substantially more complicated; in fact, for all practical purposes the formulation would become similar to body-fitted.

One approach is to let the minimum value define the effect of porosity on velocities through the surface area of the flow, others include harmonic averaging and volume averaging. Harmonic and volume averaging have been tried out in the code and seem to produce quite similar results. This might be mostly due to the fact that both of the averaging procedures result in the same values, in BWR fuel bundle geometry, for the horizontal direction, which is the main flow direction. Examples of harmonic and volume averaging are presented in Figure 6.3. The rounded shape represents the surface of the fuel rod and the shaded areas represent the fractions of the volume occupied by the fuel rod.

The lines in Figure 6.3 visualize the averaging procedures; as the line intersects with the interface, the fraction above the interface from the total length of the interface is the porosity at the interface according to the averaging procedure in question.

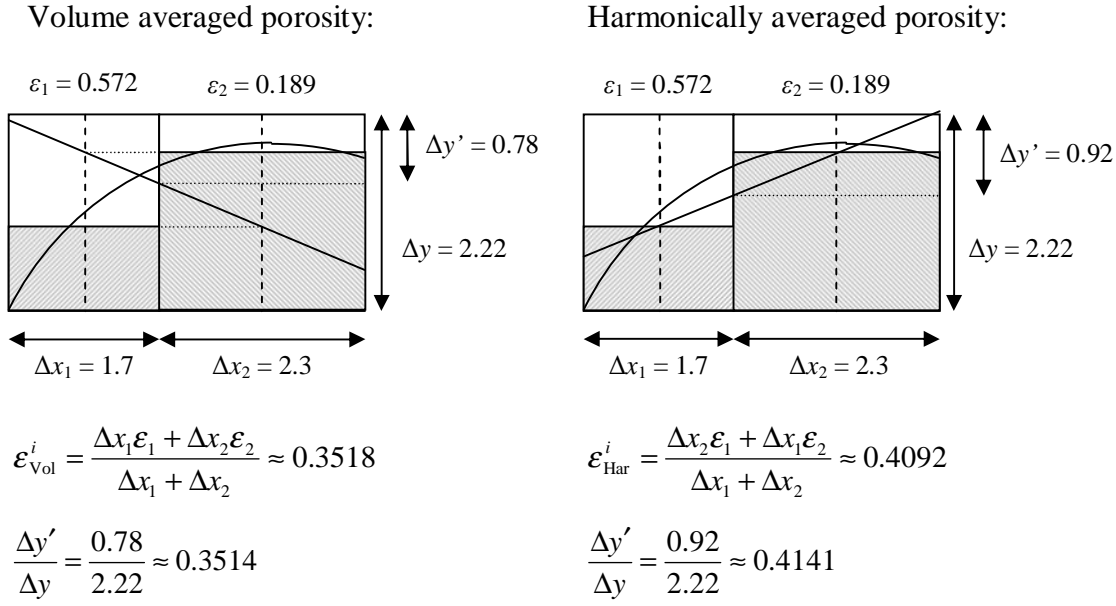


Figure 6.3: Volume averaged and harmonically averaged porosities at the interface of two adjacent nodes.

Porosities at the interfaces are chosen to be presented as harmonic averages over the interface, as shown in equations (6.4), (6.5) and (6.6). This form of averaging works well when moving parallel to the surfaces of the fuel rods, but when approaching perpendicularly to the surface of the fuel rods the surface area of the flow is often underestimated.

$$\varepsilon_{I,J,K}^i = \frac{\Delta x_{I-1,J,K} \varepsilon_{I,J,K} + \Delta x_{I,J,K} \varepsilon_{I-1,J,K}}{\Delta x_{I-1,J,K} + \Delta x_{I,J,K}} \quad (6.4)$$

$$\varepsilon_{I,J,K}^j = \frac{\Delta y_{I,J-1,K} \varepsilon_{I,J,K} + \Delta y_{I,J,K} \varepsilon_{I,J-1,K}}{\Delta y_{I,J-1,K} + \Delta y_{I,J,K}} \quad (6.5)$$

$$\varepsilon_{I,J,K}^k = \frac{\Delta z_{I,J,K-1} \varepsilon_{I,J,K} + \Delta z_{I,J,K} \varepsilon_{I,J,K-1}}{\Delta z_{I,J,K-1} + \Delta z_{I,J,K}} \quad (6.6)$$

where $\varepsilon_{I,J,K}$ porosity of node I,J,K

6.3 Discretization for the iterative methods in PORFLO

A separate subroutine for pressure-velocity solution, which utilizes SIMPLE, Semi-Implicit Method for Pressure-Linked Equations, SIMPLEC, SIMPLE-Consistent, and SIMPLER, SIMPLE-Revised, algorithms, was created and included in PORFLO during

this thesis. The conservation equations for mixture mass and momentum were formulated, discretized, and coded as a part of this thesis. In this section, the discretization of conservation equations for mixture mass and momentum is presented.

The discretization procedure follows the guidelines set by Patankar (1980) and later introduced in (Versteeg & Malalasekera 2006), with the exception that some modifications are made to accommodate two-phase flow, since the algorithms presented in the references are intended for one-phase flow. Though the pressure-velocity solution in 5-equation models consists of equations formulated for the mixture of phases, which are similar to the equations governing one-phase flow, some additional terms have to be introduced to account for the peculiarities of two-phase flow, changes in mixture density caused by phase change for instance.

The flow is assumed to be fully incompressible, which leads to an ill-conditioned system of equations for pressure corrections; there is practically no diagonal dominance in most of the domain, which in turn renders most iterative solvers, without preconditioning, unable to solve the system of equations. This will be discussed in more detail in the remainder of this thesis; the purpose here is merely to point out how much effect some basic assumptions can have on the solution procedure.

6.3.1 Discretization of the mass conservation equations

Since the object is to derive discretized equations for the mixture of the phases, the discretization could be started from conservation equations for mixture mass. However, if the derivation is begun by combining the separate mass equations for the two phases, equations (4.2) and (4.3), one of the fundamental disadvantages of 5-equation models becomes evident.

$$\frac{\partial(\alpha\rho_g)}{\partial t} + \frac{\partial(\alpha\rho_g u_g)}{\partial x} + \frac{\partial(\alpha\rho_g v_g)}{\partial y} + \frac{\partial(\alpha\rho_g w_g)}{\partial z} = +\gamma$$

$$\frac{\partial[(1-\alpha)\rho_l]}{\partial t} + \frac{\partial[(1-\alpha)\rho_l u_l]}{\partial x} + \frac{\partial[(1-\alpha)\rho_l v_l]}{\partial y} + \frac{\partial[(1-\alpha)\rho_l w_l]}{\partial z} = -\gamma$$

The conservation equations for liquid and vapour mass can be summed together to form an equation for the mixture of the two phases:

$$\begin{aligned} & \frac{\partial[\alpha\rho_g + (1-\alpha)\rho_l]}{\partial t} + \frac{\partial[\alpha\rho_g u_g + (1-\alpha)\rho_l u_l]}{\partial x} \\ & + \frac{\partial[\alpha\rho_g v_g + (1-\alpha)\rho_l v_l]}{\partial y} + \frac{\partial[\alpha\rho_g w_g + (1-\alpha)\rho_l w_l]}{\partial z} = \gamma - \gamma \end{aligned} \quad (6.7)$$

The expression inside the square brackets of the time derivative term, the first term on the left-hand side of equation (6.7), is the definition of mixture density, which is statistical in its nature; at any given instant a portion α of the control volume is filled with vapour while portion $1 - \alpha$ is filled with liquid, the mixture density is simply the volume average of the two densities. To combine the mass fluxes inside the square brackets of the second, third, and fourth terms on the left-hand side, the velocities of the two phases need to be equal for the mixture mass to be conserved.

However, after the mixture flow rates and the pressure field are solved, the phase velocities are obtained from drift-flux correlation. If velocity differences between the phases exist, the conservation equation for mixture mass based on mixture density is no longer valid. The resulting error in mass balance has to be corrected during the simulation or the errors grow prohibitively large and the simulation crashes.

If the phase velocities are assumed to be equal, the conservation equation for mixture mass can be expressed using the mixture densities:

$$\frac{\partial\rho_m}{\partial t} + \frac{\partial(\rho_m u_m)}{\partial x} + \frac{\partial(\rho_m v_m)}{\partial y} + \frac{\partial(\rho_m w_m)}{\partial z} = 0 \quad (6.8)$$

Discretized equations for conservation of mixture mass are derived by integrating equation (6.8) over the control volume shown in Figure 6.4 and time step Δt .

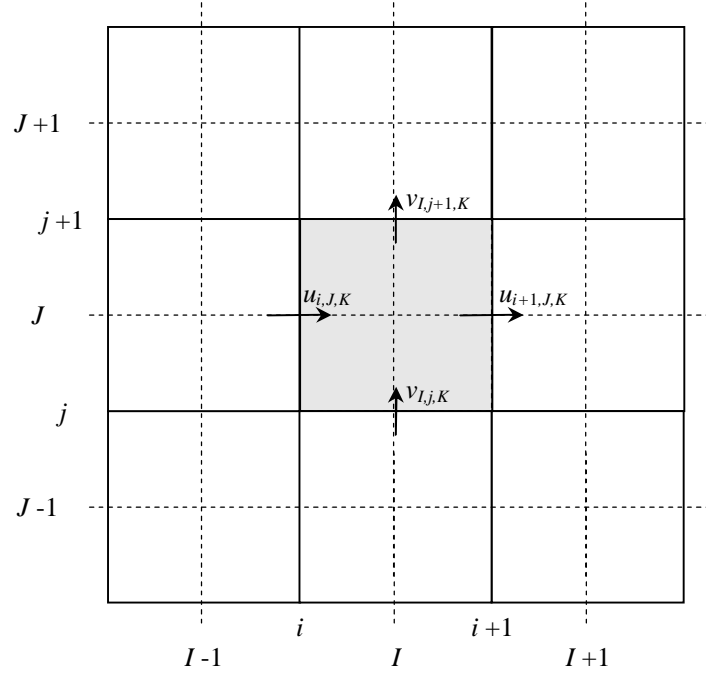


Figure 6.4: A control volume and its surrounding velocities.

$$\iiint_V \int_t^{t+\Delta t} \frac{\partial \rho_m}{\partial t} dt dV + \iiint_V \int_t^{t+\Delta t} \left[\frac{\partial(\rho_m u_m)}{\partial x} + \frac{\partial(\rho_m v_m)}{\partial y} + \frac{\partial(\rho_m w_m)}{\partial z} \right] dt dV = 0 \quad (6.9)$$

Before integration is possible an assumption is needed about how the variables, velocities for instance, vary with time. One possibility is to propose the following, shown for the net outflow of mixture mass:

$$\begin{aligned} & \iiint_V \int_t^{t+\Delta t} \left[\frac{\partial(\rho_m u_m)}{\partial x} + \frac{\partial(\rho_m v_m)}{\partial y} + \frac{\partial(\rho_m w_m)}{\partial z} \right] dt dV \\ &= \beta \left\{ \iiint_V \left[\frac{\partial(\rho_m u_m)}{\partial x} + \frac{\partial(\rho_m v_m)}{\partial y} + \frac{\partial(\rho_m w_m)}{\partial z} \right]^{n+1} dV \right\} \Delta t \\ &+ (1-\beta) \left\{ \iiint_V \left[\frac{\partial(\rho_m u_m)}{\partial x} + \frac{\partial(\rho_m v_m)}{\partial y} + \frac{\partial(\rho_m w_m)}{\partial z} \right]^n dV \right\} \Delta t \end{aligned} \quad (6.10)$$

Superscript n denotes the values at the beginning of the time step, and superscript $n + 1$ denotes the values at the end of the time step. The weighting factor β usually has values between 0 and 1, depending on the selected temporal discretization scheme: $\beta = 0$ for the explicit scheme, $\beta = 0.5$ for the Crank-Nicolson scheme, and $\beta = 1$ for the fully implicit scheme.

Since quite severe restrictions for the length of the time step exist in both the explicit and the Crank-Nicolson scheme, the fully implicit scheme is selected. In the incompressible formulation, the Courant's criterion for the velocity of the flow has to be obeyed when using explicit or Crank-Nicolson schemes, but, in principle, longer time steps could be used when implicit discretization is chosen. Courant's criterion for the speed of sound, however, is not relevant for incompressible flows, since the propagation velocity of the pressure wave is infinite.

After the discretization scheme is established, to simplify the formulation, the superscripts n and $n + 1$ are dropped and the values at the beginning of the time step are referred to with a superscript o , for old, and the values at the end of the time step have no superscripts. Furthermore, if the time rate of change in mixture density, the first term on the left-hand side of equation (6.9), is presumed to be constant during the time step Δt , the temporal integration of equation (6.9) is unambiguous.

$$\begin{aligned} \iiint_V \int_t^{t+\Delta t} \frac{\partial \rho_m}{\partial t} dt dV + \iiint_V \int_t^{t+\Delta t} \left[\frac{\partial(\rho_m u_m)}{\partial x} + \frac{\partial(\rho_m v_m)}{\partial y} + \frac{\partial(\rho_m w_m)}{\partial z} \right] dt dV &= 0 \\ \Leftrightarrow \iiint_V \frac{(\rho_m - \rho_m^o)}{\Delta t} dV \Delta t + \iiint_V \left[\frac{\partial(\rho_m u_m)}{\partial x} + \frac{\partial(\rho_m v_m)}{\partial y} + \frac{\partial(\rho_m w_m)}{\partial z} \right] dV \Delta t &= 0 \end{aligned} \quad (6.11)$$

The time rate of change of mixture density is integrated over the control volume, shown in Figure 6.4 to obtain the change in control volume mass:

$$\iiint_V \frac{(\rho_m - \rho_m^o)}{\Delta t} dV \Delta t = \varepsilon_{I,J,K} V_{I,J,K} \frac{(\rho_m - \rho_m^o)_{I,J,K}}{\Delta t} \Delta t \quad (6.12)$$

where

$V_{I,J,K}$	volume of the pressure node [m ³]
$\varepsilon_{I,J,K}$	porosity of the pressure node [-]
ρ_m	mixture density at the end of the time step [kg/m ³]
ρ_m^o	mixture density at the beginning of the time step [kg/m ³].

The second volume integral containing net outflow of mixture mass on the left-hand side of equation (6.11) is transformed into surface integrals over the surface area of the control volume shown in Figure 6.4. *The divergence theorem* (Adams 1999, p. 946) defines the

relation between the surface integral over a closed surface S and the volume integral over a volume V that is bounded by the surface S .

The relation is given through

$$\oiint_S (C_1 \bar{i} + C_2 \bar{j} + C_3 \bar{k}) \cdot \bar{n} dS = \iiint_V \left(\frac{\partial C_1}{\partial x} + \frac{\partial C_2}{\partial y} + \frac{\partial C_3}{\partial z} \right) dV \quad (6.13)$$

where \mathbf{C} vector $C = (C_1 \bar{i} + C_2 \bar{j} + C_3 \bar{k})$
 $(\bar{i}, \bar{j}, \bar{k})$ unit vectors in the directions of the coordinate axes
 \bar{n} normal vector of surface S .

The divergence theorem is applied on equation (6.11) to transform the volume integrals inside the square brackets into surface integrals over the faces of the control volume:

$$\begin{aligned} & \iiint_V \left[\frac{\partial(\rho_m u_m)}{\partial x} + \frac{\partial(\rho_m v_m)}{\partial y} + \frac{\partial(\rho_m w_m)}{\partial z} \right] dV \Delta t \\ &= \oiint_A [(\rho_m u_m) \bar{i} + (\rho_m v_m) \bar{j} + (\rho_m w_m) \bar{k}] \cdot \bar{n} dA \Delta t \\ &= \left[\varepsilon_{I+1,J,K}^i (\rho_m u_m)_{i+1,J,K} - \varepsilon_{I,J,K}^i (\rho_m u_m)_{i,J,K} \right] A_{I,J,K}^i \Delta t \\ &+ \left[\varepsilon_{I,J+1,K}^j (\rho_m v_m)_{I,j+1,K} - \varepsilon_{I,J,K}^j (\rho_m v_m)_{I,j,K} \right] A_{I,J,K}^j \Delta t \\ &+ \left[\varepsilon_{I,J,K+1}^k (\rho_m w_m)_{I,J,k+1} - \varepsilon_{I,J,K}^k (\rho_m w_m)_{I,J,k} \right] A_{I,J,K}^k \Delta t \end{aligned} \quad (6.14)$$

The densities at the node faces are taken from the node upstream of the interface, according to the upwind differencing scheme (Patankar 1980, pp. 83-85). Porosities at the interfaces are given in equations (6.4), (6.5) and (6.6).

$$\begin{aligned} & \iiint_V \left[\frac{\partial(\rho_m u_m)}{\partial x} + \frac{\partial(\rho_m v_m)}{\partial y} + \frac{\partial(\rho_m w_m)}{\partial z} \right] dV \Delta t \\ &= \left[\varepsilon_{I+1,J,K}^i (\rho_{I,J,K} \langle u_{i+1,J,K} \rangle + \rho_{I+1,J,K} \langle -u_{i+1,J,K} \rangle) \right. \\ &\quad \left. - \varepsilon_{I,J,K}^i (\rho_{I-1,J,K} \langle u_{i,J,K} \rangle + \rho_{I,J,K} \langle -u_{i,J,K} \rangle) \right] A_{I,J,K}^i \Delta t \\ &+ \left[\varepsilon_{I,J+1,K}^j (\rho_{I,J,K} \langle v_{I,j+1,K} \rangle + \rho_{I,J+1,K} \langle -v_{I,j+1,K} \rangle) \right. \\ &\quad \left. - \varepsilon_{I,J,K}^j (\rho_{I,J-1,K} \langle v_{I,j,K} \rangle + \rho_{I,J,K} \langle -v_{I,j,K} \rangle) \right] A_{I,J,K}^j \Delta t \\ &+ \left[\varepsilon_{I,J,K+1}^k (\rho_{I,J,K} \langle w_{I,J,k+1} \rangle + \rho_{I,J,K+1} \langle -w_{I,J,k+1} \rangle) \right. \\ &\quad \left. - \varepsilon_{I,J,K}^k (\rho_{I,J,K-1} \langle w_{I,J,k} \rangle + \rho_{I,J,K} \langle -w_{I,J,k} \rangle) \right] A_{I,J,K}^k \Delta t \end{aligned} \quad (6.15)$$

Notation $\langle u_{i+1,J,K} \rangle$ means maximization between $u_{i+1,J,K}$ and zero; $\max(u_{i+1,J,K}, 0)$.

The discretized equation for mixture mass is obtained by combining the results of equations (6.12) and (6.15) and dividing by the length of the time step Δt .

$$\begin{aligned}
& \varepsilon_{I,J,K} V_{I,J,K} \frac{(\rho_m - \rho_m^o)_{I,J,K}}{\Delta t} \\
&= \left[\varepsilon_{I+1,J,K}^i (\rho_{I,J,K} \langle u_{i+1,J,K} \rangle + \rho_{I+1,J,K} \langle -u_{i+1,J,K} \rangle) \right. \\
&\quad \left. - \varepsilon_{I,J,K}^i (\rho_{I-1,J,K} \langle u_{i,J,K} \rangle + \rho_{I,J,K} \langle -u_{i,J,K} \rangle) \right] A_{I,J,K}^i \\
&+ \left[\varepsilon_{I,J+1,K}^j (\rho_{I,J,K} \langle v_{I,j+1,K} \rangle + \rho_{I,J+1,K} \langle -v_{I,j+1,K} \rangle) \right. \\
&\quad \left. - \varepsilon_{I,J,K}^j (\rho_{I,J-1,K} \langle v_{I,j,K} \rangle + \rho_{I,J,K} \langle -v_{I,j,K} \rangle) \right] A_{I,J,K}^j \\
&+ \left[\varepsilon_{I,J,K+1}^k (\rho_{I,J,K} \langle w_{I,J,k+1} \rangle + \rho_{I,J,K+1} \langle -w_{I,J,k+1} \rangle) \right. \\
&\quad \left. - \varepsilon_{I,J,K}^k (\rho_{I,J,K-1} \langle w_{I,J,k} \rangle + \rho_{I,J,K} \langle -w_{I,J,k} \rangle) \right] A_{I,J,K}^k
\end{aligned} \tag{6.16}$$

6.3.2 Discretization of the volume conservation equations

Instead of trying to conserve the mixture mass, some two-phase CFD codes, phase coupled SIMPLE algorithm (Vasquez & Ivanov 2000) in Fluent for example, attempt to conserve the volume of the mixture, hence avoiding the discrepancies between mixture mass flow rates based on mixture densities and the true mass flow rates of the two phases. Stosic and Stevanovic (2002) present a method similar to the phase coupled SIMPLE in Fluent, though the name of the program the method is implemented in is not mentioned. The derivation of conservation equations for mixture volume begins with the conservation equations for liquid and vapour volume.

$$\frac{\partial \alpha}{\partial t} + \frac{\partial(\alpha u_g)}{\partial x} + \frac{\partial(\alpha v_g)}{\partial y} + \frac{\partial(\alpha w_g)}{\partial z} = + \frac{\gamma}{\rho_g} \tag{6.17}$$

$$\frac{\partial(1-\alpha)}{\partial t} + \frac{\partial[(1-\alpha)u_1]}{\partial x} + \frac{\partial[(1-\alpha)v_1]}{\partial y} + \frac{\partial[(1-\alpha)w_1]}{\partial z} = - \frac{\gamma}{\rho_1} \tag{6.18}$$

The conservation equations for liquid and vapour volume are summed together, to form an equation for the mixture:

$$\frac{\partial}{\partial t} + \frac{\partial[\alpha u_g + (1-\alpha)u_l]}{\partial x} + \frac{\partial[\alpha v_g + (1-\alpha)v_l]}{\partial y} + \frac{\partial[\alpha w_g + (1-\alpha)w_l]}{\partial z} = \gamma \left(\frac{1}{\rho_g} - \frac{1}{\rho_l} \right) \quad (6.19)$$

The expressions inside the square brackets in the second, third, and fourth terms on the left-hand side of equation (6.19) are the definitions of mixture velocities in x, y, and z-directions, respectively. The only term on the right-hand side of the equation accounts for the change in volume due to boiling or condensation. If the square brackets in equation (6.19) are replaced with the appropriate components of mixture velocity, the final form of the conservation equation for mixture volume is complete.

$$\frac{\partial}{\partial t} + \frac{\partial u_m}{\partial x} + \frac{\partial v_m}{\partial y} + \frac{\partial w_m}{\partial z} = \gamma \left(\frac{1}{\rho_g} - \frac{1}{\rho_l} \right) \quad (6.20)$$

To obtain discretized forms of the volume conservation equations, equation (6.20) is integrated over the control volume, shown in Figure 6.4, and time step Δt . Integration of the time dependent term (1) is handled first:

$$\int_t^{t+\Delta t} \iiint_V \frac{\partial}{\partial t} dV dt = \int_t^{t+\Delta t} \varepsilon_{I,J,K} V_{I,J,K} dt = \Delta(\varepsilon_{I,J,K} V_{I,J,K}) \equiv \Delta V_{I,J,K} \quad (6.21)$$

For simplicity the term $\Delta(\varepsilon_{I,J,K} V_{I,J,K})$ in equation (6.21) is marked with $\Delta V_{I,J,K}$, since it represents the change in volume during the time step, change in volume of the fluid to be exact. The second, third, and fourth terms (2) on the left-hand side of equation (6.20) constitute the divergence of velocity: hence the divergence theorem can once again be applied to transform the volume integrals into surface integrals over the control volume faces.

$$\begin{aligned} & \iiint_V \left(\frac{\partial u_m}{\partial x} + \frac{\partial v_m}{\partial y} + \frac{\partial w_m}{\partial z} \right) dV \Delta t \\ &= \oiint_A [(u_m)\bar{i} + (v_m)\bar{j} + (w_m)\bar{k}] \cdot \bar{n} dA \Delta t \\ &= [\varepsilon_{I+1,J,K}^i (u_m)_{i+1,J,K} - \varepsilon_{I,J,K}^i (u_m)_{I,J,K}] A_{I,J,K}^i \Delta t \\ &+ [\varepsilon_{I,J+1,K}^j (v_m)_{I,j+1,K} - \varepsilon_{I,J,K}^j (v_m)_{I,J,K}] A_{I,J,K}^j \Delta t \\ &+ [\varepsilon_{I,J,K+1}^k (w_m)_{I,J,k+1} - \varepsilon_{I,J,K}^k (w_m)_{I,J,k}] A_{I,J,K}^k \Delta t \end{aligned} \quad (6.22)$$

The subscripts m, denoting the values of mixture velocities, are dropped to abbreviate the formulation. Porosities at the interfaces are taken according to equations (6.4), (6.5) and (6.6).

$$\begin{aligned}
& \iiint_V \left[\frac{\partial u_m}{\partial x} + \frac{\partial v_m}{\partial y} + \frac{\partial w_m}{\partial z} \right] dV \Delta t \\
&= \left(\varepsilon_{I+1,J,K}^i u_{i+1,J,K} - \varepsilon_{I,J,K}^i u_{i,J,K} \right) A_{I,J,K}^i \Delta t \\
&+ \left(\varepsilon_{I,J+1,K}^j v_{I,j+1,K} - \varepsilon_{I,J,K}^j v_{I,j,K} \right) A_{I,J,K}^j \Delta t \\
&+ \left(\varepsilon_{I,J,K+1}^k w_{I,J,k+1} - \varepsilon_{I,J,K}^k w_{I,J,k} \right) A_{I,J,K}^k \Delta t
\end{aligned} \tag{6.23}$$

The only term (3) on the right-hand side of equation (6.20), which accounts for the change in volume of the mixture due to evaporation or condensation is integrated over the control volume and time step Δt , as the time dependent term above.

$$\iiint_V \int_t^{t+\Delta t} \gamma \left(\frac{1}{\rho_g} - \frac{1}{\rho_l} \right) dt dV = \varepsilon_{I,J,K} V_{I,J,K} \gamma \left(\frac{1}{\rho_g} - \frac{1}{\rho_l} \right) \Delta t = \Gamma_{I,J,K} \left(\frac{1}{\rho_g} - \frac{1}{\rho_l} \right) \Delta t \tag{6.24}$$

Combining the results of equations (6.21), (6.23), and (6.24) and dividing both sides of the resulting equation by the length of the time step Δt , the final versions of the discretized equations for conservation of mixture volume are obtained:

$$\begin{aligned}
& \frac{\Delta V_{I,J,K}}{\Delta t} + \left(\varepsilon_{I+1,J,K}^i u_{i+1,J,K} - \varepsilon_{I,J,K}^i u_{i,J,K} \right) A_{I,J,K}^i \\
&+ \left(\varepsilon_{I,J+1,K}^j v_{I,j+1,K} - \varepsilon_{I,J,K}^j v_{I,j,K} \right) A_{I,J,K}^j \\
&+ \left(\varepsilon_{I,J,K+1}^k w_{I,J,k+1} - \varepsilon_{I,J,K}^k w_{I,J,k} \right) A_{I,J,K}^k = \Gamma_{I,J,K} \left(\frac{1}{\rho_g} - \frac{1}{\rho_l} \right)
\end{aligned} \tag{6.25}$$

The terms inside the parenthesis on the left-hand side of equation (6.25) constitute the volumetric net outflow. The first term on the left-hand side is particularly useful: if local differences in mixture densities exist, which are not caused by phase change, but say by differences in temperatures, the equation would not conserve mass, hence inherently resulting in erroneous mass balance; the first term provides a way to correct the mass balance.

6.3.3 Discretization of the momentum equations for SIMPLE

The discretization of the momentum equations is presented only for u-momentum, momentum in x-direction, since the discretization procedure is analogous in all the three directions. The discretized momentum equations for y and z-directions are presented in appendix B. For the sake of clarity the derivation of viscous terms has been excluded from this discussion and can be seen in appendix A.

The derivation starts with the conservative form of conservation of momentum, equation (4.6). The conservative form of u-momentum, without the viscous force terms on the right-hand side, is given through

$$\frac{\partial(\rho_m u_m)}{\partial t} + \frac{\partial(\rho_m u_m u_m)}{\partial x} + \frac{\partial(\rho_m u_m v_m)}{\partial y} + \frac{\partial(\rho_m u_m w_m)}{\partial z} = -\frac{\partial p}{\partial x} - 0,5 \times \frac{f}{d_e} \rho_m u_m |u_m|. \quad (6.26)$$

Equation (6.26) is integrated over the control volume and time step Δt . Temporal discretization is presented first.

6.3.3.1 Temporal discretization

Temporal discretization is quite straightforward compared to spatial discretization: the time rate of change of control volume u-momentum, the first term on the left-hand side of equation (6.26), is presumed to be constant within the time step while fully implicit discretization is chosen for other variables. Values at the beginning of the time step are referred to with a superscript o, for old, and the variables without superscripts are considered to represent the values at the end of the time step.

$$\begin{aligned} & \int_t^{t+\Delta t} \frac{\partial(\rho_m u_m)}{\partial t} dt + \int_t^{t+\Delta t} \left[\frac{\partial(\rho_m u_m u_m)}{\partial x} + \frac{\partial(\rho_m u_m v_m)}{\partial y} + \frac{\partial(\rho_m u_m w_m)}{\partial z} \right] dt \\ & = - \int_t^{t+\Delta t} \left[\frac{\partial p}{\partial x} + 0,5 \times \frac{f}{d_e} \rho_m u_m |u_m| \right] dt \end{aligned} \quad (6.27)$$

$$\begin{aligned} & \Leftrightarrow \frac{(\rho_m u_m - \rho_m^o u_m^o)}{\Delta t} \Delta t + \left[\frac{\partial(\rho_m u_m u_m)}{\partial x} + \frac{\partial(\rho_m u_m v_m)}{\partial y} + \frac{\partial(\rho_m u_m w_m)}{\partial z} \right] \Delta t \\ & = - \left[\frac{\partial p}{\partial x} + 0,5 \times \frac{f}{d_e} \rho_m u_m |u_m| \right] \Delta t \end{aligned} \quad (6.28)$$

6.3.3.2 Spatial discretization

The spatial discretization is performed by integrating equation (6.28) over the u-control volume shown in Figure 6.5. Backward staggering has been used to create the indexing of the velocity grid; small indexes (i, j, k), which denote the faces, the locations of the velocities, are set before the capital indexes, (I, J, K), denoting the control volume centers. The mass flow rates at each boundary (F_e, F_w, F_n , etc.) of the u-control volume are handled according to the upwind differencing scheme, which means that the densities are taken from the node upstream of the interface.

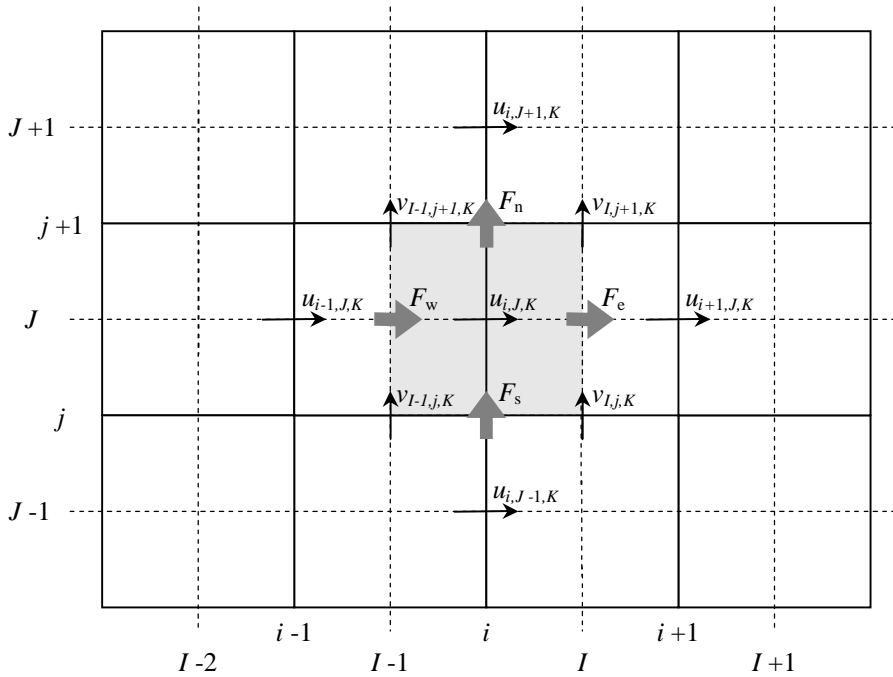


Figure 6.5: A u-control volume and its neighboring velocities.

Integration of the time dependent term, first term on the left-hand side of equation (6.28), and the forces acting on the fluid in x-direction, the terms inside the square brackets on the right-hand side of equation (6.28), is performed first.

$$\begin{aligned}
 & \iiint_V \frac{(\rho_m u_m - \rho_m^o u_m^o)}{\Delta t} dV \Delta t \\
 & = \frac{1}{2} (\epsilon_{I-1,J,K} V_{I-1,J,K} + \epsilon_{I,J,K} V_{I,J,K}) \left[\frac{\rho_{I,J,K}^i u_{i,J,K} - (\rho_{I,J,K}^i)^o u_{i,J,K}^o}{\Delta t} \right] \Delta t
 \end{aligned} \tag{6.29}$$

$$\begin{aligned}
& - \iiint_V \left(\frac{\partial p}{\partial x} + 0,5 \times \frac{f}{d_e} \rho_m u_m |u_m| \right) dV \Delta t \\
& = - \frac{1}{2} \times \frac{f}{d_e} \frac{1}{2} (\varepsilon_{I-1,J,K} V_{I-1,J,K} + \varepsilon_{I,J,K} V_{I,J,K}) \rho_{I,J,K}^i u_{i,J,K} |u_{i,J,K}^*| \Delta t \\
& \quad - (p_{I,J,K} - p_{I-1,J,K}) \varepsilon_{I,J,K}^i A_{I,J,K}^i \Delta t
\end{aligned} \tag{6.30}$$

The volume integrals of the momentum transfer terms, the terms inside the square brackets on the left-hand side of equation (6.28), are transformed into surface integrals over the u-control volume faces by implementing the divergence theorem and integrated over the surface area. Integration over the surface of the control volume yields the net outflow of u-momentum:

$$\begin{aligned}
& \iiint_V \left[\frac{\partial(\rho_m u_m u_m)}{\partial x} + \frac{\partial(\rho_m u_m v_m)}{\partial y} + \frac{\partial(\rho_m u_m w_m)}{\partial z} \right] dV \\
& = \oiint_A (\rho_m u_m u_m \bar{i} + \rho_m u_m v_m \bar{j} + \rho_m u_m w_m \bar{k}) \cdot \bar{n} dA \\
& = \oiint_{A_e} (\rho_m u_m u_m \bar{i}) \cdot \bar{i} dA_e + \oiint_{A_w} (\rho_m u_m u_m \bar{i}) \cdot (-\bar{i}) dA_w \\
& \quad + \oiint_{A_n} (\rho_m u_m v_m \bar{j}) \cdot \bar{j} dA_n + \oiint_{A_s} (\rho_m u_m v_m \bar{j}) \cdot (-\bar{j}) dA_s \\
& \quad + \oiint_{A_u} (\rho_m u_m w_m \bar{k}) \cdot \bar{k} dA_u + \oiint_{A_d} (\rho_m u_m w_m \bar{k}) \cdot (-\bar{k}) dA_d \\
& = F_e u_e - F_w u_w + F_n u_n - F_s u_s + F_u u_u - F_d u_d
\end{aligned} \tag{6.31}$$

The subscripts m, in equation (6.31) denoting values of the mixture of phases, are dropped in the last stage to avoid multiple subscripts. The mass flow rates at the u-control volume faces, presented below, are handled according to the upwind differencing scheme: the densities are taken from the node upstream of the interface.

$$F_e = \frac{1}{2} \rho_{I,J,K} \varepsilon_{I,J,K} A_{I,J,K}^i (u_{i,J,K} + u_{i+1,J,K}), \tag{6.32}$$

$$F_w = \frac{1}{2} \rho_{I-1,J,K} \varepsilon_{I-1,J,K} A_{I,J,K}^i (u_{i-1,J,K} + u_{i,J,K}), \tag{6.33}$$

$$F_s = \frac{1}{2} \varepsilon_{I-1,J,K}^j A_{I-1,J,K}^j \left[\langle v_{I-1,j,K} \rangle \rho_{I-1,J-1,K} - \langle -v_{I-1,j,K} \rangle \rho_{I-1,J,K} \right] + \frac{1}{2} \varepsilon_{I,J,K}^j A_{I,J,K}^j \left[\langle v_{I,j,K} \rangle \rho_{I,J-1,K} - \langle -v_{I,j,K} \rangle \rho_{I,J,K} \right], \quad (6.34)$$

$$F_n = \frac{1}{2} \varepsilon_{I-1,J+1,K}^j A_{I-1,J+1,K}^j \left[\langle v_{I-1,j+1,K} \rangle \rho_{I-1,J,K} - \langle -v_{I-1,j+1,K} \rangle \rho_{I-1,J+1,K} \right] + \frac{1}{2} \varepsilon_{I,J+1,K}^j A_{I,J+1,K}^j \left[\langle v_{I,j+1,K} \rangle \rho_{I,J,K} - \langle -v_{I,j+1,K} \rangle \rho_{I,J+1,K} \right], \quad (6.35)$$

$$F_d = \frac{1}{2} \varepsilon_{I-1,J,K}^k A_{I-1,J,K}^k \left[\langle w_{I-1,J,k} \rangle \rho_{I-1,J,K-1} - \langle -w_{I-1,J,k} \rangle \rho_{I-1,J,K} \right] + \frac{1}{2} \varepsilon_{I,J,K}^k A_{I,J,K}^k \left[\langle w_{I,J,k} \rangle \rho_{I,J,K-1} - \langle -w_{I,J,k} \rangle \rho_{I,J,K} \right] \quad \text{and} \quad (6.36)$$

$$F_u = \frac{1}{2} \varepsilon_{I-1,J,K+1}^k A_{I-1,J,K+1}^k \left[\langle w_{I-1,J,k+1} \rangle \rho_{I-1,J,K} - \langle -w_{I-1,J,k+1} \rangle \rho_{I-1,J,K+1} \right] + \frac{1}{2} \varepsilon_{I,J,K+1}^k A_{I,J,K+1}^k \left[\langle w_{I,J,k+1} \rangle \rho_{I,J,K} - \langle -w_{I,J,k+1} \rangle \rho_{I,J,K+1} \right]. \quad (6.37)$$

Notation $\langle v_{I-1,j,K} \rangle$ means maximization between $v_{I-1,j,K}$ and zero; $\max(v_{I-1,j,K}, 0)$. It can be seen, from equation (6.31) and equations (6.32) through (6.37), that the momentum transfer terms are nonlinear in terms of velocity. To make solution possible, the momentum transfer terms have to be linearized. In most implicitly formulated iterative methods the velocities from which the mass flow rates at the boundaries are calculated, the velocities in equations (6.32) through (6.37), are taken from the previous iteration, and the velocities that are conveyed by the mass flow rates are solved, the velocities that are multiplied by the mass flow rates in the last stage of equation (6.31).

The u-components of the velocities at the u-control volume boundaries in equation (6.31) have to be considered next. One approach is to assume that the velocities at the boundaries are merely averages of the adjacent nodes. However, perhaps a better approach is to take the values of the velocities from upstream of the boundaries letting the mass flow rates, calculated from the velocities of the previous iteration, determine the direction of the flow at the interfaces. The latter approach leads to the following two forms:

$$\begin{aligned}
& \iiint_V \left[\frac{\partial(\rho_m u_m u_m)}{\partial x} + \frac{\partial(\rho_m u_m v_m)}{\partial y} + \frac{\partial(\rho_m u_m w_m)}{\partial z} \right] dV \\
& = F_e u_e - F_w u_w + F_n u_n - F_s u_s + F_u u_u - F_d u_d \\
& = (\langle F_e \rangle u_{i,J,K} - \langle -F_e \rangle u_{i+1,J,K}) - (\langle F_w \rangle u_{i-1,J,K} - \langle -F_w \rangle u_{i,J,K}) + (\langle F_n \rangle u_{i,J,K} - \langle -F_n \rangle u_{i,J+1,K}) \\
& \quad - (\langle F_s \rangle u_{i,J-1,K} - \langle -F_s \rangle u_{i,J,K}) + (\langle F_u \rangle u_{i,J,K} - \langle -F_u \rangle u_{i,J,K+1}) - (\langle F_d \rangle u_{i,J,K-1} - \langle -F_d \rangle u_{i,J,K}) \\
& = (\langle F_e \rangle + \langle -F_w \rangle + \langle F_n \rangle + \langle -F_s \rangle + \langle F_u \rangle + \langle -F_d \rangle) u_{i,J,K} \\
& \quad - \langle -F_e \rangle u_{i+1,J,K} - \langle F_w \rangle u_{i-1,J,K} - \langle -F_n \rangle u_{i,J+1,K} - \langle F_s \rangle u_{i,J-1,K} - \langle -F_u \rangle u_{i,J,K+1} - \langle F_d \rangle u_{i,J,K-1}
\end{aligned} \tag{6.38}$$

OR

$$\begin{aligned}
& \iiint_V \left[\frac{\partial(\rho_m u_m u_m)}{\partial x} + \frac{\partial(\rho_m u_m v_m)}{\partial y} + \frac{\partial(\rho_m u_m w_m)}{\partial z} \right] dV \\
& = (\langle F_w \rangle + \langle F_s \rangle + \langle F_d \rangle + \langle -F_e \rangle + \langle -F_n \rangle + \langle -F_u \rangle + (F_e - F_w) + (F_n - F_s) + (F_u - F_d)) u_{i,J,K} \\
& \quad - \langle -F_e \rangle u_{i+1,J,K} - \langle F_w \rangle u_{i-1,J,K} - \langle -F_n \rangle u_{i,J+1,K} - \langle F_s \rangle u_{i,J-1,K} - \langle -F_u \rangle u_{i,J,K+1} - \langle F_d \rangle u_{i,J,K-1}
\end{aligned} \tag{6.39}$$

These two seemingly different forms are in fact equivalent; the maximizations are merely performed differently. The form in equation (6.39) is equivalent to the 1-dimensional representation in (Versteeg & Malalasekera 2006, pp. 146-147) though the derivation procedure is quite different. When the results of equations (6.29), (6.30), and (6.39) are substituted into the temporally discretized equation (6.28) the momentum equation for x-direction can be expressed through

$$\begin{aligned}
& \frac{1}{2} (\varepsilon_{I-1,J,K} V_{I-1,J,K} + \varepsilon_{I,J,K} V_{I,J,K}) \frac{[\rho_{I,J,K}^i u_{i,J,K} - (\rho_{I,J,K}^i)^o u_{i,J,K}^o]}{\Delta t} \\
& + [\langle F_w \rangle + \langle F_s \rangle + \langle F_d \rangle + \langle -F_e \rangle + \langle -F_n \rangle + \langle -F_u \rangle + (F_e - F_w) + (F_n - F_s) + (F_u - F_d)] u_{i,J,K} . \tag{6.40} \\
& = \langle F_w \rangle u_{i-1,J,K} + \langle F_s \rangle u_{i,J-1,K} + \langle F_d \rangle u_{i,J,K-1} + \langle -F_e \rangle u_{i+1,J,K} + \langle -F_n \rangle u_{i,J+1,K} + \langle -F_u \rangle u_{i,J,K+1} \\
& \quad - \frac{1}{2} \times \frac{f}{d_e} \frac{1}{2} (\varepsilon_{I-1,J,K} V_{I-1,J,K} + \varepsilon_{I,J,K} V_{I,J,K}) \rho_{I,J,K}^i u_{i,J,K} |u_{i,J,K}^*| - (p_{I,J,K} - p_{I-1,J,K}) \varepsilon_{I,J,K}^i A_{I,J,K}^i
\end{aligned}$$

The terms in equation (6.40) can be rearranged so that all the terms containing velocities $u_{i,J,K}$ are moved to the left-hand side and the others to the right-hand side of the equation. Thus,

$$\begin{aligned}
& \left[\langle F_w \rangle + \langle F_s \rangle + \langle F_d \rangle + \langle -F_e \rangle + \langle -F_n \rangle + \langle -F_u \rangle + (F_e - F_w) + (F_n - F_s) + (F_u - F_d) + e_{I,J,K}^i \right] u_{i,J,K} \\
& = \langle F_w \rangle u_{i-1,J,K} + \langle F_s \rangle u_{i,J-1,K} + \langle F_d \rangle u_{i,J,K-1} + \langle -F_e \rangle u_{i+1,J,K} + \langle -F_n \rangle u_{i,J+1,K} + \langle -F_u \rangle u_{i,J,K+1} \\
& - (p_{I,J,K} - p_{I-1,J,K}) \varepsilon_{I,J,K}^i A_{I,J,K}^i + c_{I,J,K}^i
\end{aligned} \quad (6.41)$$

where

$$e_{I,J,K}^i = \frac{1}{2} (\varepsilon_{I-1,J,K} V_{I-1,J,K} + \varepsilon_{I,J,K} V_{I,J,K}) \rho_{I,J,K}^i \left(\frac{1}{\Delta t} + \frac{1}{2} \frac{f}{d_e} |u_{i,J,K}^*| \right) \text{ and} \quad (6.42)$$

$$c_{I,J,K}^i = \frac{1}{2} (\varepsilon_{I-1,J,K} V_{I-1,J,K} + \varepsilon_{I,J,K} V_{I,J,K}) (\rho_{I,J,K}^i)^o \frac{u_{i,J,K}^o}{\Delta t}. \quad (6.43)$$

Finally, if the coefficients of velocities are marked ($a_{i,J,K}$, $a_{i-1,J,K}$, ...), equation (6.41) can be written in a more compact form:

$$\begin{aligned}
a_{i,J,K} u_{i,J,K} & = a_{i-1,J,K} u_{i-1,J,K} + a_{i,J-1,K} u_{i,J-1,K} + a_{i,J,K-1} u_{i,J,K-1} \\
& + a_{i+1,J,K} u_{i+1,J,K} + a_{i,J+1,K} u_{i,J+1,K} + a_{i,J,K+1} u_{i,J,K+1}, \\
& - (p_{I,J,K} - p_{I-1,J,K}) \varepsilon_{I,J,K}^i A_{I,J,K}^i + c_{I,J,K}^i
\end{aligned} \quad (6.44)$$

where the coefficients of velocities are given through

$$\begin{aligned}
a_{i,J,K} & = \left[\langle F_w \rangle + \langle F_s \rangle + \langle F_d \rangle + \langle -F_e \rangle + \langle -F_n \rangle + \langle -F_u \rangle \right. \\
& \left. + (F_e - F_w) + (F_n - F_s) + (F_u - F_d) + e_{I,J,K}^i \right]
\end{aligned} \quad (6.45)$$

$$\begin{aligned}
a_{i-1,J,K} & = \langle F_w \rangle & a_{i,J-1,K} & = \langle F_s \rangle & a_{i,J,K-1} & = \langle F_d \rangle \\
a_{i+1,J,K} & = \langle -F_e \rangle & a_{i,J+1,K} & = \langle -F_n \rangle & a_{i,J,K+1} & = \langle -F_u \rangle
\end{aligned}$$

6.4 Discretization for the direct method in PORFLO

The procedure of the direct method for pressure-velocity solution implemented in PORFLO is presented in this section. There were three subroutines in PORFLO for pressure-velocity solution before this thesis, which all implemented the same direct method; only the solution of the resulting system of equations was done differently. These subroutines were originally intended for particle bed simulations, in which the solution of pressure and velocity fields is in many ways less complicated than in BWR fuel bundle geometry, since the effects of diffusion and momentum convection in the cross flow direction can be ignored in momentum equations governing the flow in particle beds. Nevertheless, these new features have been implemented in the old solution procedure.

The direct method for pressure-velocity solution in PORFLO combines the conservation equations for mixture mass with the three mixture momentum equations to obtain a single system of equations for pressure. The pressure equations have been formulated to be slightly compressible, which under BWR conditions is questionable. Solution of the pressure equations by iterative solvers is facilitated by this formulation, however, the time accuracy is most likely impaired. After the pressure field is obtained, it is used to derive the velocity fields algebraically. Since the derivation of the discretized equations used in the direct method for pressure-velocity solution in PORFLO is lengthy and the scope of this thesis is more on representing the work done during this thesis, the discretized forms are merely given or the derivation is presented only partially.

6.4.1 Discretized forms of the volume conservation equations

To be precise, the form of the conservation equations, which are combined with the momentum equations in PORFLO, is actually conservation of mixture volume. Nevertheless, the formulation has been started from conservation equations for vapour and liquid mass. The final form of the discretized equation for conservation of mixture volume is given through

$$\begin{aligned}
& \varepsilon_{I,J,K} V_{I,J,K} \left[\frac{\alpha}{\rho_g} \frac{\partial \rho_g}{\partial p} + \frac{(1-\alpha)}{\rho_l} \frac{\partial \rho_l}{\partial p} \right]_{I,J,K} \frac{(p_{I,J,K} - p_{I,J,K}^o)}{\Delta t} \\
& + [(J_m)_{i+1,J,K} - (J_m)_{i,J,K}] \\
& + [(J_m)_{I,j+1,K} - (J_m)_{I,j,K}] \\
& + [(J_m)_{I,J,k+1} - (J_m)_{I,J,k}] \\
& = \Gamma_{I,J,K} \left(\frac{1}{\rho_g} - \frac{1}{\rho_l} \right)_{I,J,K}
\end{aligned} \tag{6.46}$$

Superscript o is used to refer to the values at the beginning of the time step and the variables without superscripts are taken from the end of the time step, whenever possible. The first term on the left-hand side of the equation constitutes the change in volume due to changes in control volume pressure, and the terms inside the square brackets constitute the compressibility of the two-phase fluid. The second, third, and fourth terms on the left-hand

side form the volumetric net outflow. The only term on the right-hand side represents the change in mixture volume due to phase change.

6.4.2 Discretized forms of the momentum equations

Unlike the discretization procedure for the iterative methods, the discretization of the momentum equations for the direct method in PORFLO starts with the non-conservative, or primitive, forms of the momentum equations. The non-conservative form of u-momentum, momentum in x-direction, without the viscous terms is shown below.

$$\rho_m \frac{\partial u_m}{\partial t} + \rho_m u_m \frac{\partial u_m}{\partial x} + \rho_m v_m \frac{\partial u_m}{\partial y} + \rho_m w_m \frac{\partial u_m}{\partial z} = -\frac{\partial p}{\partial x} - 0,5 \times \frac{f}{d_e} \rho_m u_m |u_m| \quad (6.47)$$

Equation (6.47) is integrated over the control volume, shown in Figure 6.6, and time step Δt .

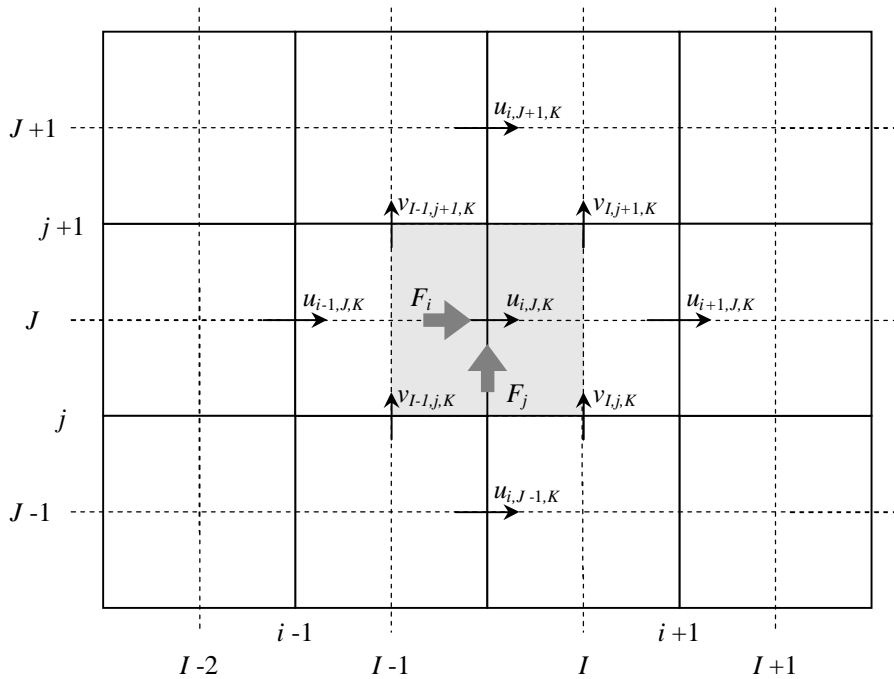


Figure 6.6: U-control volume and its surrounding velocities.

$$\begin{aligned}
& \frac{1}{2} (\varepsilon_{I-1,J,K} V_{I-1,J,K} + \varepsilon_{I,J,K} V_{I,J,K}) \frac{[\rho_{I,J,K}^i u_{i,J,K} - (\rho_{I,J,K}^i)^o u_{i,J,K}^o]}{\Delta t} \\
& + \langle F_i \rangle (u_{i,J,K} - u_{i-1,J,K}) + \langle -F_i \rangle (u_{i+1,J,K} - u_{i,J,K}) \\
& + \langle F_j \rangle (u_{i,J,K} - u_{i,J-1,K}) + \langle -F_j \rangle (u_{i,J+1,K} - u_{i,J,K}) \\
& + \langle F_k \rangle (u_{i,J,K} - u_{i,J,K-1}) + \langle -F_k \rangle (u_{i,J,K+1} - u_{i,J,K}) \\
& = -\frac{1}{2} \times \frac{f}{d_e} \frac{1}{2} (\varepsilon_{I-1,J,K} V_{I-1,J,K} + \varepsilon_{I,J,K} V_{I,J,K}) \rho_{I,J,K}^i u_{i,J,K} |u_{i,J,K}^o| \\
& \quad - (p_{I,J,K} - p_{I-1,J,K}) \varepsilon_{I,J,K}^i A_{I,J,K}^i
\end{aligned} \tag{6.48}$$

Notation $\langle F_i \rangle$ means maximization between F_i and zero; $\max(F_i, 0)$. The fully implicit discretization scheme has been used in integration: superscript o denotes the values at the beginning of the time step and the variables without superscripts are considered to be the values at the end of the time step.

In the non-conservative formulation, the mass flow rates in each direction of the coordinate axes are averaged over the u-control volume and assumed to go through both of the faces perpendicular to the direction of the mass flow rate. Mass flow rates F_j are calculated using velocities $v_{I,j,K}$, $v_{I-1,j,K}$, $v_{I,j+1,K}$, and $v_{I-1,j+1,K}$, F_k are calculated using $w_{I,J,k}$, $w_{I-1,J,k}$, $w_{I,J,k+1}$, and $w_{I-1,J,k+1}$, and F_i are calculated using only $u_{i,J,K}$. The mass flow rates F_i , F_j , and F_k in u-momentum equations, equation (6.48) are given through

$$F_i = \varepsilon_{I,J,K}^i A_{I,J,K}^i (\rho_{I-1,J,K} \langle u_{i,J,K} \rangle - \rho_{I,J,K} \langle -u_{i,J,K} \rangle) \tag{6.49}$$

$$\begin{aligned}
F_j &= \frac{1}{4} \varepsilon_{I-1,J+1,K}^j A_{I-1,J+1,K}^j (\rho_{I-1,J,K} \langle v_{I-1,j+1,K} \rangle - \rho_{I-1,J+1,K} \langle -v_{I-1,j+1,K} \rangle) \\
&+ \frac{1}{4} \varepsilon_{I,J+1,K}^j A_{I,J+1,K}^j (\rho_{I,J,K} \langle v_{I,j+1,K} \rangle - \rho_{I,J+1,K} \langle -v_{I,j+1,K} \rangle) \\
&+ \frac{1}{4} \varepsilon_{I-1,J,K}^j A_{I-1,J,K}^j (\rho_{I-1,J-1,K} \langle v_{I-1,j,K} \rangle - \rho_{I-1,J,K} \langle -v_{I-1,j,K} \rangle) \\
&+ \frac{1}{4} \varepsilon_{I,J,K}^j A_{I,J,K}^j (\rho_{I,J-1,K} \langle v_{I,j,K} \rangle - \rho_{I,J,K} \langle -v_{I,j,K} \rangle)
\end{aligned} \tag{6.50}$$

$$\begin{aligned}
F_k &= \frac{1}{4} \varepsilon_{I-1,J,K+1}^k A_{I-1,J,K+1}^k \left(\rho_{I-1,J,K} \langle w_{I-1,J,k+1} \rangle - \rho_{I-1,J,K+1} \langle -w_{I-1,J,k+1} \rangle \right) \\
&+ \frac{1}{4} \varepsilon_{I,J,K+1}^k A_{I,J,K+1}^k \left(\rho_{I,J,K} \langle w_{I,J,k+1} \rangle - \rho_{I,J,K+1} \langle -w_{I,J,k+1} \rangle \right) \\
&+ \frac{1}{4} \varepsilon_{I-1,J,K}^k A_{I-1,J,K}^k \left(\rho_{I-1,J,K-1} \langle w_{I-1,J,k} \rangle - \rho_{I-1,J,K} \langle -w_{I-1,J,k} \rangle \right) \\
&+ \frac{1}{4} \varepsilon_{I,J,K}^k A_{I,J,K}^k \left(\rho_{I,J,K-1} \langle w_{I,J,k} \rangle - \rho_{I,J,K} \langle -w_{I,J,k} \rangle \right)
\end{aligned} \tag{6.51}$$

The direct method in PORFLO is formulated using mixture flow rates, J_m , instead of velocities. Equation (6.48) is rearranged so that the terms containing the central velocity $u_{i,J,K}$ are moved to the left-hand side and all the other terms to the right-hand side of the equation. Then, the velocities are transformed into flow rates using the flow areas the particular velocity goes through.

$$\begin{aligned}
&\left[\frac{1}{2} (\varepsilon_{I-1,J,K} V_{I-1,J,K} + \varepsilon_{I,J,K} V_{I,J,K}) \rho_{I,J,K}^i \left(\frac{1}{\Delta t} + \frac{1}{2} \frac{f}{d_e} \frac{|(J_m)_{i,J,K}^o|}{\varepsilon_{I,J,K}^i A_{I,J,K}^i} \right) \right. \\
&\quad \left. + F_i + F_j + F_k \right] \frac{1}{\varepsilon_{I,J,K}^i A_{I,J,K}^i} (J_m)_{i,J,K} \\
&= \frac{\langle F_i \rangle}{\varepsilon_{I-1,J,K}^i A_{I,J,K}^i} (J_m)_{i-1,J,K} - \frac{\langle -F_i \rangle}{\varepsilon_{I+1,J,K}^i A_{I,J,K}^i} (J_m)_{i+1,J,K} \\
&\quad + \frac{\langle F_j \rangle}{\varepsilon_{I,J-1,K}^j A_{I,J-1,K}^j} (J_m)_{i,J-1,K} - \frac{\langle -F_j \rangle}{\varepsilon_{I,J+1,K}^j A_{I,J+1,K}^j} (J_m)_{i,J+1,K} \\
&\quad + \frac{\langle F_k \rangle}{\varepsilon_{I,J,K-1}^k A_{I,J,K-1}^k} (J_m)_{i,J,K-1} - \frac{\langle -F_k \rangle}{\varepsilon_{I,J,K+1}^k A_{I,J,K+1}^k} (J_m)_{i,J,K+1} \\
&\quad + \frac{1}{2} \frac{(\varepsilon_{I-1,J,K} V_{I-1,J,K} + \varepsilon_{I,J,K} V_{I,J,K})}{\varepsilon_{I,J,K}^i A_{I,J,K}^i} (\rho_{I,J,K}^i)^o \frac{(J_m)_{i,J,K}^o}{\varepsilon_{I,J,K}^i A_{I,J,K}^i} \\
&\quad - (p_{I,J,K} - p_{I-1,J,K}) \varepsilon_{I,J,K}^i A_{I,J,K}^i
\end{aligned} \tag{6.52}$$

6.4.3 Combining the volume conservation and momentum equations

In the current version of the direct method for pressure-velocity solution in PORFLO the pressure equation, obtained by combining the volume conservation and momentum

equations, is solved only once during each time step. Due to both the nonlinearity of the momentum equations and the fact that information about the direction of the flow is needed when calculating the mass flow rates, some values have to be known, hence the pressure equation can not be solved fully implicitly, even though fully implicit discretization has been used to derive the discretized equations. As the pressure equation is solved only once during each time step, these known values are taken from the beginning of the time step, which makes the overall solution procedure more explicit and therefore stringent to Courant's criteria.

To combine the volume conservation and momentum equations, the central flow rates of each momentum equation are solved and substituted into the volume conservation equations. The central flow rate $(J_m)_{i,J,K}$ of equation (6.52) is solved by dividing both sides of the equation by the coefficient of the central flow rate. All the variables on the left-hand side of equation (6.52) which are included in terms that do not contain pressures, as well as the variables in the coefficient of the central velocity, are given values from the beginning of the time step, hence they can be combined and handled as a constant, $c_{i,J,K}$. Furthermore, if the terms inside the brackets in the coefficients of the central flow rates in u-momentum equations are denoted as $a_{i,J,K}$, the central flow rate $(J_m)_{i,J,K}$ can be solved:

$$(J_m)_{i,J,K} = c_{i,J,K} - \frac{(\epsilon_{I,J,K}^i A_{I,J,K}^i)^2}{a_{i,J,K}} (p_{I,J,K} - p_{I-1,J,K}) \quad (6.53)$$

The momentum equations in other directions are handled similarly:

$$(J_m)_{I,j,K} = c_{I,j,K} - \frac{(\epsilon_{I,J,K}^j A_{I,J,K}^j)^2}{a_{I,j,K}} (p_{I,J,K} - p_{I,J-1,K}) \quad (6.54)$$

$$(J_m)_{I,J,k} = c_{I,J,k} - \frac{(\epsilon_{I,J,K}^k A_{I,J,K}^k)^2}{a_{I,J,k}} (p_{I,J,K} - p_{I,J,K-1}) \quad (6.55)$$

Equations (6.53), (6.54), and (6.55) are written for each flow rate at the boundaries of the pressure node and substituted into the volume conservation equation, (6.46), to yield an equation for the pressure:

$$\begin{aligned}
& \varepsilon_{I,J,K} V_{I,J,K} \left[\frac{\alpha}{\rho_g} \frac{\partial \rho_g}{\partial p} + \frac{(1-\alpha)}{\rho_1} \frac{\partial \rho_1}{\partial p} \right]_{I,J,K} \frac{(p_{I,J,K} - p_{I,J,K}^o)}{\Delta t} \\
& + \left[c_{i+1,J,K} - \frac{(\varepsilon_{I+1,J,K}^i A_{I+1,J,K}^i)^2}{a_{i+1,J,K}} (p_{I+1,J,K} - p_{I,J,K}) - c_{i,J,K} + \frac{(\varepsilon_{I,J,K}^i A_{I,J,K}^i)^2}{a_{i,J,K}} (p_{I,J,K} - p_{I-1,J,K}) \right] \\
& + \left[c_{I,j+1,K} - \frac{(\varepsilon_{I,J+1,K}^j A_{I,J+1,K}^j)^2}{a_{I,j+1,K}} (p_{I+1,J,K} - p_{I,J,K}) - c_{I,j,K} + \frac{(\varepsilon_{I,J,K}^j A_{I,J,K}^j)^2}{a_{I,j,K}} (p_{I,J,K} - p_{I,J-1,K}) \right] \\
& + \left[c_{I,J,k+1} - \frac{(\varepsilon_{I,J,K+1}^k A_{I,J,K+1}^k)^2}{a_{I,J,k+1}} (p_{I,J,K+1} - p_{I,J,K}) - c_{I,J,k} + \frac{(\varepsilon_{I,J,K}^k A_{I,J,K}^k)^2}{a_{I,J,k}} (p_{I,J,K} - p_{I,J,K-1}) \right] \\
& = \Gamma_{I,J,K} \left(\frac{1}{\rho_g} - \frac{1}{\rho_1} \right)_{I,J,K}
\end{aligned} \tag{6.56}$$

The terms are rearranged to obtain the final form of the pressure equation:

$$\begin{aligned}
& \left\{ \frac{(\varepsilon_{I+1,J,K}^i A_{I+1,J,K}^i)^2}{a_{i+1,J,K}} + \frac{(\varepsilon_{I,J,K}^i A_{I,J,K}^i)^2}{a_{i,J,K}} + \frac{(\varepsilon_{I,J+1,K}^j A_{I,J+1,K}^j)^2}{a_{I,j+1,K}} + \frac{(\varepsilon_{I,J,K}^j A_{I,J,K}^j)^2}{a_{I,j,K}} \right. \\
& + \frac{(\varepsilon_{I,J,K+1}^k A_{I,J,K+1}^k)^2}{a_{I,J,k+1}} + \frac{(\varepsilon_{I,J,K}^k A_{I,J,K}^k)^2}{a_{I,J,k}} + \varepsilon_{I,J,K} V_{I,J,K} \left[\frac{\alpha}{\rho_g} \frac{\partial \rho_g}{\partial p} + \frac{(1-\alpha)}{\rho_1} \frac{\partial \rho_1}{\partial p} \right]_{I,J,K} \left. \right\} p_{I,J,K} \\
& - \frac{(\varepsilon_{I+1,J,K}^i A_{I+1,J,K}^i)^2}{a_{i+1,J,K}} p_{I+1,J,K} - \frac{(\varepsilon_{I,J,K}^i A_{I,J,K}^i)^2}{a_{i,J,K}} p_{I-1,J,K} \\
& - \frac{(\varepsilon_{I,J+1,K}^j A_{I,J+1,K}^j)^2}{a_{I,j+1,K}} p_{I+1,J,K} - \frac{(\varepsilon_{I,J,K}^j A_{I,J,K}^j)^2}{a_{I,j,K}} p_{I,J-1,K} \\
& - \frac{(\varepsilon_{I,J,K+1}^k A_{I,J,K+1}^k)^2}{a_{I,J,k+1}} p_{I,J,K+1} - \frac{(\varepsilon_{I,J,K}^k A_{I,J,K}^k)^2}{a_{I,J,k}} p_{I,J,K-1} \\
& = c_{i,J,K} - c_{i+1,J,K} + c_{I,j,K} - c_{I,j+1,K} + c_{I,J,k} - c_{I,J,k+1} + \Gamma_{I,J,K} \left(\frac{1}{\rho_g} - \frac{1}{\rho_1} \right)_{I,J,K} \\
& + \frac{\varepsilon_{I,J,K} V_{I,J,K}}{\Delta t} \left[\frac{\alpha}{\rho_g} \frac{\partial \rho_g}{\partial p} + \frac{(1-\alpha)}{\rho_1} \frac{\partial \rho_1}{\partial p} \right]_{I,J,K} p_{I,J,K}^o
\end{aligned} \tag{6.57}$$

It will become evident in the next chapter that the pressure equation of the direct method in PORFLO bears a strong resemblance to the pressure equation of the SIMPLER algorithm. After the pressure field is solved, the flow rates are calculated from equations (6.53), (6.54), and (6.55).

6.5 Discretization of the energy conservation equations

Recalling the enthalpy equations for vapour and liquid phase presented previously:

$$\frac{\partial(\alpha\rho_g h_g)}{\partial t} + \frac{\partial(\alpha\rho_g h_g u_g)}{\partial x} + \frac{\partial(\alpha\rho_g h_g v_g)}{\partial y} + \frac{\partial(\alpha\rho_g h_g w_g)}{\partial z} = q_{wg}''' + q_{lg}''' \quad (6.58)$$

$$\frac{\partial[(1-\alpha)\rho_l h_l]}{\partial t} + \frac{\partial[(1-\alpha)\rho_l h_l u_l]}{\partial x} + \frac{\partial[(1-\alpha)\rho_l h_l v_l]}{\partial y} + \frac{\partial[(1-\alpha)\rho_l h_l w_l]}{\partial z} = q_{wl}''' - q_{lg}''' \quad (6.59)$$

where q_{wg}''' heat rate from the fuel rod to vapour per unit volume [W/m^3],
 q_{lg}''' heat rate from liquid to vapour per unit volume [W/m^3] and
 q_{wl}''' heat rate from the fuel rod to liquid per unit volume [W/m^3].

As before with the other conservation equations discussed, the conservation equations of vapour and liquid are integrated over the control volume and time step to obtain the discretized forms. Fully implicit time discretization is chosen, and the time rate of change term is presumed to be constant during the time step. The variables without superscripts are considered to be the values at the end of the time step; $t + \Delta t$. Temporal integration is performed first. For vapour:

$$\begin{aligned} & \int_t^{t+\Delta t} \frac{\partial(\alpha\rho_g h_g)}{\partial t} dt + \int_t^{t+\Delta t} \left[\frac{\partial(\alpha\rho_g h_g u_g)}{\partial x} + \frac{\partial(\alpha\rho_g h_g v_g)}{\partial y} + \frac{\partial(\alpha\rho_g h_g w_g)}{\partial z} \right] dt = \int_t^{t+\Delta t} (q_{wg}''' + q_{lg}''') dt \\ \Leftrightarrow & \frac{[(\alpha\rho_g h_g) - (\alpha\rho_g h_g)^o]}{\Delta t} \Delta t + \left[\frac{\partial(\alpha\rho_g h_g u_g)}{\partial x} + \frac{\partial(\alpha\rho_g h_g v_g)}{\partial y} + \frac{\partial(\alpha\rho_g h_g w_g)}{\partial z} \right] \Delta t \\ & = (q_{wg}''' + q_{lg}''') \Delta t \end{aligned} \quad (6.60)$$

And for liquid:

$$\begin{aligned}
& \int_t^{t+\Delta t} \frac{\partial[(1-\alpha)\rho_1 h_1]}{\partial t} dt + \int_t^{t+\Delta t} \left\{ \frac{\partial[(1-\alpha)\rho_1 h_1 u_1]}{\partial x} + \frac{\partial[(1-\alpha)\rho_1 h_1 v_1]}{\partial y} + \frac{\partial[(1-\alpha)\rho_1 h_1 w_1]}{\partial z} \right\} dt \\
&= \int_t^{t+\Delta t} (q_{wl}''' - q_{lg}''') \\
&\Leftrightarrow \frac{\{[(1-\alpha)\rho_1 h_1] - [(1-\alpha)\rho_1 h_1]^\circ\}}{\Delta t} \Delta t \\
&\quad + \left\{ \frac{\partial[(1-\alpha)\rho_1 h_1 u_1]}{\partial x} + \frac{\partial[(1-\alpha)\rho_1 h_1 v_1]}{\partial y} + \frac{\partial[(1-\alpha)\rho_1 h_1 w_1]}{\partial z} \right\} \Delta t \\
&= (q_{wl}''' - q_{lg}''') \Delta t
\end{aligned} \tag{6.61}$$

Spatial integration is performed over the control volume in Figure 6.4. The transient and source terms are integrated first. For vapour:

$$\iiint_V \frac{[(\alpha \rho_g h_g) - (\alpha \rho_g h_g)^\circ]}{\Delta t} dV \Delta t = \varepsilon_{I,J,K} V_{I,J,K} \frac{[(\alpha \rho_g h_g)_{I,J,K} - (\alpha \rho_g h_g)_{I,J,K}^\circ]}{\Delta t} \Delta t \tag{6.62}$$

$$\iiint_V (q_{wg}''' + q_{lg}''') dV \Delta t = \varepsilon_{I,J,K} V_{I,J,K} (q_{wg}''' + q_{lg}''') \Delta t \tag{6.63}$$

And for liquid:

$$\begin{aligned}
& \iiint_V \frac{\{[(1-\alpha)\rho_1 h_1] - [(1-\alpha)\rho_1 h_1]^\circ\}}{\Delta t} dV \Delta t \\
&= \varepsilon_{I,J,K} V_{I,J,K} \frac{\{[(1-\alpha)\rho_1 h_1]_{I,J,K} - [(1-\alpha)\rho_1 h_1]_{I,J,K}^\circ\}}{\Delta t} \Delta t
\end{aligned} \tag{6.64}$$

$$\iiint_V (q_{wl}''' - q_{lg}''') dV \Delta t = \varepsilon_{I,J,K} V_{I,J,K} (q_{wl}''' - q_{lg}''') \Delta t \tag{6.65}$$

If the local values of void fraction and the densities of the phases at the end of the time step are unknown, which is the case when the void fractions and material properties are solved only once during the time step, values at the beginning of the time step have to be used instead. By doing so, the solution procedure as a whole becomes more explicit. If the solution of the enthalpy equations, void fractions and material properties is moved inside the SIMPLE iteration loop, the enthalpy equations could be solved during each SIMPLE

iteration. Then the values at the end of the previous iteration could be used to approximate the values at the end of the time step. Iterative solution over the entire solution procedure, together with the subroutine that implements the SIMPLE family of algorithms, is presented in section 8.3.

The divergence theorem is once again applied to transform the volume integrals of the convective terms, in equations (6.60) and (6.61), into surface integrals over the faces of the control volume. The implementation of the divergence theorem on the convective terms of the temporally integrated conservation equation for vapour enthalpy, equation (6.60) is presented below.

$$\begin{aligned}
& \iiint_V \left[\frac{\partial(\alpha \rho_g h_g u_g)}{\partial x} + \frac{\partial(\alpha \rho_g h_g v_g)}{\partial y} + \frac{\partial(\alpha \rho_g h_g w_g)}{\partial z} \right] dV \Delta t \\
&= \oint_A (\alpha \rho_g h_g u_g \bar{i} + \alpha \rho_g h_g v_g \bar{j} + \alpha \rho_g h_g w_g \bar{k}) \cdot \bar{n} dA \\
&= \oint_{A_e} (\alpha \rho_g h_g u_g \bar{i})_{i+1,J,K} \cdot \bar{i} dA_e + \oint_{A_w} (\alpha \rho_g h_g u_g \bar{i})_{i,J,K} \cdot (-\bar{i}) dA_w \\
&+ \oint_{A_n} (\alpha \rho_g h_g v_g \bar{j})_{I,j+1,K} \cdot \bar{j} dA_n + \oint_{A_s} (\alpha \rho_g h_g v_g \bar{j})_{I,j,K} \cdot (-\bar{j}) dA_s \\
&+ \oint_{A_u} (\alpha \rho_g h_g w_g \bar{k})_{I,J,k+1} \cdot \bar{k} dA_u + \oint_{A_d} (\alpha \rho_g h_g w_g \bar{k})_{I,J,k} \cdot (-\bar{k}) dA_d \\
&= \varepsilon_{i+1,J,K}^i A_{i+1,J,K}^i (\alpha \rho_g h_g u_g)_{i+1,J,K} - \varepsilon_{I,J,K}^i A_{I,J,K}^i (\alpha \rho_g h_g u_g)_{i,J,K} \\
&+ \varepsilon_{I,J+1,K}^j A_{I,J+1,K}^j (\alpha \rho_g h_g v_g)_{I,j+1,K} - \varepsilon_{I,J,K}^j A_{I,J,K}^j (\alpha \rho_g h_g v_g)_{I,j,K} \\
&+ \varepsilon_{I,J,K+1}^k A_{I,J,K+1}^k (\alpha \rho_g h_g w_g)_{I,J,k+1} - \varepsilon_{I,J,K}^k A_{I,J,K}^k (\alpha \rho_g h_g w_g)_{I,J,k} \tag{6.66}
\end{aligned}$$

The separate terms consist of the mass flow rate of vapour times the enthalpy at each boundary of the pressure node. The values of the enthalpies at the boundaries are defined by the direction of the mass flow rate, according to the upwind differencing scheme. When all the results of the spatial integration for the vapour phase, equations (6.62), (6.63) and (6.66), are combined, after some algebra the final form of the discretized equation for conservation vapour enthalpy is given through:

$$\begin{aligned}
& \left[\langle G_e \rangle + \langle -G_w \rangle + \langle G_n \rangle + \langle -G_s \rangle + \langle G_u \rangle + \langle -G_d \rangle + \frac{(M_g)_{I,J,K}}{\Delta t} \right] (h_g)_{I,J,K} \\
& - \langle -G_e \rangle (h_g)_{I+1,J,K} - \langle G_w \rangle (h_g)_{I-1,J,K} \\
& - \langle -G_n \rangle (h_g)_{I,J+1,K} - \langle G_s \rangle (h_g)_{I,J-1,K} \\
& - \langle -G_u \rangle (h_g)_{I,J,K+1} - \langle G_d \rangle (h_g)_{I,J,K-1} \\
& = \varepsilon_{I,J,K} V_{I,J,K} (q_{wg}'' + q_{lg}'') + \frac{(M_g)_{I,J,K}^o}{\Delta t}
\end{aligned} \tag{6.67}$$

where

$$G_e = \varepsilon_{I+1,J,K}^i A_{I+1,J,K}^i \left[(\alpha \rho_g)_{I,J,K} \langle (u_g)_{i+1,J,K} \rangle - (\alpha \rho_g)_{I+1,J,K} \langle -(u_g)_{i+1,J,K} \rangle \right] \tag{6.68}$$

$$G_w = \varepsilon_{I-1,J,K}^i A_{I-1,J,K}^i \left[(\alpha \rho_g)_{I-1,J,K} \langle (u_g)_{I,J,K} \rangle - (\alpha \rho_g)_{I,J,K} \langle -(u_g)_{I,J,K} \rangle \right] \tag{6.69}$$

$$G_n = \varepsilon_{I,J+1,K}^j A_{I,J+1,K}^j \left[(\alpha \rho_g)_{I,J,K} \langle (v_g)_{I,j+1,K} \rangle - (\alpha \rho_g)_{I,J+1,K} \langle -(v_g)_{I,j+1,K} \rangle \right] \tag{6.70}$$

$$G_s = \varepsilon_{I,J,K}^j A_{I,J,K}^j \left[(\alpha \rho_g)_{I,J-1,K} \langle (v_g)_{I,j,K} \rangle - (\alpha \rho_g)_{I,J,K} \langle -(v_g)_{I,j,K} \rangle \right] \tag{6.71}$$

$$G_u = \varepsilon_{I,J,K+1}^k A_{I,J,K+1}^k \left[(\alpha \rho_g)_{I,J,K} \langle (w_g)_{I,J,k+1} \rangle - (\alpha \rho_g)_{I,J,K+1} \langle -(w_g)_{I,J,k+1} \rangle \right] \tag{6.72}$$

$$G_d = \varepsilon_{I,J,K}^k A_{I,J,K}^k \left[(\alpha \rho_g)_{I,J,K-1} \langle (w_g)_{I,J,k} \rangle - (\alpha \rho_g)_{I,J,K} \langle -(w_g)_{I,J,k} \rangle \right] \tag{6.73}$$

$$(M_g)_{I,J,K} = \varepsilon_{I,J,K} V_{I,J,K} (\alpha \rho_g)_{I,J,K} \tag{6.74}$$

The vapour mass flow rates at the boundaries, (G_e , G_w , G_n , ...), are referred to with a subscript according to the direction of the boundary in relation to the center point of the node. Notation $\langle G_e \rangle$ means maximization between the vapour mass flow rate at the boundary east of the center point, G_e , and zero.

When the same procedure is done with the equations of the liquid phase, the discretized form of the conservation equation for liquid enthalpy is obtained.

$$\begin{aligned}
& \left[\langle W_e \rangle + \langle -W_w \rangle + \langle W_n \rangle + \langle -W_s \rangle + \langle W_u \rangle + \langle -W_d \rangle + \frac{(M_1)_{I,J,K}}{\Delta t} \right] (h_1)_{I,J,K} \\
& - \langle -W_e \rangle (h_1)_{I+1,J,K} - \langle W_w \rangle (h_1)_{I-1,J,K} \\
& - \langle -W_n \rangle (h_1)_{I,J+1,K} - \langle W_s \rangle (h_1)_{I,J-1,K} \\
& - \langle -W_u \rangle (h_1)_{I,J,K+1} - \langle W_d \rangle (h_1)_{I,J,K-1} \\
& = \varepsilon_{I,J,K} V_{I,J,K} (q_{wl}^m - q_{lg}^m) + \frac{(M_1)_{I,J,K}^o}{\Delta t}
\end{aligned} \tag{6.75}$$

where

$$W_e = \varepsilon_{I+1,J,K}^i A_{I+1,J,K}^i \left\{ [(1-\alpha)\rho_1]_{I,J,K} \langle (u_1)_{i+1,J,K} \rangle - [(1-\alpha)\rho_1]_{I+1,J,K} \langle -(u_1)_{i+1,J,K} \rangle \right\} \tag{6.76}$$

$$W_w = \varepsilon_{I,J,K}^i A_{I,J,K}^i \left\{ [(1-\alpha)\rho_1]_{I-1,J,K} \langle (u_1)_{i,J,K} \rangle - [(1-\alpha)\rho_1]_{I,J,K} \langle -(u_1)_{i,J,K} \rangle \right\} \tag{6.77}$$

$$W_n = \varepsilon_{I,J+1,K}^j A_{I,J+1,K}^j \left\{ [(1-\alpha)\rho_1]_{I,J,K} \langle (v_1)_{I,j+1,K} \rangle - [(1-\alpha)\rho_1]_{I,J+1,K} \langle -(v_1)_{I,j+1,K} \rangle \right\} \tag{6.78}$$

$$W_s = \varepsilon_{I,J,K}^j A_{I,J,K}^j \left\{ [(1-\alpha)\rho_1]_{I,J-1,K} \langle (v_1)_{I,j,K} \rangle - [(1-\alpha)\rho_1]_{I,J,K} \langle -(v_1)_{I,j,K} \rangle \right\} \tag{6.79}$$

$$W_u = \varepsilon_{I,J,K+1}^k A_{I,J,K+1}^k \left\{ [(1-\alpha)\rho_1]_{I,J,K} \langle (w_1)_{I,J,k+1} \rangle - [(1-\alpha)\rho_1]_{I,J,K+1} \langle -(w_1)_{I,J,k+1} \rangle \right\} \tag{6.80}$$

$$W_d = \varepsilon_{I,J,K}^k A_{I,J,K}^k \left\{ [(1-\alpha)\rho_1]_{I,J,K-1} \langle (w_1)_{I,J,k} \rangle - [(1-\alpha)\rho_1]_{I,J,K} \langle -(w_1)_{I,J,k} \rangle \right\} \tag{6.81}$$

$$(M_1)_{I,J,K} = \varepsilon_{I,J,K} V_{I,J,K} [(1-\alpha)\rho_1]_{I,J,K} \tag{6.82}$$

7 THE SIMPLE FAMILY OF ALGORITHMS

As mentioned above in Chapter 5, SIMPLE, Semi-Implicit Method for Pressure-Linked Equations, algorithm is an iterative method for pressure-velocity solution, in which the pressure and velocity fields are coupled through pressure corrections. The pressure corrections are used to obtain improved values for pressures and velocities at the end of each iteration. Iteration is continued until the pressure and velocity fields satisfy each other.

There are two distinctively different version of the SIMPLE algorithm: steady-state and transient. The steady-state SIMPLE algorithm is easily derived from its transient counterpart, by omitting the time dependent terms. Although steady-state results are presented in Chapter 10, the form of the SIMPLE algorithm implemented in PORFLO is in fact transient, since the original solution procedure in PORFLO was also transient.

The SIMPLE algorithm, upon which the other algorithms of this group are based, was first introduced by S. V. Patankar. Presentation of the SIMPLE algorithm can be found in (Patanekar 1980, pp. 113-131). Since then, several minor adjustments have been proposed, to further improve the algorithm, many of which are referred to with an additional suffix, SIMPLEC for instance. The base of the SIMPLE algorithm, however, has remained relatively unchanged through the years. Another fact that indicates the usefulness of the SIMPLE algorithm is its relatively recent implementations in multi-phase CFD codes: at least Fluent versions 6.0 and above include Phase Coupled SIMPLE algorithm, presented in (Vasquez & Ivanov 2000), as an optional solution method.

The SIMPLE algorithm is presented in the next section, and after that the modifications made in SIMPLER and SIMPLEC explained. As a part of this thesis a subroutine was created, which implements the three SIMPLE variants presented in the following sections.

7.1 The SIMPLE algorithm

The SIMPLE algorithm uses the discretized equations for mixture mass and momentum to formulate a correction for the pressure field. The pressure corrections are needed, since the velocity field that results from the solution of the momentum equations does not necessarily satisfy continuity. The pressure correction is a way to correct the imbalances in the conservation of mass, or volume, depending on the conservation equations the pressure corrections are based on.

For the sake of clarity and brevity, the viscous terms have been excluded from the equations, since it's quite straightforward to include them in the velocity coefficients of the momentum equations. The discretized conservation equations for mixture momentum can be presented for x, y and z-direction respectively as follows:

$$a_{i,J,K}u_{i,J,K} = a_{i-1,J,K}u_{i-1,J,K} + a_{i,J-1,K}u_{i,J-1,K} + a_{i,J,K-1}u_{i,J,K-1} + a_{i+1,J,K}u_{i+1,J,K} + a_{i,J+1,K}u_{i,J+1,K} + a_{i,J,K+1}u_{i,J,K+1} - (p_{I,J,K} - p_{I-1,J,K})\epsilon_{I,J,K}^i A_{I,J,K}^i + c_{I,J,K}^i \quad (7.1)$$

$$a_{I,j,k}v_{I,j,k} = a_{I-1,j,k}v_{I-1,j,k} + a_{I,j-1,k}v_{I,j-1,k} + a_{I,j,k-1}v_{I,j,k-1} + a_{I+1,j,k}v_{I+1,j,k} + a_{I,j+1,k}v_{I,j+1,k} + a_{I,j,k+1}v_{I,j,k+1} - (p_{I,J,K} - p_{I,J-1,K})\epsilon_{I,J,K}^j A_{I,J,K}^j + c_{I,J,K}^j \quad (7.2)$$

$$a_{I,J,k}w_{I,J,k} = a_{I-1,J,k}w_{I-1,J,k} + a_{I,J-1,k}w_{I,J-1,k} + a_{I,J,k-1}w_{I,J,k-1} + a_{I+1,J,k}w_{I+1,J,k} + a_{I,J+1,k}w_{I,J+1,k} + a_{I,J,k+1}w_{I,J,k+1} - (p_{I,J,K} - p_{I,J,K-1})\epsilon_{I,J,K}^k A_{I,J,K}^k + c_{I,J,K}^k \quad (7.3)$$

SIMPLE algorithm starts with a guessed pressure field p^* and guessed velocity fields u^* , v^* and w^* , which are used to calculate the velocity coefficients ($a_{i,J,K}$, $a_{i-1,J,K}$, etc.), and the momentum source terms in equations (7.1) through (7.3). The discretized momentum equations, (7.1) through (7.3), are solved to obtain improved velocities u^{**} , v^{**} and w^{**} , shown for x-direction below.

$$a_{i,J,K}u_{i,J,K}^{**} = a_{i-1,J,K}u_{i-1,J,K}^{**} + a_{i,J-1,K}u_{i,J-1,K}^{**} + a_{i,J,K-1}u_{i,J,K-1}^{**} + a_{i+1,J,K}u_{i+1,J,K}^{**} + a_{i,J+1,K}u_{i,J+1,K}^{**} + a_{i,J,K+1}u_{i,J,K+1}^{**} - (p_{I,J,K}^* - p_{I-1,J,K}^*)\epsilon_{I,J,K}^i A_{I,J,K}^i + c_{I,J,K}^i \quad (7.4)$$

Corrected values and corrections are related as shown below:

$$p = p^* + p' \quad (7.5)$$

$$u = u^{**} + u' \quad (7.6)$$

$$v = v^{**} + v' \text{ and} \quad (7.7)$$

$$w = w^{**} + w'. \quad (7.8)$$

Here, superscript ' denotes the correction and the variables without superscripts are the corrected values of the variables in question. The corrected pressure and velocity fields have to satisfy the momentum equations as well as the guessed fields. To formulate equations for the corrections the momentum equations for the improved velocities are subtracted from the momentum equations for the corrected fields.

For x-direction, subtracting (7.4) from (7.1) gives

$$\begin{aligned} a_{i,J,K}(u_{i,J,K} - u_{i,J,K}^{**}) &= a_{i-1,J,K}(u_{i-1,J,K} - u_{i-1,J,K}^{**}) + a_{i,J-1,K}(u_{i,J-1,K} - u_{i,J-1,K}^{**}) \\ &+ a_{i,J,K-1}(u_{i,J,K-1} - u_{i,J,K-1}^{**}) + a_{i+1,J,K}(u_{i+1,J,K} - u_{i+1,J,K}^{**}) + a_{i,J+1,K}(u_{i,J+1,K} - u_{i,J+1,K}^{**}) \\ &+ a_{i,J,K+1}(u_{i,J,K+1} - u_{i,J,K+1}^{**}) - [(p_{I,J,K} - p_{I,J,K}^*) - (p_{I-1,J,K} - p_{I-1,J,K}^*)] \mathcal{E}_{I,J,K}^i A_{I,J,K}^i \end{aligned} \quad (7.9)$$

It is seen that the terms in the parentheses are the corrections p' , in equation (7.5), and u' , in equation (7.6), defined above. Substituting the corrections into equation (7.9) leads to the following form:

$$\begin{aligned} a_{i,J,K}u'_{i,J,K} &= a_{i-1,J,K}u'_{i-1,J,K} + a_{i,J-1,K}u'_{i,J-1,K} + a_{i,J,K-1}u'_{i,J,K-1} \\ &+ a_{i+1,J,K}u'_{i+1,J,K} + a_{i,J+1,K}u'_{i,J+1,K} + a_{i,J,K+1}u'_{i,J,K+1} - (p'_{I,J,K} - p'_{I-1,J,K}) \mathcal{E}_{I,J,K}^i A_{I,J,K}^i \end{aligned} \quad (7.10)$$

At this point, an approximation is introduced to simplify the velocity correction: the effects of the neighboring velocity terms on the velocity correction are neglected. After the neighbouring velocity terms are omitted, the velocity correction can be solved from equation (7.10).

$$u'_{i,J,K} = -\frac{\mathcal{E}_{I,J,K}^i A_{I,J,K}^i}{a_{i,J,K}} (p'_{I,J,K} - p'_{I-1,J,K}) \quad (7.11)$$

Applying the velocity correction, (7.11), back to equation (7.6), the corrected velocities for x-direction can be obtained.

$$u_{i,J,K} = u_{i,J,K}^{**} - \frac{\mathcal{E}_{I,J,K}^i A_{I,J,K}^i}{a_{i,J,K}} (p'_{I,J,K} - p'_{I-1,J,K}) \quad (7.12)$$

Corrected velocity components for other directions can be derived using the same procedure.

$$v_{I,j,K} = v_{I,j,K}^{**} - \frac{\varepsilon_{I,J,K}^j A_{I,J,K}^j}{a_{I,j,K}} (p'_{I,J,K} - p'_{I,J-1,K}) \quad (7.13)$$

$$w_{I,J,k} = w_{I,J,k}^{**} - \frac{\varepsilon_{I,J,K}^k A_{I,J,K}^k}{a_{I,J,k}} (p'_{I,J,K} - p'_{I,J,K-1}) \quad (7.14)$$

The equations for corrected velocities contain pressure corrections. In most of the SIMPLE algorithms intended for single-phase flow, such as the original version proposed by Patankar (1980, pp. 113-131), the mass conservation equation is used together with the continuity equation to provide these pressure corrections. The same procedure is followed here, with the exception that conservation equations for **mixture** mass and momentum are used, since two-phase flow is in question. An alternative approach using mixture volume, instead of mixture mass, as the basis for the pressure correction equations is presented in section 8.1. The discretized forms of conservation equations for mixture mass were given in equation (6.16) and are repeated here in equation (7.15) for convenience.

$$\begin{aligned} & \varepsilon_{I,J,K} V_{I,J,K} \frac{(\rho_{I,J,K} - \rho_{I,J,K}^o)}{\Delta t} \\ & + \left[\varepsilon_{I+1,J,K}^i (\rho_{I,J,K} \langle u_{i+1,J,K} \rangle + \rho_{I+1,J,K} \langle -u_{i+1,J,K} \rangle) \right. \\ & \quad \left. - \varepsilon_{I,J,K}^i (\rho_{I-1,J,K} \langle u_{i,J,K} \rangle + \rho_{I,J,K} \langle -u_{i,J,K} \rangle) \right] A_{I,J,K}^i \\ & + \left[\varepsilon_{I,J+1,K}^j (\rho_{I,J,K} \langle v_{I,j+1,K} \rangle + \rho_{I,J+1,K} \langle -v_{I,j+1,K} \rangle) \right. \\ & \quad \left. - \varepsilon_{I,J,K}^j (\rho_{I,J-1,K} \langle v_{I,j,K} \rangle + \rho_{I,J,K} \langle -v_{I,j,K} \rangle) \right] A_{I,J,K}^j \\ & + \left[\varepsilon_{I,J,K+1}^k (\rho_{I,J,K} \langle w_{I,J,k+1} \rangle + \rho_{I,J,K+1} \langle -w_{I,J,k+1} \rangle) \right. \\ & \quad \left. - \varepsilon_{I,J,K}^k (\rho_{I,J,K-1} \langle w_{I,J,k} \rangle + \rho_{I,J,K} \langle -w_{I,J,k} \rangle) \right] A_{I,J,K}^k = 0 \end{aligned} \quad (7.15)$$

To clarify the formulation, the cumbersome maximization terms are combined and the densities at the boundaries are denoted with ρ_m , referring to the mixture densities at the boundaries.

$$\begin{aligned}
& \varepsilon_{I,J,K} V_{I,J,K} \frac{(\rho_{I,J,K} - \rho_{I,J,K}^{\circ})}{\Delta t} \\
& + \left[\varepsilon_{I+1,J,K}^i (\rho_m u_{i+1,J,K}) - \varepsilon_{I,J,K}^i (\rho_m u_{i,J,K}) \right] A_{I,J,K}^i \\
& + \left[\varepsilon_{I,J+1,K}^j (\rho_m v_{I,j+1,K}) - \varepsilon_{I,J,K}^j (\rho_m v_{I,j,K}) \right] A_{I,J,K}^j \\
& + \left[\varepsilon_{I,J,K+1}^k (\rho_m w_{I,J,k+1}) - \varepsilon_{I,J,K}^k (\rho_m w_{I,J,k}) \right] A_{I,J,K}^k = 0
\end{aligned} \tag{7.16}$$

Substituting the corrected velocities, (7.12), (7.13) and (7.14), into the discretized continuity equation (7.16) yields:

$$\begin{aligned}
& \varepsilon_{I,J,K} V_{I,J,K} \frac{(\rho_{I,J,K} - \rho_{I,J,K}^{\circ})}{\Delta t} \\
& + \varepsilon_{I+1,J,K}^i A_{I,J,K}^i \left[\rho_m \left(u_{i+1,J,K}^* - \frac{\varepsilon_{I+1,J,K}^i A_{I+1,J,K}^i}{a_{i+1,J,K}} (p'_{I+1,J,K} - p'_{I,J,K}) \right) \right]_{i+1,J,K} \\
& - \varepsilon_{I,J,K}^i A_{I,J,K}^i \left[\rho_m \left(u_{i,J,K}^* - \frac{\varepsilon_{I,J,K}^i A_{I,J,K}^i}{a_{i,J,K}} (p'_{I,J,K} - p'_{I-1,J,K}) \right) \right]_{i,J,K} \\
& + \varepsilon_{I,J+1,K}^j A_{I,J,K}^j \left[\rho_m \left(v_{I,j+1,K}^* - \frac{\varepsilon_{I,J+1,K}^j A_{I,J+1,K}^j}{a_{I,j+1,K}} (p'_{I,J+1,K} - p'_{I,J,K}) \right) \right]_{I,j+1,K} \\
& - \varepsilon_{I,J,K}^j A_{I,J,K}^j \left[\rho_m \left(v_{I,j,K}^* - \frac{\varepsilon_{I,J,K}^j A_{I,J,K}^j}{a_{I,j,K}} (p'_{I,J,K} - p'_{I,J-1,K}) \right) \right]_{I,j,K} \\
& + \varepsilon_{I,J,K+1}^k A_{I,J,K}^k \left[\rho_m \left(w_{I,J,k+1}^* - \frac{\varepsilon_{I,J,K+1}^k A_{I,J,K+1}^k}{a_{I,J,k+1}} (p'_{I,J,K+1} - p'_{I,J,K}) \right) \right]_{I,J,k+1} \\
& - \varepsilon_{I,J,K}^k A_{I,J,K}^k \left[\rho_m \left(w_{I,J,k}^* - \frac{\varepsilon_{I,J,K}^k A_{I,J,K}^k}{a_{I,J,k}} (p'_{I,J,K} - p'_{I,J,K-1}) \right) \right]_{I,J,k} = 0
\end{aligned} \tag{7.17}$$

Here, coefficients $(a_{i,J,K}, a_{i+1,J,K}, \dots)$ are the central coefficients of the corresponding momentum equations; $a_{i,J,K}$ and $a_{i-1,J,K}$ are taken from u-momentum equations, $a_{I,j,K}$ and $a_{I,j+1,K}$ from v-momentum equations, and $a_{I,J,k}$ and $a_{I,J,k+1}$ are taken from w-momentum equations. The mixture densities at each boundary of the pressure node are handled according to the upwind differencing scheme: the latest values of the velocities at each boundary are used to provide the direction where the densities are taken from. With some manipulation the pressure correction equation, (7.17), can be rearranged so that the pressure terms are shown separately:

$$\begin{aligned}
& \left[\left(\varepsilon_{I+1,J,K}^i A_{I,J,K}^i \right)^2 \left(\frac{\rho_m}{a} \right)_{i+1,J,K} + \left(\varepsilon_{I,J,K}^i A_{I,J,K}^i \right)^2 \left(\frac{\rho_m}{a} \right)_{i,J,K} \right. \\
& + \left(\varepsilon_{I,J+1,K}^j A_{I,J,K}^j \right)^2 \left(\frac{\rho_m}{a} \right)_{I,j+1,K} + \left(\varepsilon_{I,J,K}^j A_{I,J,K}^j \right)^2 \left(\frac{\rho_m}{a} \right)_{I,j,K} \\
& \left. + \left(\varepsilon_{I,J,K+1}^k A_{I,J,K}^k \right)^2 \left(\frac{\rho_m}{a} \right)_{I,J,k+1} + \left(\varepsilon_{I,J,K}^k A_{I,J,K}^k \right)^2 \left(\frac{\rho_m}{a} \right)_{I,J,k} \right] p'_{I,J,K} \\
& = \left(\varepsilon_{I+1,J,K}^i A_{I,J,K}^i \right)^2 \left(\frac{\rho_m}{a} \right)_{i+1,J,K} p'_{I+1,J,K} + \left(\varepsilon_{I,J,K}^i A_{I,J,K}^i \right)^2 \left(\frac{\rho_m}{a} \right)_{i,J,K} p'_{I-1,J,K} \\
& + \left(\varepsilon_{I,J+1,K}^j A_{I,J,K}^j \right)^2 \left(\frac{\rho_m}{a} \right)_{I,j+1,K} p'_{I,J+1,K} + \left(\varepsilon_{I,J,K}^j A_{I,J,K}^j \right)^2 \left(\frac{\rho_m}{a} \right)_{I,j,K} p'_{I,J-1,K} \\
& + \left(\varepsilon_{I,J,K+1}^k A_{I,J,K}^k \right)^2 \left(\frac{\rho_m}{a} \right)_{I,J,k+1} p'_{I,J,K+1} + \left(\varepsilon_{I,J,K}^k A_{I,J,K}^k \right)^2 \left(\frac{\rho_m}{a} \right)_{I,J,k} p'_{I,J,K-1} \\
& \left[+ \left(\rho_m u^{**} \varepsilon^i A^i \right)_{i,J,K} - \left(\rho_m u^{**} \varepsilon^i A^i \right)_{i+1,J,K} + \left(\rho_m v^{**} \varepsilon^j A^j \right)_{I,j,K} - \left(\rho_m v^{**} \varepsilon^j A^j \right)_{I,j+1,K} \right. \\
& \left. + \left(\rho_m w^{**} \varepsilon^k A^k \right)_{I,J,k} - \left(\rho_m w^{**} \varepsilon^k A^k \right)_{I,J,k+1} - \varepsilon_{I,J,K} V_{I,J,K} \frac{(\rho_{I,J,K} - \rho_{I,J,K}^o)}{\Delta t} \right] \tag{7.18}
\end{aligned}$$

Using coefficients ($b_{I,J,K}$, $b_{I-1,J,K}, \dots$) for the pressure corrections and denoting the terms inside the brackets on the right-hand side with $d'_{I,J,K}$ leads to the final form of the pressure correction equation:

$$\begin{aligned}
b_{I,J,K} p'_{I,J,K} &= b_{I+1,J,K} p'_{I+1,J,K} + b_{I-1,J,K} p'_{I-1,J,K} + b_{I,J+1,K} p'_{I,J+1,K} \\
&+ b_{I,J-1,K} p'_{I,J-1,K} + b_{I,J,K+1} p'_{I,J,K+1} + b_{I,J,K-1} p'_{I,J,K-1} + d'_{I,J,K} \tag{7.19}
\end{aligned}$$

$$b_{I,J,K} p'_{I,J,K} = \sum b_{nb} p'_{nb} + d'_{I,J,K} \tag{7.20}$$

The pressure corrections, which are obtained by solving the system of equations (7.19), are used to correct the pressure and velocity fields using equations (7.5), (7.12), (7.13) and (7.14). The corrected pressures and velocities are in turn used as the guessed values in the beginning of the next iteration. Iteration is continued until convergence is established. The main phases and the sequence of operations of the transient SIMPLE algorithm are shown in Figure 7.1.

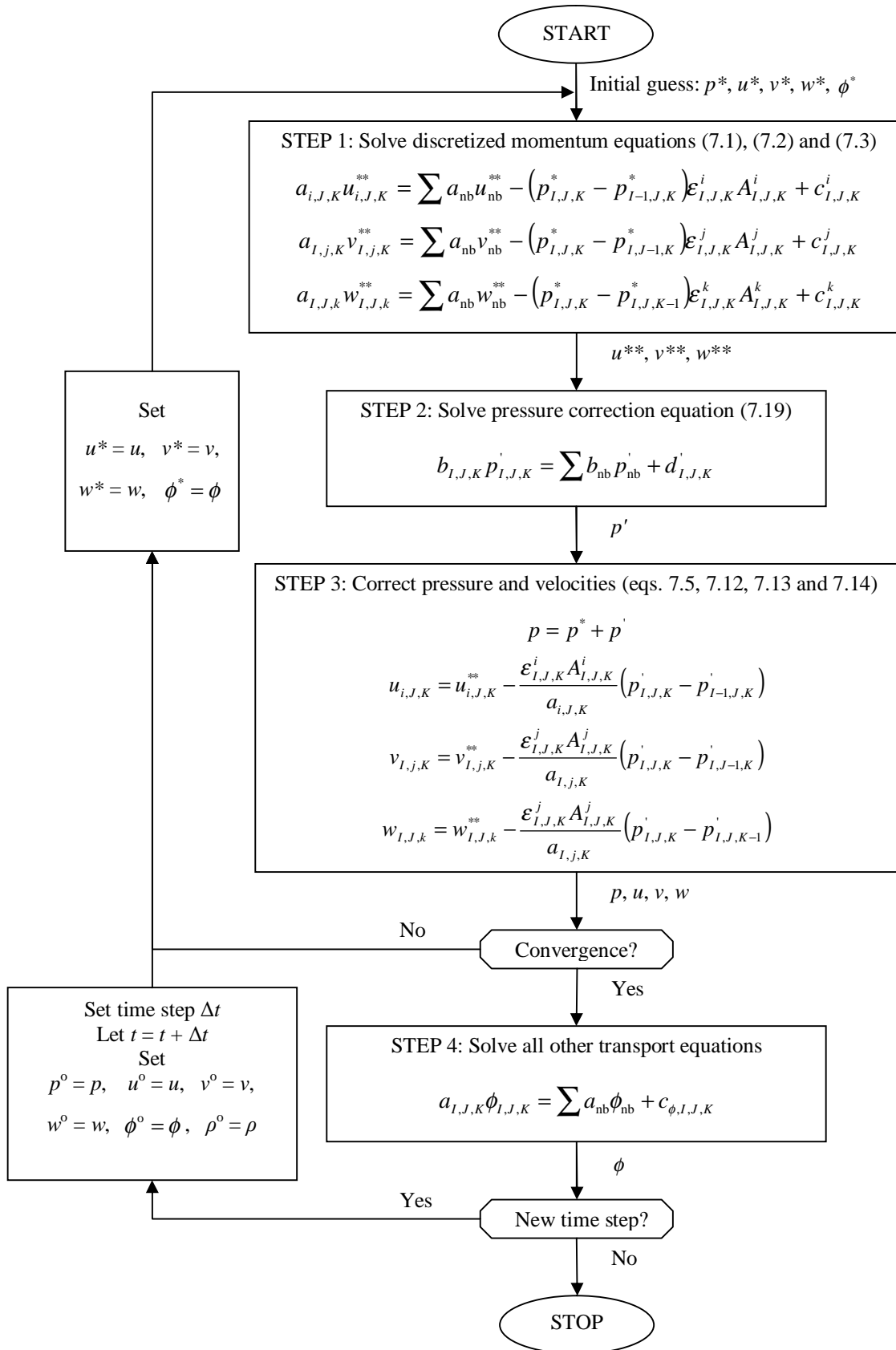


Figure 7.1: The transient SIMPLE algorithm.

7.2 The SIMPLER algorithm

The most profound drawback of the SIMPLE algorithm is that it doesn't preserve a good initial guess for the velocity field, if the pressure field is guessed poorly. In the SIMPLER, SIMPLE Revised, algorithm the discretized continuity equation and the momentum equations are used to derive an additional equation for pressure, which is solved first to provide a more accurate guess for the pressure to be input into the discretized momentum equations. The rest of the procedure is the same as in SIMPLE, with the exception that the pressure correction is used to update only the velocities. In other words, compared to the SIMPLE algorithm, SIMPLER employs a more accurate form for the pressure to preserve a good initial guess for the velocity. The SIMPLER algorithm is presented in (Patankar 1980, pp. 131-133).

The discretized momentum equations (7.1), (7.2) and (7.3) are rearranged as follows:

$$u_{i,J,K} = \frac{\sum a_{nb} u_{nb} + c_{I,J,K}^i}{a_{i,J,K}} - (p_{I,J,K} - p_{I-1,J,K}) \frac{\epsilon_{I,J,K}^i A_{I,J,K}^i}{a_{i,J,K}} \quad (7.21)$$

$$v_{I,j,K} = \frac{\sum a_{nb} v_{nb} + c_{I,J,K}^j}{a_{I,j,K}} - (p_{I,J,K} - p_{I,J-1,K}) \frac{\epsilon_{I,J,K}^j A_{I,J,K}^j}{a_{I,j,K}} \quad (7.22)$$

$$w_{I,J,k} = \frac{\sum a_{nb} w_{nb} + c_{I,J,K}^k}{a_{I,J,k}} - (p_{I,J,K} - p_{I,J,K-1}) \frac{\epsilon_{I,J,K}^k A_{I,J,K}^k}{a_{I,J,k}} \quad (7.23)$$

At this point, the first terms on the right-hand sides of the equations are defined as pseudo-velocities

$$\hat{u}_{i,J,K} = \frac{\sum a_{nb} u_{nb} + c_{I,J,K}^i}{a_{i,J,K}}, \quad (7.24)$$

$$\hat{v}_{I,j,K} = \frac{\sum a_{nb} v_{nb} + c_{I,J,K}^j}{a_{I,j,K}} \text{ and} \quad (7.25)$$

$$\hat{w}_{I,J,k} = \frac{\sum a_{nb} w_{nb} + c_{I,J,K}^k}{a_{I,J,k}}. \quad (7.26)$$

Applying the pseudo-velocities in the discretized momentum equations, (7.21), (7.22) and (7.23), leads to the following forms:

$$u_{i,j,k} = \hat{u}_{i,j,k} - \frac{\varepsilon_{i,j,k}^i A_{i,j,k}^i}{a_{i,j,k}} (p_{i,j,k} - p_{i-1,j,k}), \quad (7.27)$$

$$v_{i,j,k} = \hat{v}_{i,j,k} - \frac{\varepsilon_{i,j,k}^j A_{i,j,k}^j}{a_{i,j,k}} (p_{i,j,k} - p_{i,j-1,k}) \text{ and} \quad (7.28)$$

$$w_{i,j,k} = \hat{w}_{i,j,k} - \frac{\varepsilon_{i,j,k}^k A_{i,j,k}^k}{a_{i,j,k}} (p_{i,j,k} - p_{i,j,k-1}). \quad (7.29)$$

Next step is to combine these with the continuity equation for conservation of mixture mass to obtain the pressure equation, shown below.

$$\begin{aligned} & \varepsilon_{i,j,k} V_{i,j,k} \frac{(\rho_{i,j,k} - \rho_{i,j,k}^o)}{\Delta t} \\ & + \varepsilon_{i+1,j,k}^i A_{i+1,j,k}^i \left[\rho_m \left(\hat{u}_{i+1,j,k} - \frac{\varepsilon_{i+1,j,k}^i A_{i+1,j,k}^i}{a_{i+1,j,k}} (p_{i+1,j,k} - p_{i,j,k}) \right) \right]_{i+1,j,k} \\ & - \varepsilon_{i,j,k}^i A_{i,j,k}^i \left[\rho_m \left(\hat{u}_{i,j,k} - \frac{\varepsilon_{i,j,k}^i A_{i,j,k}^i}{a_{i,j,k}} (p_{i,j,k} - p_{i-1,j,k}) \right) \right]_{i,j,k} \\ & + \varepsilon_{i,j+1,k}^j A_{i,j+1,k}^j \left[\rho_m \left(\hat{v}_{i,j+1,k} - \frac{\varepsilon_{i,j+1,k}^j A_{i,j+1,k}^j}{a_{i,j+1,k}} (p_{i,j+1,k} - p_{i,j,k}) \right) \right]_{i,j+1,k} \\ & - \varepsilon_{i,j,k}^j A_{i,j,k}^j \left[\rho_m \left(\hat{v}_{i,j,k} - \frac{\varepsilon_{i,j,k}^j A_{i,j,k}^j}{a_{i,j,k}} (p_{i,j,k} - p_{i,j-1,k}) \right) \right]_{i,j,k} \\ & + \varepsilon_{i,j,k+1}^k A_{i,j,k+1}^k \left[\rho_m \left(\hat{w}_{i,j,k+1} - \frac{\varepsilon_{i,j,k+1}^k A_{i,j,k+1}^k}{a_{i,j,k+1}} (p_{i,j,k+1} - p_{i,j,k}) \right) \right]_{i,j,k+1} \\ & - \varepsilon_{i,j,k}^k A_{i,j,k}^k \left[\rho_m \left(\hat{w}_{i,j,k} - \frac{\varepsilon_{i,j,k}^k A_{i,j,k}^k}{a_{i,j,k}} (p_{i,j,k} - p_{i,j,k-1}) \right) \right]_{i,j,k} = 0 \end{aligned} \quad (7.30)$$

The equation (7.30) can be further rearranged.

$$\begin{aligned}
& \left[\left(\varepsilon_{i+1,J,K}^i A_{i+1,J,K}^i \right)^2 \left(\frac{\rho_m}{a} \right)_{i+1,J,K} + \left(\varepsilon_{I,J,K}^i A_{I,J,K}^i \right)^2 \left(\frac{\rho_m}{a} \right)_{I,J,K} \right. \\
& + \left(\varepsilon_{I,J+1,K}^j A_{I,J+1,K}^j \right)^2 \left(\frac{\rho_m}{a} \right)_{I,J+1,K} + \left(\varepsilon_{I,J,K}^j A_{I,J,K}^j \right)^2 \left(\frac{\rho_m}{a} \right)_{I,J,K} \\
& \left. + \left(\varepsilon_{I,J,K+1}^k A_{I,J,K+1}^k \right)^2 \left(\frac{\rho_m}{a} \right)_{I,J,K+1} + \left(\varepsilon_{I,J,K}^k A_{I,J,K}^k \right)^2 \left(\frac{\rho_m}{a} \right)_{I,J,K} \right] p_{I,J,K} \\
& = \left(\varepsilon_{i+1,J,K}^i A_{i+1,J,K}^i \right)^2 \left(\frac{\rho_m}{a} \right)_{i+1,J,K} p_{i+1,J,K} + \left(\varepsilon_{I,J,K}^i A_{I,J,K}^i \right)^2 \left(\frac{\rho_m}{a} \right)_{I,J,K} p_{I-1,J,K} \\
& + \left(\varepsilon_{I,J+1,K}^j A_{I,J+1,K}^j \right)^2 \left(\frac{\rho_m}{a} \right)_{I,J+1,K} p_{I,J+1,K} + \left(\varepsilon_{I,J,K}^j A_{I,J,K}^j \right)^2 \left(\frac{\rho_m}{a} \right)_{I,J,K} p_{I,J-1,K} \\
& + \left(\varepsilon_{I,J,K+1}^k A_{I,J,K+1}^k \right)^2 \left(\frac{\rho_m}{a} \right)_{I,J,K+1} p_{I,J,K+1} + \left(\varepsilon_{I,J,K}^k A_{I,J,K}^k \right)^2 \left(\frac{\rho_m}{a} \right)_{I,J,K} p_{I,J,K-1} \\
& \left[+ \left(\rho_m \hat{u} \varepsilon^i A^i \right)_{i,J,K} - \left(\rho_m \hat{u} \varepsilon^i A^i \right)_{i+1,J,K} + \left(\rho_m \hat{v} \varepsilon^j A^j \right)_{I,j,K} - \left(\rho_m \hat{v} \varepsilon^j A^j \right)_{I,j+1,K} \right. \\
& \left. + \left(\rho_m \hat{w} \varepsilon^k A^k \right)_{I,J,k} - \left(\rho_m \hat{w} \varepsilon^k A^k \right)_{I,J,k+1} - \varepsilon_{I,J,K} V_{I,J,K} \frac{(\rho_{I,J,K} - \rho_{I,J,K}^o)}{\Delta t} \right] \quad (7.31)
\end{aligned}$$

Using coefficients ($b_{I,J,K}$, $b_{I-1,J,K}$, ...) for discretized pressures leads to the final form of the pressure equation:

$$\begin{aligned}
b_{I,J,K} p_{I,J,K} &= b_{i+1,J,K} p_{i+1,J,K} + b_{I-1,J,K} p_{I-1,J,K} + b_{I,J+1,K} p_{I,J+1,K} \\
&+ b_{I,J-1,K} p_{I,J-1,K} + b_{I,J,K+1} p_{I,J,K+1} + b_{I,J,K-1} p_{I,J,K-1} + d_{I,J,K} \quad , \quad (7.32)
\end{aligned}$$

$$b_{I,J,K} p_{I,J,K} = \sum b_{nb} p_{nb} + d_{I,J,K} \quad (7.33)$$

This pressure field is used as an input for the SIMPLE algorithm, the rest of the procedure is unaffected, with the exception that the obtained pressure correction is only used to correct the velocities, **not the pressure**. The sequence of operations for the transient SIMPLER algorithm is presented in Figure 7.2.

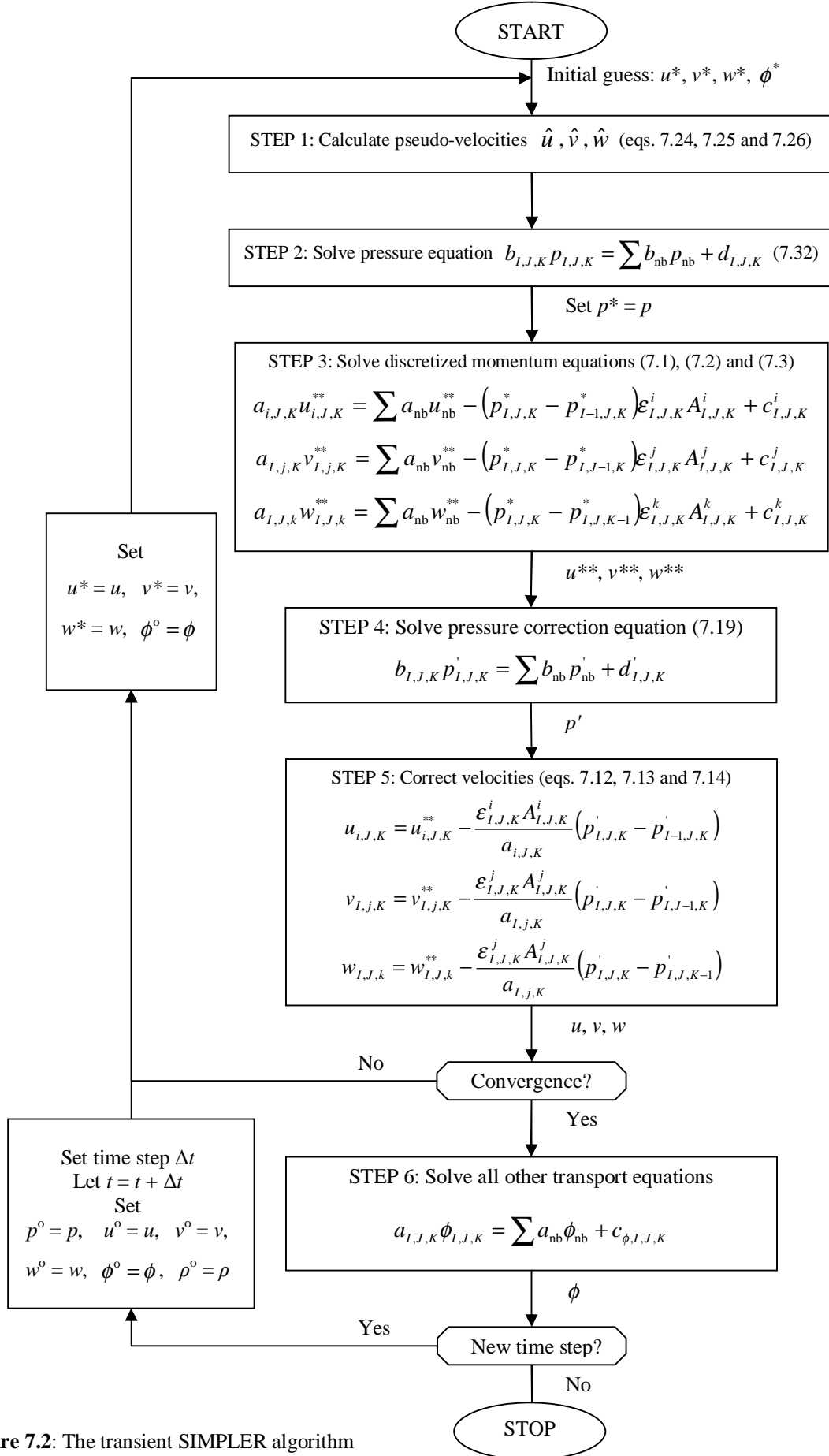


Figure 7.2: The transient SIMPLER algorithm

7.3 The SIMPLEC algorithm

The SIMPLEC, SIMPLE Consistent, algorithm follows the same approach as SIMPLE, with the exception that the effect of the neighbouring velocity corrections on the pressure correction of the central node is attempted to be included in the pressure correction equations. In SIMPLE the whole neighbouring velocity correction terms were dropped from the equation, whereas in SIMPLEC the neighbouring velocity corrections are assumed to be so close to one another that the coefficients can be summed together. Approximations introduced in SIMPLEC are shown below for x-direction:

$$a_{i,J,K}u'_{i,J,K} = a_{i-1,J,K}u'_{i-1,J,K} + a_{i,J-1,K}u'_{i,J-1,K} + a_{i,J,K-1}u'_{i,J,K-1} + a_{i+1,J,K}u'_{i+1,J,K} + a_{i,J+1,K}u'_{i,J+1,K} + a_{i,J,K+1}u'_{i,J,K+1} - (p'_{I,J,K} - p'_{I-1,J,K})\epsilon_{I,J,K}^i A_{I,J,K}^i \quad (7.34)$$

$$\Rightarrow a_{i,J,K}u'_{i,J,K} \approx a_{i-1,J,K}u'_{i-1,J,K} + a_{i,J-1,K}u'_{i,J-1,K} + a_{i,J,K-1}u'_{i,J,K-1} + a_{i+1,J,K}u'_{i+1,J,K} + a_{i,J+1,K}u'_{i,J+1,K} + a_{i,J,K+1}u'_{i,J,K+1} - (p'_{I,J,K} - p'_{I-1,J,K})\epsilon_{I,J,K}^i A_{I,J,K}^i \quad (7.35)$$

$$\Leftrightarrow (a_{i,J,K} - \sum a_{nb})u'_{i,J,K} = -(p'_{I,J,K} - p'_{I-1,J,K})\epsilon_{I,J,K}^i A_{I,J,K}^i \quad (7.36)$$

$$\Leftrightarrow u'_{i,J,K} = -\frac{\epsilon_{I,J,K}^i A_{I,J,K}^i}{a_{i,J,K} - \sum a_{nb}} (p'_{I,J,K} - p'_{I-1,J,K}) \quad (7.37)$$

Velocity corrections for other directions can be obtained using the same approach. Corrected velocities for all three directions are given through:

$$u_{i,J,K} = u_{i,J,K}^{**} - \frac{\epsilon_{I,J,K}^i A_{I,J,K}^i}{a_{i,J,K} - \sum a_{nb}} (p'_{I,J,K} - p'_{I-1,J,K}), \quad (7.38)$$

$$v_{I,j,K} = v_{I,j,K}^{**} - \frac{\epsilon_{I,j,K}^j A_{I,j,K}^j}{a_{I,j,K} - \sum a_{nb}} (p'_{I,J,K} - p'_{I,J-1,K}) \text{ and} \quad (7.39)$$

$$w_{I,J,k} = w_{I,J,k}^{**} - \frac{\epsilon_{I,J,k}^k A_{I,J,k}^k}{a_{I,J,k} - \sum a_{nb}} (p'_{I,J,K} - p'_{I,J,K-1}). \quad (7.40)$$

The pressure correction equation is otherwise the same as in SIMPLE, but the coefficients of pressure corrections contain the sum of the neighbouring coefficients of the momentum equation as well.

$$\begin{aligned}
& \left[\left(\varepsilon_{I+1,J,K}^i A_{I+1,J,K}^i \right)^2 \left(\frac{\rho_m}{a - \sum a_{nb}} \right)_{i+1,J,K} + \left(\varepsilon_{I,J,K}^i A_{I,J,K}^i \right)^2 \left(\frac{\rho_m}{a - \sum a_{nb}} \right)_{i,J,K} \right. \\
& + \left(\varepsilon_{I,J+1,K}^j A_{I,J+1,K}^j \right)^2 \left(\frac{\rho_m}{a - \sum a_{nb}} \right)_{I,j+1,K} + \left(\varepsilon_{I,J,K}^j A_{I,J,K}^j \right)^2 \left(\frac{\rho_m}{a - \sum a_{nb}} \right)_{I,J,K} \\
& \left. + \left(\varepsilon_{I,J,K+1}^k A_{I,J,K+1}^k \right)^2 \left(\frac{\rho_m}{a - \sum a_{nb}} \right)_{I,J,k+1} + \left(\varepsilon_{I,J,K}^k A_{I,J,K}^k \right)^2 \left(\frac{\rho_m}{a - \sum a_{nb}} \right)_{I,J,k} \right] p'_{I,J,K} \\
& = \left(\varepsilon_{I+1,J,K}^i A_{I+1,J,K}^i \right)^2 \left(\frac{\rho_m}{a - \sum a_{nb}} \right)_{i+1,J,K} p'_{I+1,J,K} + \left(\varepsilon_{I,J,K}^i A_{I,J,K}^i \right)^2 \left(\frac{\rho_m}{a - \sum a_{nb}} \right)_{i,J,K} p'_{I-1,J,K} \\
& + \left(\varepsilon_{I,J+1,K}^j A_{I,J+1,K}^j \right)^2 \left(\frac{\rho_m}{a - \sum a_{nb}} \right)_{I,j+1,K} p'_{I,J+1,K} + \left(\varepsilon_{I,J,K}^j A_{I,J,K}^j \right)^2 \left(\frac{\rho_m}{a - \sum a_{nb}} \right)_{I,J,K} p'_{I,J-1,K} \\
& + \left(\varepsilon_{I,J,K+1}^k A_{I,J,K+1}^k \right)^2 \left(\frac{\rho_m}{a - \sum a_{nb}} \right)_{I,J,k+1} p'_{I,J,K+1} + \left(\varepsilon_{I,J,K}^k A_{I,J,K}^k \right)^2 \left(\frac{\rho_m}{a - \sum a_{nb}} \right)_{I,J,k} p'_{I,J,K-1} \\
& \left[\left(\rho_m u^{**} \varepsilon^i A^i \right)_{i,J,K} - \left(\rho_m u^{**} \varepsilon^i A^i \right)_{i+1,J,K} + \left(\rho_m v^{**} \varepsilon^j A^j \right)_{I,j,K} - \left(\rho_m v^{**} \varepsilon^j A^j \right)_{I,j+1,K} \right. \\
& \left. + \left(\rho_m w^{**} \varepsilon^k A^k \right)_{I,J,k} - \left(\rho_m w^{**} \varepsilon^k A^k \right)_{I,J,k+1} - \varepsilon_{I,J,K} V_{I,J,K} \frac{(\rho_{I,J,K} - \rho_{I,J,K}^o)}{\Delta t} \right] \tag{7.41}
\end{aligned}$$

If the coefficients of pressure corrections are denoted as $(b_{I,J,K}, b_{I-1,J,K}, \dots)$ and the terms inside the brackets on the right-hand side of the equation are denoted as $d'_{I,J,K}$.

$$\begin{aligned}
b_{I,J,K} p'_{I,J,K} &= b_{I+1,J,K} p'_{I+1,J,K} + b_{I-1,J,K} p'_{I-1,J,K} + b_{I,J+1,K} p'_{I,J+1,K} \\
&+ b_{I,J-1,K} p'_{I,J-1,K} + b_{I,J,K+1} p'_{I,J,K+1} + b_{I,J,K-1} p'_{I,J,K-1} + d'_{I,J,K}, \tag{7.42}
\end{aligned}$$

$$b_{I,J,K} p'_{I,J,K} = \sum b_{nb} p'_{nb} + d'_{I,J,K}. \tag{7.43}$$

Otherwise the SIMPLEC algorithm follows the same procedure as SIMPLE, only the coefficients of the pressure corrections and the velocity correction equations are altered. The main steps of the transient SIMPLEC algorithm are shown in Figure 7.3.

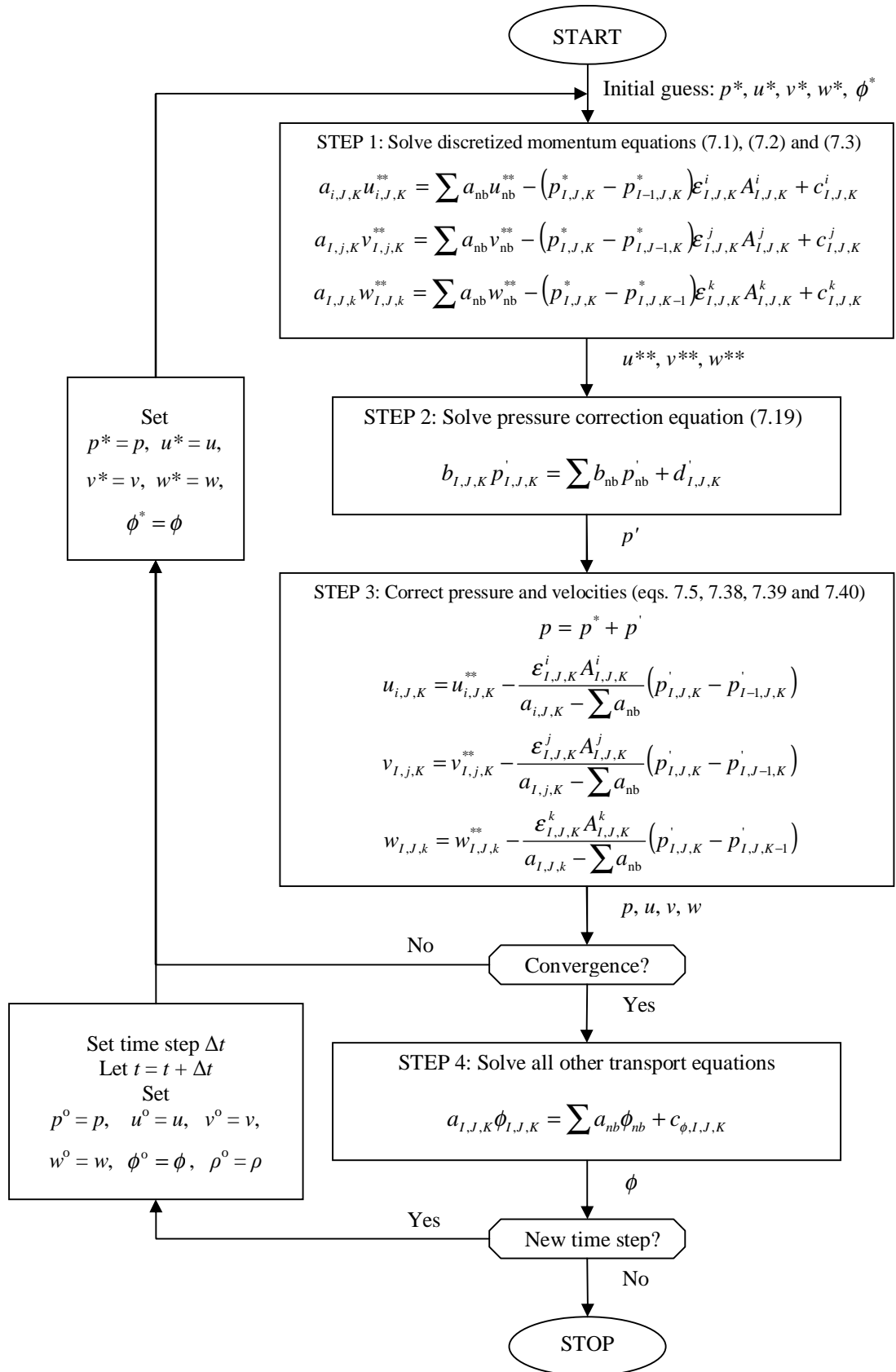


Figure 7.3: The transient SIMPLEC algorithm.

7.4 Pressure and velocity under-relaxation

The pressure and velocity corrections in the SIMPLE family of algorithms need to be under-relaxed to attain stable convergence; the corrections are not used in its entirety, only a fraction of the correction or the iteratively improved value is used. The pressure correction is under-relaxed with an under-relaxation factor α_p as follows:

$$p_{I,J,K}^{\text{new}} = p_{I,J,K}^* + \alpha_p p'_{I,J,K} \quad (7.44)$$

where

$p_{I,J,K}^{\text{new}}$	corrected pressure [Pa],
$p_{I,J,K}^*$	old pressure [Pa],
$p'_{I,J,K}$	pressure correction [Pa], and
α_p	under-relaxation factor for pressure [-].

The under-relaxation factors have values between [0, 1], however the corrections could be over-relaxed by choosing a value greater than one. The SIMPLE variants require different under-relaxation factors for pressure: while SIMPLE requires moderate under-relaxation, very little, if any, is needed in SIMPLEC. Due to the fact that pressure corrections are not used in SIMPLER to correct the pressure, no under-relaxation is needed for pressure either.

The velocities are corrected with the pressure corrections through the following equations:

$$u_{i,j,k} = u_{i,j,k}^{**} - \frac{\varepsilon_{I,J,K}^i A_{I,J,K}^i}{a_{i,j,k}} (p'_{I,J,K} - p'_{I-1,J,K}) \quad (7.45)$$

$$v_{I,j,k} = v_{I,j,k}^{**} - \frac{\varepsilon_{I,J,K}^j A_{I,J,K}^j}{a_{I,j,k}} (p'_{I,J,K} - p'_{I,J-1,K}) \quad (7.46)$$

$$w_{I,J,k} = w_{I,J,k}^{**} - \frac{\varepsilon_{I,J,K}^k A_{I,J,K}^k}{a_{I,J,k}} (p'_{I,J,K} - p'_{I,J,K-1}) \quad (7.47)$$

where

u, v, w	are the x, y and z-components of velocity respectively [m/s],
$**$	denotes the values after the solution of the momentum equations.

The velocities are under-relaxed with a factor α_u . All the velocity components are under-relaxed with the same factor, despite the fact that different under-relaxation factors could be defined for each direction. Velocity under-relaxation is shown for x-direction:

$$u_{i,J,K}^{\text{new}} = \alpha_u u_{i,J,K} + (1 - \alpha_u) u_{i,J,K}^{n-1} \quad (7.48)$$

where u^{new} under-relaxed new velocity [m/s]
 u corrected new velocity [m/s]
 u^{n-1} corrected velocity at the previous iteration [m/s].

The momentum equations can be modified to contain the velocity under-relaxations, so that the under-relaxations do not have to be performed separately. The velocities that are input to the momentum equations have been corrected using the pressure corrections in equations (7.45), (7.46) and (7.47). Momentum equation for x-direction can be written as

$$a_{i,J,K} u_{i,J,K} = \sum a_{\text{nb}} u_{\text{nb}} - (p_{I,J,K} - p_{I-1,J,K}) \epsilon_{I,J,K}^i A_{I,J,K}^i + c_{I,J,K}^i \quad (7.49)$$

To get the under-relaxed form of the momentum equation, equation (7.49) is first divided by the coefficient of the central velocity node, $a_{i,J,K}$.

$$u_{i,J,K} = \frac{1}{a_{i,J,K}} \left[\sum a_{\text{nb}} u_{\text{nb}} - (p_{I,J,K} - p_{I-1,J,K}) \epsilon_{I,J,K}^i A_{I,J,K}^i + c_{I,J,K}^i \right] \quad (7.50)$$

Then, both sides of the momentum equation are multiplied by the factor α_u and after that $(1 - \alpha_u) u_{i,J,K}^{n-1}$ is added to both sides:

$$\alpha_u u_{i,J,K} + (1 - \alpha_u) u_{i,J,K}^{n-1} = \frac{\alpha_u}{a_{i,J,K}} \left[\sum a_{\text{nb}} u_{\text{nb}} - (p_{I,J,K} - p_{I-1,J,K}) \epsilon_{I,J,K}^i A_{I,J,K}^i + c_{I,J,K}^i \right] + (1 - \alpha_u) u_{i,J,K}^{n-1} \quad (7.51)$$

It can be noticed that the left-hand side of the equation is just the under-relaxed new velocity:

$$u_{i,J,K}^{\text{new}} = \frac{\alpha_u}{a_{i,J,K}} \left[\sum a_{\text{nb}} u_{\text{nb}} - (p_{I,J,K} - p_{I-1,J,K}) \epsilon_{I,J,K}^i A_{I,J,K}^i + c_{I,J,K}^i \right] + (1 - \alpha_u) u_{i,J,K}^{n-1} \quad (7.52)$$

As the momentum equations are solved in the beginning of each iteration, the neighbouring velocities, in equation (7.52), are taken from the end of the previous iteration without relaxation and $u_{i,J,K}^{n-1}$ is the velocity obtained two iterations earlier without relaxation.

8 DEVELOPMENT OF THE CODE

When developing new code or applying old codes to new conditions, much of the coding effort is spent on testing and debugging the code –this work makes no exception. The first few months of development were spent on getting the simulations started. The combined effects of the errors, both in the older main code and in the subroutine which implements the SIMPLE variants, complicated the development in the beginning. The errors in the code are harder to backtrack when the effects of several errors are combined; in addition some of the errors only manifest themselves after the simulation reaches a certain point, and sufficient amount of void fraction has been created, for example.

Apart from the obvious bugs in the code, problematic behaviour inherent to the solution algorithm or the disposition of the governing equations was encountered on few occasions: these findings are discussed in this Chapter.

8.1 Basis for the pressure correction equation

The single-phase versions of the SIMPLE algorithm use the mass conservation equation to formulate the pressure correction equation, as presented in (Patankar 1980) and (Versteeg & Malalasekera 2007), but due to the relative differences in phase velocities, the conservation equation for mixture mass in 5-equation models based on mixture density is not accurate; a topic which was briefly visited in section 6.3.1. A term needs to be introduced to correct the inherent error in mass balance resulting from the use of mixture density.

During the development of the code it became apparent that as soon as sufficient boiling occurs the pressure correction equation based on conservation of mixture mass can no longer provide velocity fields that satisfy continuity and the resulting mass errors increase gradually, even though the mass errors accumulated up until a certain time step are corrected during the next. In an attempt to counter this, the pressure correction equations were formulated again starting from the conservation of mixture volume instead of mass.

The conservation equation for mixture volume is not flawless either: if local differences in mixture densities exist, the mass balance is not preserved, since the conservation equation for mixture volume only preserves the volume of the mixture and has no bearing on the conservation of mass. However, the resulting error in mass balance can be corrected, as opposed to the previously discussed formulation based on conservation of mixture mass. It seems that the crucial factor that prevents the mass conservation equation from correcting itself is the fact that the correction term itself contains the flawed mixture density; the correction term of the volume conservation equation, on the other hand, does not contain the mixture density, nor do the other terms in the equation for that matter.

If the velocities at each boundary of the pressure node in the conservation equation for mixture volume, equation (6.25), are replaced with the corrected velocities in equations (7.12), (7.13) and (7.14) the pressure correction equations based on conservation of mixture volume are obtained.

$$\begin{aligned} \frac{\Delta V_{I,J,K}}{\Delta t} + (\varepsilon_{I+1,J,K}^i u_{i+1,J,K} - \varepsilon_{I,J,K}^i u_{i,J,K}) A_{I,J,K}^i \\ + (\varepsilon_{I,J+1,K}^j v_{I,j+1,K} - \varepsilon_{I,J,K}^j v_{I,j,K}) A_{I,J,K}^j \\ + (\varepsilon_{I,J,K+1}^k w_{I,J,k+1} - \varepsilon_{I,J,K}^k w_{I,J,k}) A_{I,J,K}^k = \Gamma_{I,J,K} \left(\frac{1}{\rho_g} - \frac{1}{\rho_l} \right) \end{aligned} \quad (8.1)$$

$$\begin{aligned} \Leftrightarrow \frac{\Delta V_{I,J,K}}{\Delta t} + \left\{ \varepsilon_{I+1,J,K}^i \left[u_{i+1,J,K}^{**} - \frac{\varepsilon_{I+1,J,K}^i A_{I,J,K}^i}{a_{i+1,J,K}} (p'_{I+1,J,K} - p'_{I,J,K}) \right] \right. \\ \left. - \varepsilon_{I,J,K}^i \left[u_{i,J,K}^{**} - \frac{\varepsilon_{I,J,K}^i A_{I,J,K}^i}{a_{i,J,K}} (p'_{I,J,K} - p'_{I-1,J,K}) \right] \right\} A_{I,J,K}^i \\ + \left\{ \varepsilon_{I,J+1,K}^j \left[v_{I,j+1,K}^{**} - \frac{\varepsilon_{I,J+1,K}^j A_{I,J,K}^j}{a_{I,j+1,K}} (p'_{I,J+1,K} - p'_{I,J,K}) \right] \right. \\ \left. - \varepsilon_{I,J,K}^j \left[v_{I,j,K}^{**} - \frac{\varepsilon_{I,J,K}^j A_{I,J,K}^j}{a_{I,j,K}} (p'_{I,J,K} - p'_{I,J-1,K}) \right] \right\} A_{I,J,K}^j \\ + \left\{ \varepsilon_{I,J,K+1}^k \left[w_{I,J,k+1}^{**} - \frac{\varepsilon_{I,J,K+1}^k A_{I,J,K}^k}{a_{I,J,k+1}} (p'_{I,J,K+1} - p'_{I,J,K}) \right] \right. \\ \left. - \varepsilon_{I,J,K}^k \left[w_{I,J,k}^{**} - \frac{\varepsilon_{I,J,K}^k A_{I,J,K}^k}{a_{I,J,k}} (p'_{I,J,K} - p'_{I,J,K-1}) \right] \right\} A_{I,J,K}^k = \Gamma_{I,J,K} \left(\frac{1}{\rho_g} - \frac{1}{\rho_l} \right) \end{aligned} \quad (8.2)$$

Equation (8.2) is rearranged so that the terms containing the pressure corrections remain on the left-hand side, the terms containing the pressure correction of the central node, $p'_{I,J,K}$, are combined and the rest is moved to the right-hand side of the equation.

$$\begin{aligned}
& \left[\frac{(\varepsilon^i_{I+1,J,K} A^i_{I,J,K})^2}{a_{i+1,J,K}} + \frac{(\varepsilon^i_{I,J,K} A^i_{I,J,K})^2}{a_{i,J,K}} + \frac{(\varepsilon^j_{I,J+1,K} A^j_{I,J,K})^2}{a_{I,j+1,K}} \right. \\
& \left. + \frac{(\varepsilon^j_{I,J,K} A^j_{I,J,K})^2}{a_{I,j,K}} + \frac{(\varepsilon^k_{I,J,K+1} A^k_{I,J,K})^2}{a_{I,J,k+1}} + \frac{(\varepsilon^k_{I,J,K} A^k_{I,J,K})^2}{a_{I,J,k}} \right] p'_{I,J,K} \\
& - \frac{(\varepsilon^i_{I+1,J,K} A^i_{I,J,K})^2}{a_{i+1,J,K}} p'_{I+1,J,K} - \frac{(\varepsilon^i_{I,J,K} A^i_{I,J,K})^2}{a_{i,J,K}} p'_{I-1,J,K} - \frac{(\varepsilon^j_{I,J+1,K} A^j_{I,J,K})^2}{a_{I,j+1,K}} p'_{I,J+1,K} \\
& - \frac{(\varepsilon^j_{I,J,K} A^j_{I,J,K})^2}{a_{I,j,K}} p'_{I,J-1,K} - \frac{(\varepsilon^k_{I,J,K+1} A^k_{I,J,K})^2}{a_{I,J,k+1}} p'_{I,J,K+1} - \frac{(\varepsilon^k_{I,J,K} A^k_{I,J,K})^2}{a_{I,J,k}} p'_{I,J,K-1} \\
& = \left[(\varepsilon^i A^i u^{**})_{i,J,K} - (\varepsilon^i A^i u^{**})_{i+1,J,K} + (\varepsilon^j A^j v^{**})_{I,j,K} - (\varepsilon^j A^j v^{**})_{I,j+1,K} \right. \\
& \left. + (\varepsilon^k A^k w^{**})_{I,J,k} - (\varepsilon^k A^k w^{**})_{I,J,k+1} + \Gamma_{I,J,K} \left(\frac{1}{\rho_g} - \frac{1}{\rho_l} \right) - \frac{\Delta V_{I,J,K}}{\Delta t} \right] \quad (8.3)
\end{aligned}$$

The right-hand side of the pressure correction equation is essentially the conservation equation for mixture volume, which is comprised of the volumetric flow rates at the boundaries, the change in mixture volume due to boiling and the time rate of change in mixture volume $\Delta V_{I,J,K}/\Delta t$. The time rate of change in mixture volume is used to introduce the effect of the explicitly calculated mass error correction into the pressure correction equations. At the end of the time step, the mass inventories of both liquid and vapour in each node are given. These can be used together with the densities of the phases to calculate the volume the mass content of the node requires. The difference of the required volume and the fluid volume of the node is used as a correction term in the pressure correction equations as follows:

$$\frac{\Delta V_{I,J,K}}{\Delta t} = - \left[\frac{(M_l)^\circ_{I,J,K}}{(\rho_l)_{I,J,K}} + \frac{(M_g)^\circ_{I,J,K}}{(\rho_g)_{I,J,K}} - \varepsilon_{I,J,K} V_{I,J,K} \right] \cdot \frac{\omega_{me}}{\Delta t} \quad (8.4)$$

The term containing the square brackets in equation (8.4) is called mass error, despite the fact that it has the same units as volumetric flow rates, m^3/s . It is nevertheless called mass error since it is derived from the vapour and liquid masses inside the control volume at the

end of the previous time step. The portion of the mass error corrected during the time step is controlled by the factor ω_{me} .

8.2 Diagonal dominance of the pressure correction equations

The most profound difficulty in the solution of SIMPLE-type algorithms formulated assuming incompressible flow, from a strictly numerical perspective, is the weakly diagonally dominant coefficient matrix of the pressure correction equations, which makes iterative solution of the pressure correction equations challenging. The pressure correction equations, or pressure equations for that matter, bear a noticeable resemblance to Poisson equations, hence they are frequently called the pressure Poisson equations (Wesseling 2001, p. 251). A two-dimensional Poisson equation is given in Kreyszig (1999, p. 962) which can easily be expanded to a three-dimensional domain:

$$\nabla^2 \mathbf{u} = f(x, y, z). \quad (8.5)$$

To point out the similarity between pressure correction equations and Poisson equations, the pressure correction equations are examined briefly. The pressure correction equations, as used in this thesis, begin with the conservation of mixture volume

$$\frac{\partial}{\partial t} + \frac{\partial u_m}{\partial x} + \frac{\partial v_m}{\partial y} + \frac{\partial w_m}{\partial z} = \gamma \left(\frac{1}{\rho_g} - \frac{1}{\rho_l} \right). \quad (8.6)$$

In the incompressible formulation the time dependent term, the first term on the left-hand side of equation (8.6), is constant, independent of pressure, as is the only term on the right-hand side. The second, third and fourth terms on the left-hand side constitute the divergence of velocity. After combining the constant terms into c , equation (8.6) can be written as follows:

$$\nabla \cdot \mathbf{u} = c \quad (8.7)$$

The next step is to introduce the effects of pressure corrections on each velocity component to the conservation equation for mixture volume. If each velocity component of \mathbf{u} is replaced with the essence of the corrected velocities, equations (7.12) through (7.14), (note that the corrections (7.12) through (7.14) are discretized while equation (8.7) is not) the following form is obtained:

$$\nabla \cdot \left(u^* - \frac{\Delta p'}{\Delta x}, \quad v^* - \frac{\Delta p'}{\Delta y}, \quad w^* - \frac{\Delta p'}{\Delta z} \right) = c. \quad (8.8)$$

Divergence of the known velocity components, which constitutes the volumetric net outflow, is moved to the right-hand side and combined with the constant c . The terms inside the parentheses containing the pressure corrections are nothing more than the spatial derivatives of pressure corrections in each direction of the coordinate axes; hence equation (8.8) is reduced to the following form:

$$\nabla \cdot \nabla p' = \nabla^2 p' = c \quad (8.9)$$

The constant term c , which is essentially the sum volumetric net outflow and the correction terms over each node, is a function of space, $c = f(x, y, z)$, as in equation (8.5).

When the pressure Poisson equation obtained by assuming incompressible flow is discretized over a three-dimensional domain, a set of equations, presented previously in equation (8.3), results:

$$\begin{aligned} & \left[\frac{(\varepsilon_{i+1,J,K}^i A_{I,J,K}^i)^2}{a_{i+1,J,K}} + \frac{(\varepsilon_{I,J,K}^i A_{I,J,K}^i)^2}{a_{i,J,K}} + \frac{(\varepsilon_{I,J+1,K}^j A_{I,J,K}^j)^2}{a_{I,j+1,K}} \right. \\ & \left. + \frac{(\varepsilon_{I,J,K}^j A_{I,J,K}^j)^2}{a_{I,j,K}} + \frac{(\varepsilon_{I,J,K+1}^k A_{I,J,K}^k)^2}{a_{I,J,k+1}} + \frac{(\varepsilon_{I,J,K}^k A_{I,J,K}^k)^2}{a_{I,J,k}} \right] p'_{I,J,K} \\ & - \frac{(\varepsilon_{i+1,J,K}^i A_{I,J,K}^i)^2}{a_{i+1,J,K}} p'_{i+1,J,K} - \frac{(\varepsilon_{I,J,K}^i A_{I,J,K}^i)^2}{a_{i,J,K}} p'_{I-1,J,K} - \frac{(\varepsilon_{I,J+1,K}^j A_{I,J,K}^j)^2}{a_{I,j+1,K}} p'_{I,J+1,K} \\ & - \frac{(\varepsilon_{I,J,K}^j A_{I,J,K}^j)^2}{a_{I,j,K}} p'_{I,J-1,K} - \frac{(\varepsilon_{I,J,K+1}^k A_{I,J,K}^k)^2}{a_{I,J,k+1}} p'_{I,J,K+1} - \frac{(\varepsilon_{I,J,K}^k A_{I,J,K}^k)^2}{a_{I,J,k}} p'_{I,J,K-1} \\ & = \left[+ (\varepsilon^i A^i u^{**})_{i+1,J,K} - (\varepsilon^i A^i u^{**})_{i-1,J,K} + (\varepsilon^j A^j v^{**})_{I,j,K} - (\varepsilon^j A^j v^{**})_{I,j+1,K} \right. \\ & \left. + (\varepsilon^k A^k w^{**})_{I,J,k} - (\varepsilon^k A^k w^{**})_{I,J,k+1} - \frac{\Delta V_{I,J,K}}{\Delta t} \right] \quad (8.10) \end{aligned}$$

It is seen that the diagonal term, the terms inside the square brackets on the left-hand side, consists of the sum of off-diagonal entries: the consequences of this will be explained

shortly. The pressure correction equations can be rewritten compiling the diagonal and off-diagonal terms into a coefficient matrix \mathbf{A} .

$$\mathbf{A}\bar{x} = \bar{b} \quad (8.11)$$

where \mathbf{A} coefficient matrix of pressure corrections
 \bar{x} a vector containing the pressure corrections
 \bar{b} the entries on right-hand side of the pressure correction equations.

In order to specify the type of the coefficient matrix of the pressure correction equations, some definitions need to be introduced.

According to Kreyszig (1999, p. 922), a diagonally dominant matrix $\mathbf{A} = [a_{jk}]$ is an $n \times n$ matrix such that

$$|a_{jj}| \geq \sum_{k \neq j} |a_{jk}| \quad j = 1, \dots, n \quad (8.12)$$

where the sum is taken over all the off-diagonal entries in row j . The matrix is **strictly diagonally dominant** if there is a strong inequality in equation (8.12) for all j .

By definition, (Kreyszig 1999, p. 923), an **irreducible matrix** \mathbf{A} cannot be brought into the form

$$\begin{bmatrix} \mathbf{B} & \mathbf{C} \\ \mathbf{0} & \mathbf{F} \end{bmatrix} \quad (8.13)$$

by interchanging rows or columns (or both); here $\mathbf{0}$ is a zero matrix and \mathbf{B} and \mathbf{F} are any $r \times r$ and $(n-r) \times (n-r)$ matrices.

And finally, by definition in (Stewart 1998, p. 219) a matrix \mathbf{A} is said to be **irreducibly diagonally dominant** if:

1. \mathbf{A} is irreducible,
2. \mathbf{A} is diagonally dominant with strict inequality in at least one row (in eq. 8.12).

According to these definitions the coefficient matrix of the pressure correction equations is **irreducibly diagonally dominant**, since it is irreducible and the sum of off-diagonal entries equals the diagonal in the whole domain except in the outlet, where the diagonal entries are greater than the sum of off-diagonals. Iterative solution of systems as $\mathbf{A}\bar{x} = \bar{b}$ with irreducibly or weakly diagonally dominant coefficient matrixes is well known to be troublesome; small changes in the coefficient matrix \mathbf{A} or the solution \bar{b} cause huge changes in the iteratively solved vector \bar{x} , and vice versa. Truncation errors make the matter even worse.

To facilitate iterative solution of the pressure correction equation, a small artificial increase in the diagonal terms of the coefficient matrix in pressure correction equations was proposed. Wesseling (2001, p. 240) provides a brief overview of the procedure which is called the artificial compressibility method. Manipulation of the sort is only possible when the final solution of the converged state at the end of the time step remains unaltered. While it is evident that, by artificially increasing the diagonal terms of the coefficient matrix, the solution of the pressure correction equations after each iteration is altered, the converged state at the end of the time step, however, remains the same, since the effect of the artificial increase in the diagonal of the coefficient matrix approaches zero when the pressure corrections approach zero, which is the case when approaching a converged solution. In other words: the path to convergence is altered by artificially increasing the diagonal dominance of the coefficient matrix, but the final solution of the flow field is not.

The pressure correction equations were solved using a direct solver, Gaussian elimination, and the number of SIMPLE iterations needed to reach a converged solution was observed. Though the goal of this test was to study the possibility to use iterative solvers already coded in PORFLO, and the usability of iterative solvers in general, a direct method was used to eliminate the effect of convergence criterion of the iterative solver on the number of SIMPLE iterations.

The tests revealed that a relative increase of approximately 1% in the diagonal entries increased the number of SIMPLE iterations by a factor of 10-1000, depending on the flow conditions. In a situation where most of the CPU-time is spent solving the pressure

correction equations, this would mean that iterative solvers would have to be substantially faster than direct methods, in order to gain any benefit from the artificial increase.

8.3 Increasing the implicitness of the overall solution

The former structure of the solution procedure in PORFLO, presented in Figure 4.1, regardless of the choice between direct or iterative methods for pressure-velocity solution, was non-iterative as a whole; meaning that, as the procedure advances, each stage of the solution procedure is visited only once during the time step. Then, the values of many variables, such as mixture densities, have to be taken from the beginning of the time step, even though fully implicit discretization scheme was used to formulate the discretized mass and momentum conservation equations. This increases the explicitness of the overall solution procedure, and renders it more conditional on Courant's criterion, which means that the flow cannot travel more than the length of the node during the time step.

To make the solution procedure more implicit, an option was added which allows iterative solution over the whole solution procedure when using the subroutine that implements the SIMPLE family of algorithms. In essence the solution of all the variables, temperatures, densities, void fractions, mass flow rates and masses of the two phases, are brought inside the SIMPLE iteration loop. The iterative solution procedure is shown in Figure 8.1.

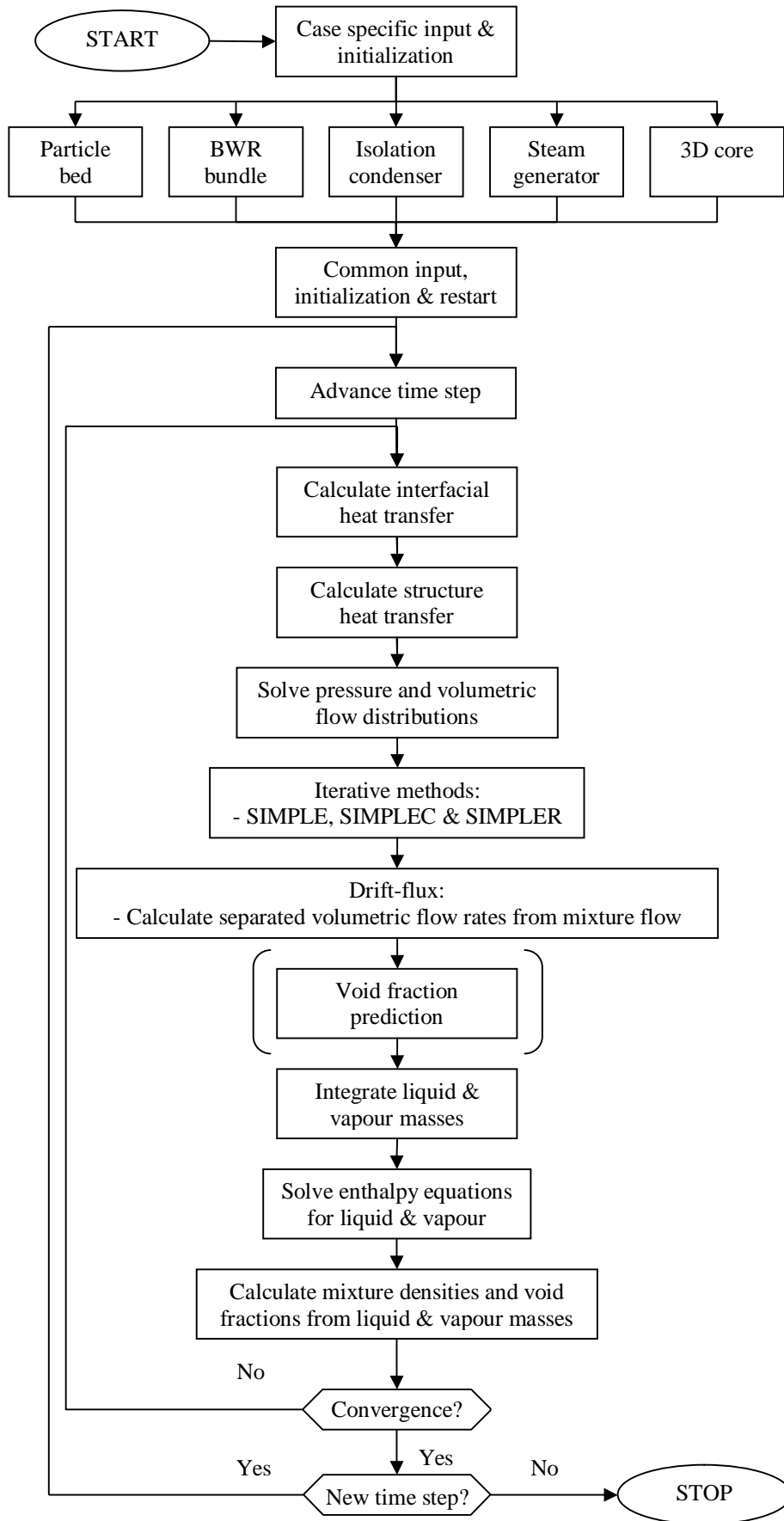


Figure 8.1: Iterative solution procedure in PORFLO. (cf. Figure 4.1)

The iterative solution mode is more sensitive to disturbances and prone to oscillations, since there are more variables that are updated during the iteration; more moving parts, so to say. When using the iterative solution mode, shown in Figure 8.1, the void fraction prediction is not needed; actually it may be an unnecessary source of disturbance.

Some tests have been performed to study the usefulness of the iterative solution mode, which indicate that the iterative mode performs as well as the non-iterative mode when using short time steps. Time steps longer than the Courant's criterion suggests have not been tested, even though fully implicit discretization combined with the iterative solution mode should be able to handle them. Using equal time steps the iterative and non-iterative solution modes converge after the same number of iterations, which indicates that with short time steps the essence of SIMPLE-type algorithms, the pressure correction, limits the rate of convergence, while changes in transported properties have little effect.

As mentioned, the iterative solution mode is less stable than the non-iterative mode. Oscillatory behaviour was encountered during the tests. While the definitive cause for this behaviour is unknown, it seems that a poor choice of parameters in the drift-flux model was at least partly responsible. If problems with stability persist, the transported properties, such as mixture density and void fraction, could be under-relaxed in a similar manner the velocities are under-relaxed at the end of each iteration.

9 BWR FULL-SIZE FINE-MESH BUNDLE TESTS

Measurements for the BFBT (**BWR Full-size Fine-mesh Bundle Tests**) benchmark were conducted in an out-of-pile test facility by Nuclear Power Engineering Corporation (NUPEC). NUPEC has carried out void fraction measurement tests as a part of a national project sponsored by the Japanese Ministry of International Trade (MITI). The BFBT benchmark problems are based on a vast library of measurements under a full scale of BWR operating conditions and several transients as well. (Inoue 1995, p. 629)

The detailed fine-mesh void fraction distribution and critical power data provided in the BFBT benchmark lay a solid foundation for advanced understanding and modeling of the two-phase flow phenomena in real BWR bundles and provide a great opportunity to assess and compare the results of simulations with other participants. Until recently such a high quality measurements of the void fraction distribution inside a real BWR geometry have not been available, but under proprietary possession instead. As opposed to the prevailing empirical approach, the development of more mechanistic models for the requirements of the design concepts of future reactors require detailed measurements in order to elucidate the separate mechanism leading to a certain result: the only way to improve the probability of accurate results in untested conditions.

9.1 Description of the test facility

The test facility is shown in Figure 9.1. Demineralized water is used as a coolant, which is circulated by the circulation pump (1). Three valves (3) of different sizes are used to control the coolant flow. The coolant is preheated in a tubular preheater (4) before it flows into the test section (5), which contains the test assembly. Water heats up in the test section and forms a two-phase flow, which is directed to the separator (7). The steam separated from the two-phase mixture in the separator is then condensed in the steam drum (8) by a spray of subcooled water. A part of the condensed water is directed to the spray pump (10) that drives the coolant through two air-cooled heat exchangers into the spray lines (9), the rest is returned back to the circulation pump. The system pressure is controlled by four valves of different sizes connected to the spray lines. The pressurizer (6) controls the system pressure at low power levels. The maximum operating conditions for the test

facility are 10.3 MPa in pressure, 315°C in temperature, 12 MW in heating power, and 33 kg/s in coolant flow rate. (Nuclear Energy Agency 2005, pp. 15-16)

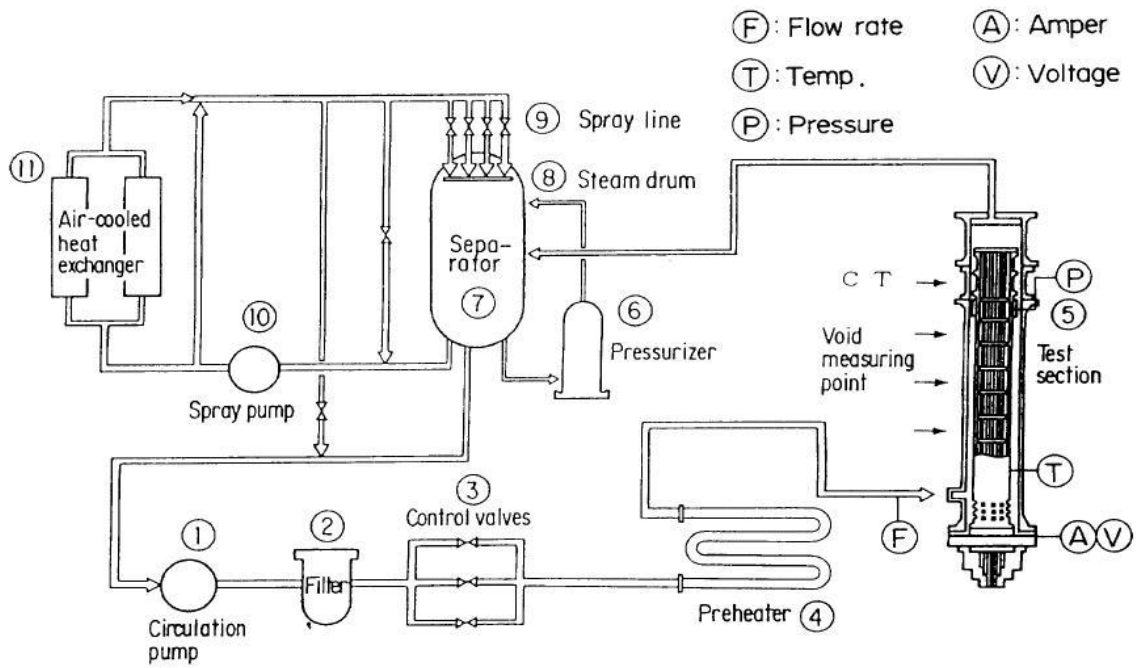


Figure 9.1: Diagram of the test facility. (Nuclear Energy Agency 2005, p. 16)

The test section is a pressure vessel that contains a flow channel and the test assembly. The test assembly consists of electrically heated rods, shown in Figure 9.2, that simulate the fuel rods. Each of these rods can be individually heated to simulate the power profile of an actual reactor. Five different types of test assemblies were used to simulate the effects of different types of fuel bundles with different amount of unheated rods and different axial power profile. A view of the test section is shown in Figure 9.3. (Nuclear Energy Agency 2005, pp. 15-16)

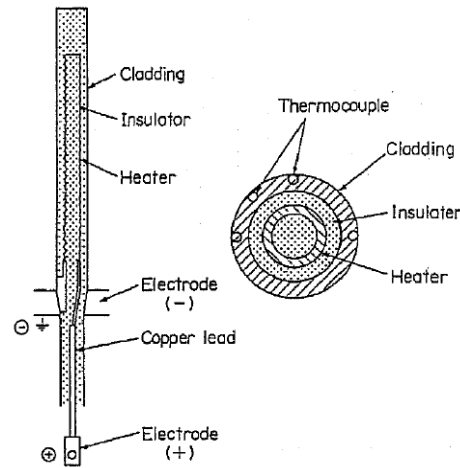


Figure 9.2: Cross-sectional view of a heated rod. (Inoue 1995, p. 632)

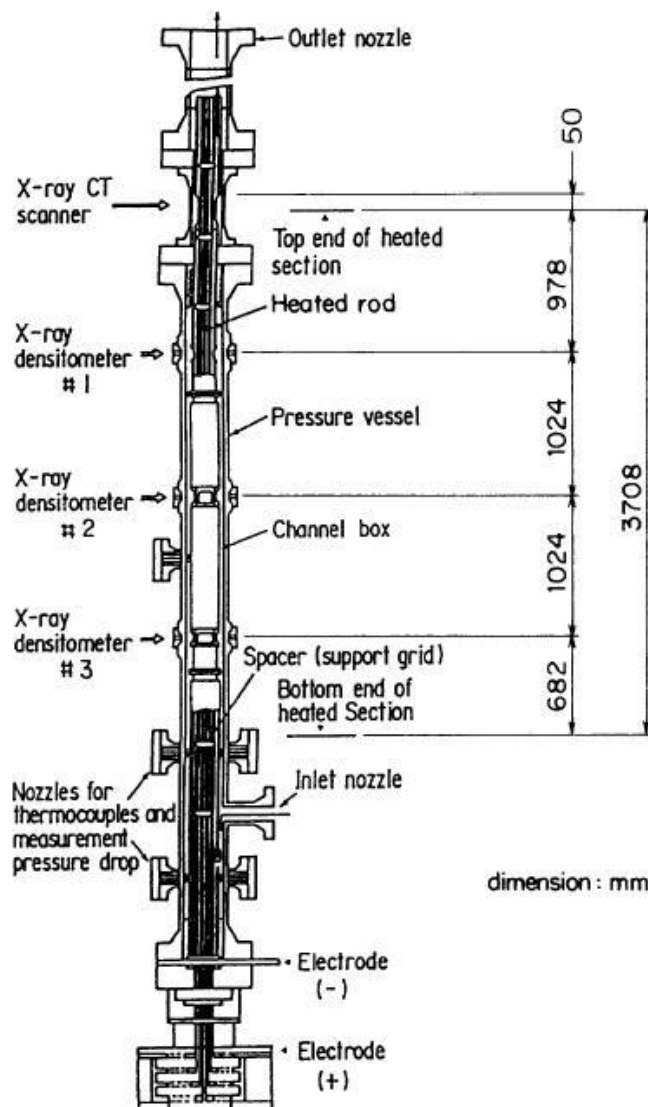


Figure 9.3: Cross-sectional view of the test section. (Nuclear Energy Agency 2005, p. 16)

9.2 Void fraction measurement

The void fraction measurement system consists of two different types of X-ray measuring devices: The X-ray CT-scanner (Computed or Computerized Tomography) and the X-ray densitometer, which are shown in Figure 9.4. The X-ray CT-scanner measures the void fraction distribution at a point just above the heated length. The X-ray densitometers are placed at three different locations along the heated length. (Nuclear Energy Agency 2005, pp. 17-21)

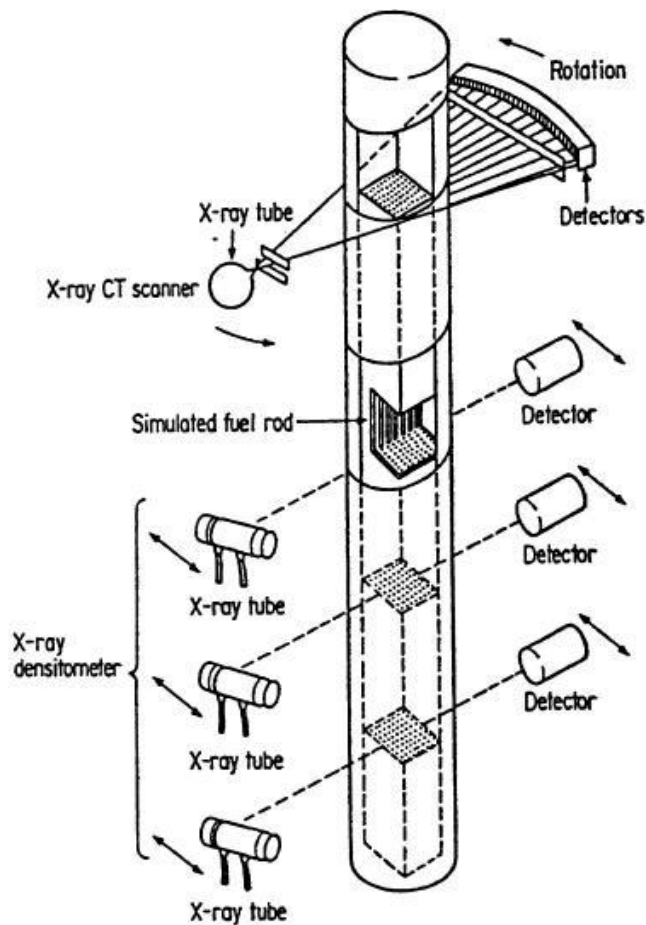


Figure 9.4: Void fraction measurement system. (Nuclear Energy Agency 2005, p. 18)

Fine mesh void distributions were measured under steady-state conditions using the X-Ray CT-scanner which was located at 5 cm above the heated length. The X-ray CT-scanner consists of an X-ray tube and 512 detectors. In fine mesh void distribution measurements the CT-scanner is rotated around the test section at a fixed axial position. Complete projection data are obtained with a 360° rotation around the test section. The channel walls and rods at the path of the X-ray CT-scanner are made of Be and the pressure vessel is

made of Ti to reduce X-ray attenuation in the structures. The effects of two-phase flow fluctuations are avoided by time-averaging the data of repeated measurements. The measuring system is capable of a resolution as small as 0.3 mm times 0.3 mm. (Nuclear Energy Agency 2005, pp. 17-21)

The X-ray CT-scanner is also used to measure the cross-sectional void fraction in transient situations, in which case the scanner is not rotated but fixed. The cross-sectional void fraction is averaged over nine repetitions of the same transient. (Nuclear Energy Agency 2005, p. 17)

The X-ray densitometer measurements were performed at three different axial positions. The X-ray beam was aimed between the rows of heated rods. One measurement was taken of each gap between the rows. As the measurements were repeated nine times, the whole cross-section of the bundle was covered. The data attained using this method is called “Densitometer Chordal Averaged Void Fraction”, which were used to evaluate the axial void fraction distribution and the bundle averaged void fraction. (Nuclear Energy Agency 2005, p. 17)

10 SIMULATIONS

VTT has participated in the NUPEC BFBT benchmark and this thesis is closely related to the work done during the benchmark. The objective of this thesis originally was to simulate the steady-state exercises of the BFBT benchmark using the porous media model PORFLO. Due to unexpected difficulties during the development of the code, the current status of the program is not as far as expected at the beginning of this thesis, and thus the benchmark exercises cannot be simulated using the full (8×8) fuel bundle, but a smaller (2×2) fuel bundle is used instead.

The foremost limiting factor is the time needed for the simulations; the current code is not parallelized in any way, so the simulations have to be performed on a single processor. In addition to having to settle for the use of a single processor, the only solver capable of solving the linear system of equations, the pressure correction equations formulated assuming incompressible flow, already coded in PORFLO is based on Gaussian elimination, which is both CPU and memory-intensive. To sum up: the time needed for the simulations with this limitation reduces the maximum number of nodes to about 30,000.

Another limiting factor is the proportions of the fuel bundle; the length of the fuel bundle is 3.6 m, while the width of the channel box is 132.5 mm, which forces the length of the fuel bundle to be divided into sufficiently large number of consecutive nodes. Therefore, a compromise has to be made between the horizontal and vertical resolution of the grid. It was proposed in the early stages of testing that, with the absence of a turbulence model, the grid needed to be relatively much finer in the horizontal than in the vertical direction in order to capture any cross-flow effects. It was decided that 18 nodes would be appropriate for the horizontal direction, and the length of the fuel bundle, 3.6 m, was divided into 36 nodes for the parameter variations and into 90 nodes for the transient simulation, both of which are presented below, to keep the number of the nodes manageable.

Now that the horizontal resolution is limited to 18 times 18 nodes, attempts to simulate the BFBT benchmark exercises using the full (8×8) fuel bundle were abandoned. This is simply because the horizontal resolution, of 18 times 18 nodes, is not sufficient for the (8×8) fuel bundle, since each fuel rod and the annular flow channel surrounding it would

have to be described with only four nodes. If each subchannel is described using only four nodes, calculations of phase separation and heat transfer would be pointless, since all the variables would not have any gradients in the horizontal direction inside the fluid and, for all practical purposes, the same results could be obtained with 1D calculations.

As soon as an iterative solver capable of solving the pressure correction equations is included in PORFLO, the number of the nodes and the size of the calculation domain can be increased and the horizontal resolution of the grid can be refined. At the moment simulations with the SIMPLE-type algorithms using the full-size (8×8) fuel bundle are out of reach.

10.1 Variations of the under-relaxation factors

Variations of the under-relaxation factors were performed on a (2×2) fuel bundle. The calculation grid was constructed of 18 consecutive nodes in the horizontal directions and 36 in the vertical direction. A horizontal cross-section of the calculation grid fitted over the (2×2) fuel bundle and is presented in Figure 10.1. The channel box is 36.4 mm by 36.4 mm and the corners are rounded with a corner radius of 4 mm. The fuel rods are 12.3 mm in diameter and the pitch is set at 16.2 mm.

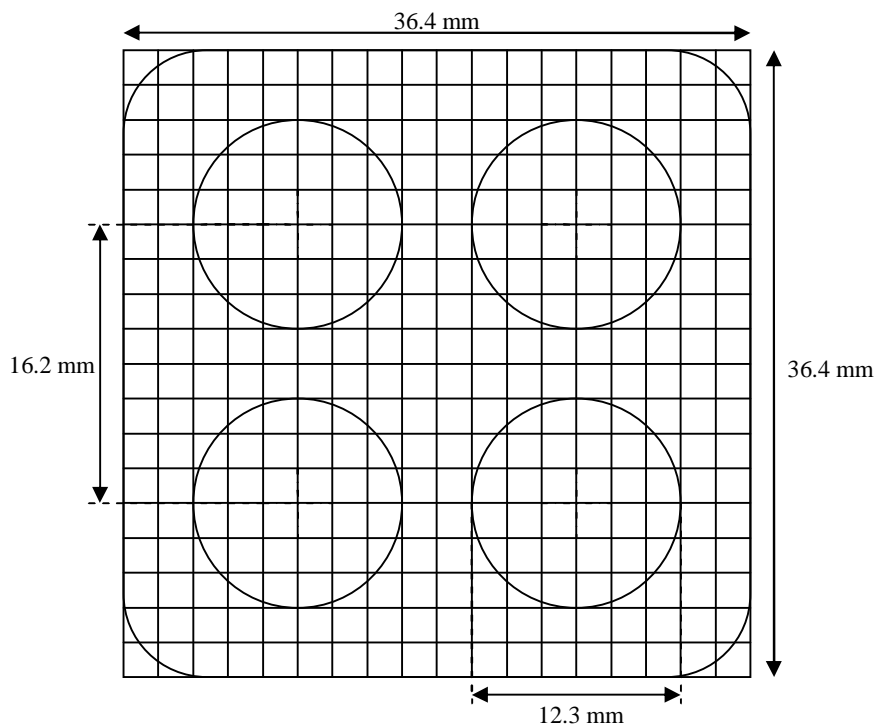


Figure 10.1: A horizontal cross-section of the calculation grid.

While the under-relaxation parameters were varied the rest of the parameters affecting the solution were kept constant. The constant parameters and flow conditions are presented in Table 10.1. The simulations were started from a previously simulated state, in which the heating power had been kept constant at 140 kW for some time, to allow the temperatures to settle. During the parameter variations, the power was linearly increased to 240 kW in two seconds, after which the power level was maintained constant. The purpose of this power transient was to provide more demanding conditions for the algorithms in order to make any differences between the results more distinct.

Table 10.1: Constant parameters and flow conditions in parameter variations.

Parameter	Value	Unit
System pressure (pressure at outlet)	60	bar
Mass flux at inlet	1500	kg/m ² s
Inlet enthalpy	1100	kJ/kg
Inlet density	778,7	kg/m ³
Heating power	$\min\left(140\text{kW} + 50\frac{\text{kW}}{\text{s}} \times \Delta t, 240\text{kW}\right)$	kW
Time step	0.002	s
Friction factor for horizontal flow	0.01	-
Friction factor for vertical flow	0.01	-

The number of iterations needed to reach a converged solution at the end of each time step was observed throughout the simulations. Convergence at the end of the time step is determined by observing the convergence criteria; two conditions need to be fulfilled: the maximum residual of the mass conservation equation, or equally the right-hand side of the pressure correction equation, has to be less than 10^{-13} kg/s and the sum of the residuals of the mass conservation equation has to be less than 10^{-10} kg/s.

10.1.1 Variations of the under-relaxation factors in SIMPLE

The under-relaxation factor variations were performed in simulations that lasted two seconds, the length of the power transient. The constant parameters presented above were used and the total number of SIMPLE iterations to complete the two second power transient was calculated. The parameter variations and results are compiled in Table 10.2.

Table 10.2: The total number of SIMPLE iterations at 2 seconds after the start of the power transient.

Under-relaxation factor for pressure α_p	Under-relaxation factor for velocities α_u	Number of iterations at 2 seconds
0.30	0.70	34,007
0.50	0.30	18,944
0.50	0.40	18,879
0.50	0.50	18,783
0.50	0.60	18,705
0.50	0.70	18,639
0.60	0.30	15,195
0.60	0.40	15,063
0.60	0.50	14,982
0.60	0.60	14,881
0.60	0.70	14,784
0.70	0.30	12,467
0.70	0.40	12,347
0.70	0.50	12,229
0.70	0.60	12,108
0.70	0.70	12,019

The number of iterations needed to obtain a converged solution at the end of each time step remained relatively constant during the simulations, only a slight increase, of similar proportion in each variation, was observed towards the end of the simulations, which indicates a slight dependence to either increasing velocities or void fractions. It is seen, from Table 10.2, that the cumulative number of iterations is strongly dependent on the under-relaxation factor for pressure, α_p , while the influence of the velocity under-relaxation, α_u , is moderate compared to pressure under-relaxation. Increase in either the under-relaxation factor for pressure or velocities decreases the cumulative number of iterations. According to these results the most aggressive set of under-relaxation factors, $\alpha_p = 0.7$ and $\alpha_u = 0.7$, converges the fastest.

10.1.2 Variations of the under-relaxation factors in SIMPLEC

The under-relaxation factors for pressure were varied a bit differently in SIMPLEC, compared to SIMPLE, since SIMPLEC requires very little, if any, pressure under-relaxation. The under-relaxation factor for pressure was varied as 0.9, 0.95 and 0.99, while the velocities were under-relaxed with a factor ranging from 0.5 to 0.8. The SIMPLEC simulations lasted four seconds; hence the number of iterations at the end of the power

transient, at two seconds, is presented for comparison between SIMPLE and SIMPLEC. The power level was kept constant at 240 kW after the two second mark; otherwise the conditions stated for SIMPLE variations are applied in SIMPLEC simulations as well. The under-relaxation parameter variations and results at the end of the power transient, at 2 seconds, and at the end of the simulation, 4 seconds, are compiled in Table 10.3.

Table 10.3: The total number of SIMPLEC-iterations at 2 and 4 seconds after the start of the power transient.

Under-relaxation factor for pressure α_p	Under-relaxation factor for velocities α_u	Number of iterations at 2 seconds	Number of iterations at 4 seconds
0.90	0.50	10,277	21,361
0.90	0.60	10,177	21,241
0.90	0.70	10,059	21,093
0.90	0.80	9,886	20,826
0.95	0.50	9,395	19,482
0.95	0.60	9,266	19,328
0.95	0.70	9,167	19,200
0.95	0.80	9,044	19,045
0.99	0.50	8,555	17,830
0.99	0.60	8,499	17,656
0.99	0.70	8,441	17,522
0.99	0.80	8,327	17,386

As with SIMPLE variations above, a slight increase in the number of iterations needed to obtain a converged solution was observed towards the end of the simulations, indicating a slight dependence to either increasing velocities or void fractions, and again, the cumulative number of iterations is strongly dependent on the under-relaxation factor for pressure, α_p , while the effect of the velocity under-relaxation factor, α_u , is marginal. Increase in either of the under-relaxation factors decreases the cumulative number of iterations. Since divergent behaviour was not encountered, the use of the most aggressive set of under-relaxation factors, $\alpha_p = 0.99$ and $\alpha_u = 0.80$, is suggested.

10.2 Transient simulation

The development of boiling two-phase flow and the transient behavior of the code were studied in a test case, in which the mass flux at inflow was first accelerated from 150 kg/m²s to the desired level of 1500 kg/m²s, which corresponds to an acceleration of 0.2 to 2.0 m/s in the flow velocity. After the flow was accelerated, the heating power was

gradually increased to 240 kW. Otherwise, the constant parameters and flow conditions presented in Table 10.1 are valid for this test case as well. The simulation was performed using the SIMPLEC algorithm with 0.90 and 0.70 for the under-relaxation factors of pressure and velocities, respectively. The calculation grid fitted over the (2×2) fuel bundle is identical to the grid used in the parameter variations above in the horizontal direction: the grid consists of 18 consecutive nodes in the horizontal directions, see Figure 10.1. The length of the fuel bundle is divided into 90 nodes, instead of the 36 used in the parameter variations, which brings the total number of nodes to 29,160.

Some variables, which are relevant mainly for debugging purposes, are monitored during the simulation in PORFLO; these variables are chosen so that the development of the simulation is easy to follow and unrealistic states are clearly indicated. The most informative ones, maximum void fraction, maximum mixture velocity, maximum cladding temperature and maximum pressure are presented in Figures 10.2 through 10.5 (blue lines), with the heating power (red lines) plotted on the second y-axes in all the figures. Since the figures represent the maximum values of the chosen variables, the location of the values can vary during the simulation.

The sudden increase in heating power at 3.7 seconds was caused by a malfunction in the restart procedure: a system failure on the computer, which the test case was executed on, ended the simulation prematurely and, as the simulation was restarted, a bug in the restart routine increased the power to 240 kW immediately after the restart. Since this 7.7 second run lasted 7 weeks on a single 2390 MHz AMD Opteron CPU operating on Linux 2.4.21-20.ELsmp (x86_64) platform, and since the initial goal of this run was to obtain the steady-state void fraction distribution at the end of the run, the simulation was not repeated due to this minor setback.

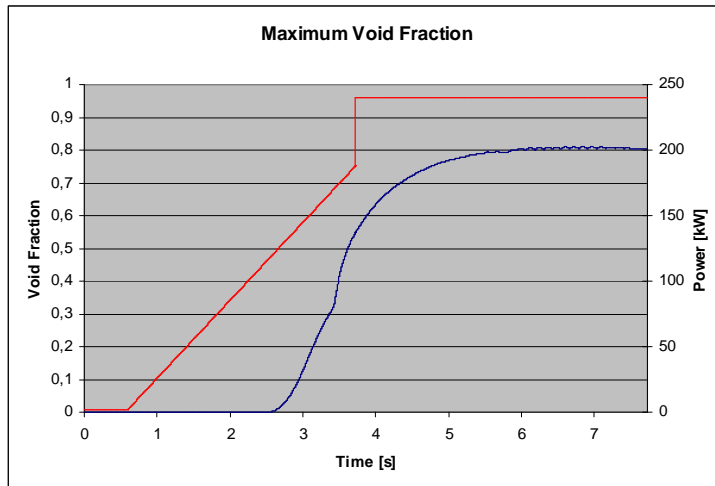


Figure 10.2: Maximum void fraction (blue) and heating power (red).

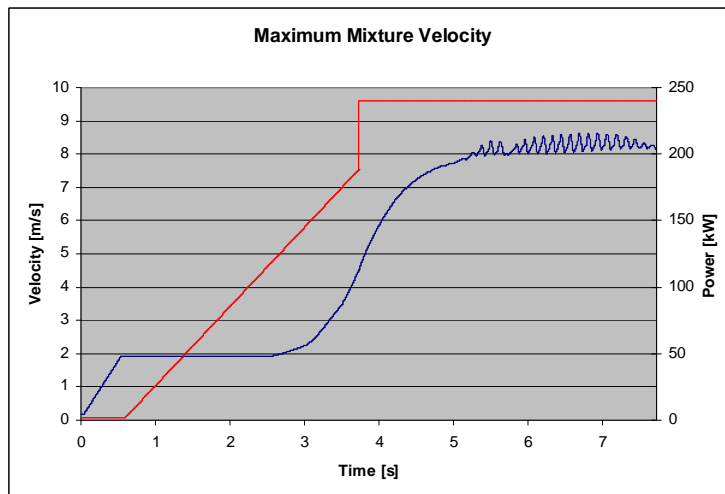


Figure 10.3: Maximum mixture velocity (blue) and heating power (red).

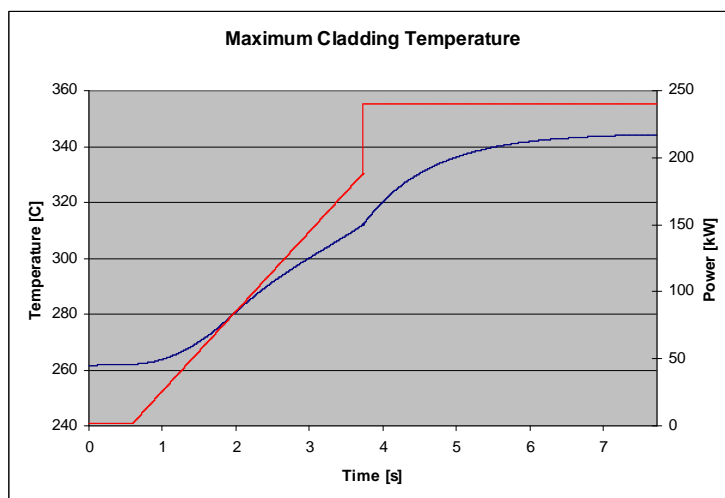


Figure 10.4: Maximum cladding temperature (blue) and heating power (red).

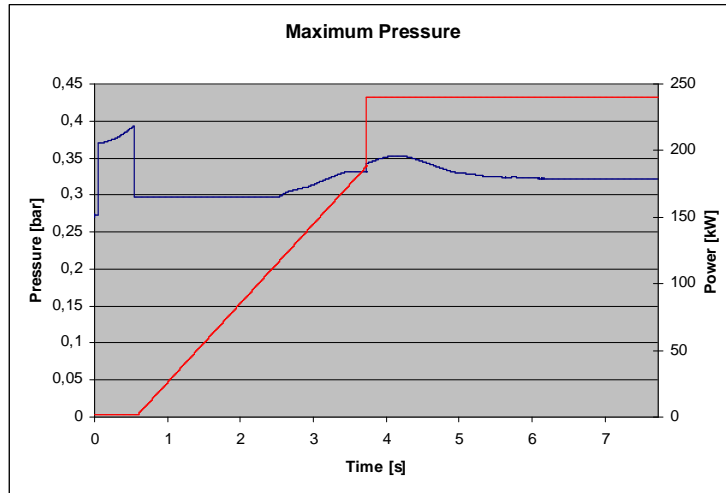


Figure 10.5: Maximum pressure (blue) and heating power (red).

10.3 Steady-state results

The steady-state results, such as the void fraction distribution and the velocity profiles, were obtained as the transient simulation, presented above, reached a converged state. It is seen that especially maximum void fraction in Figure 10.2, maximum cladding temperature in Figure 10.4, and maximum pressure in Figure 10.5, have converged quite nicely. Some oscillation can be seen in the maximum velocity in Figure 10.3, but the amplitude of the oscillation is decreasing towards the end of the simulation. The following results, which are plotted on 3D contours at 1.0 m, 2.0 m, 3.0 m and 3.54 m elevations, for the void fraction distribution in Figure 10.6, for the velocity difference between vapour and liquid in Figure 10.7, for the temperature profile in Figure 10.8, and for the mixture velocity profile in Figure 10.9, were obtained and are presented below.

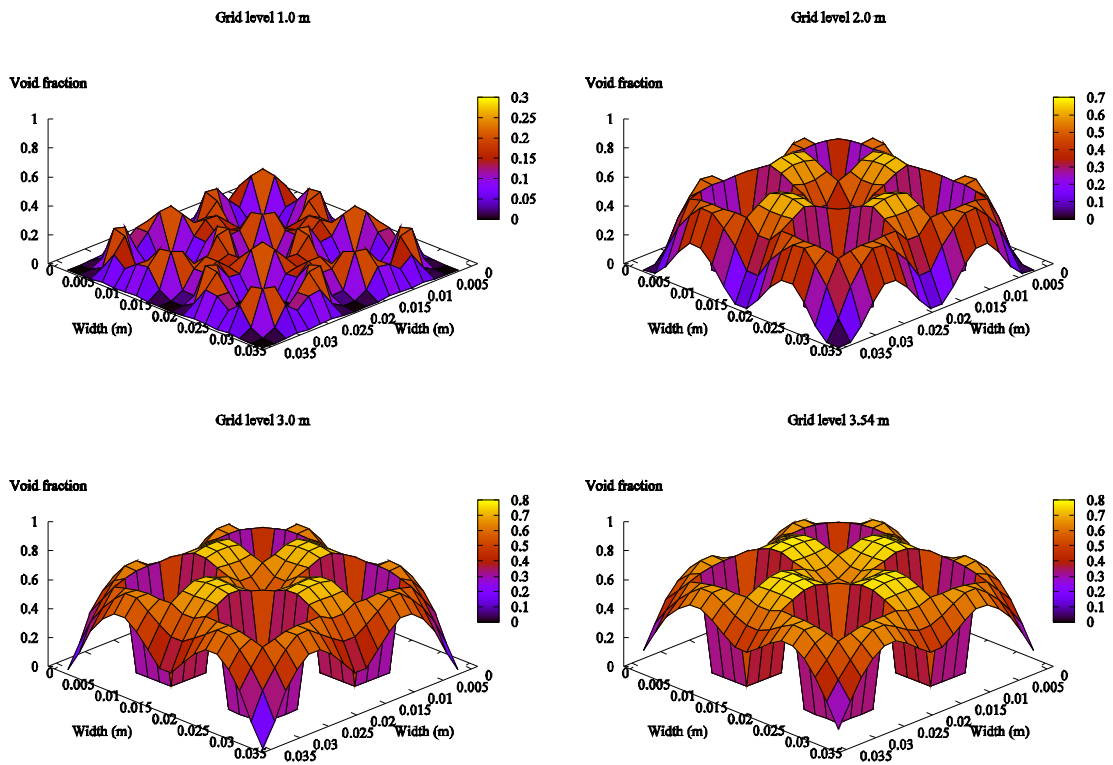


Figure 10.6: Void fraction distributions at 1.0 m, 2.0 m, 3.0 m and 3.54 m elevations.

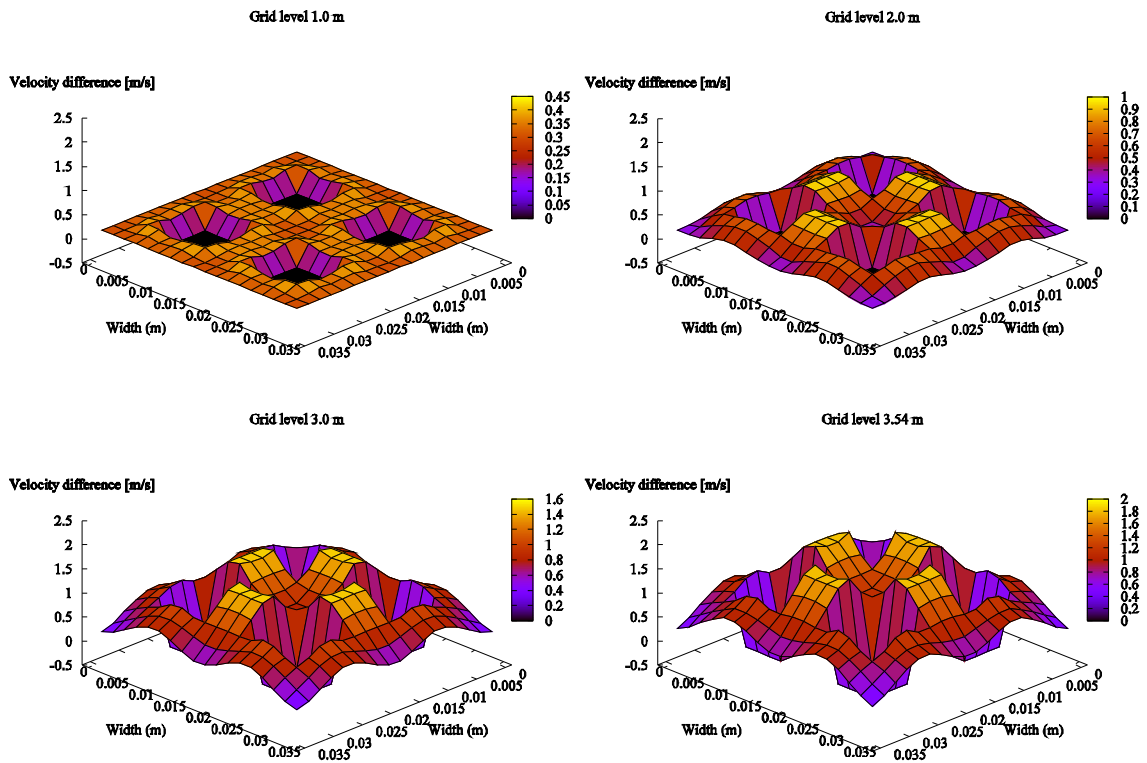


Figure 10.7: Velocity difference between vapour and liquid at 1.0 m, 2.0 m, 3.0 m and 3.54 m elevations.

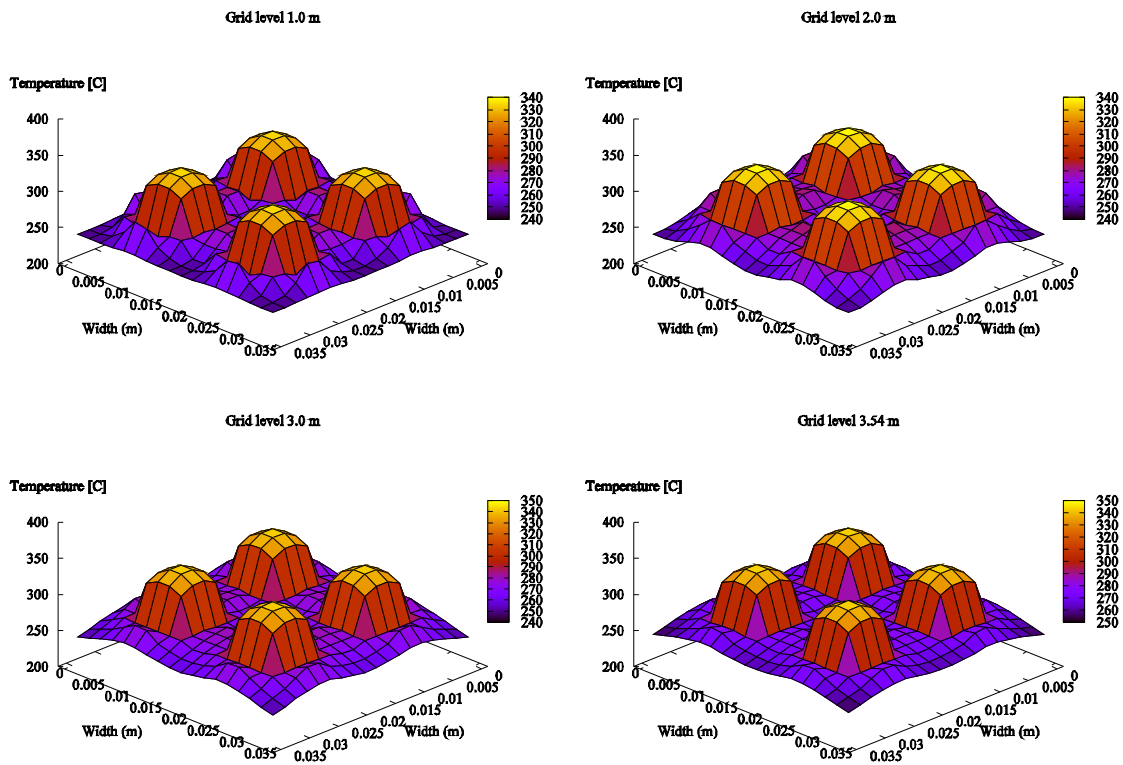


Figure 10.8: Temperature distributions at 1.0 m, 2.0 m, 3.0 m and 3.54 m elevations.

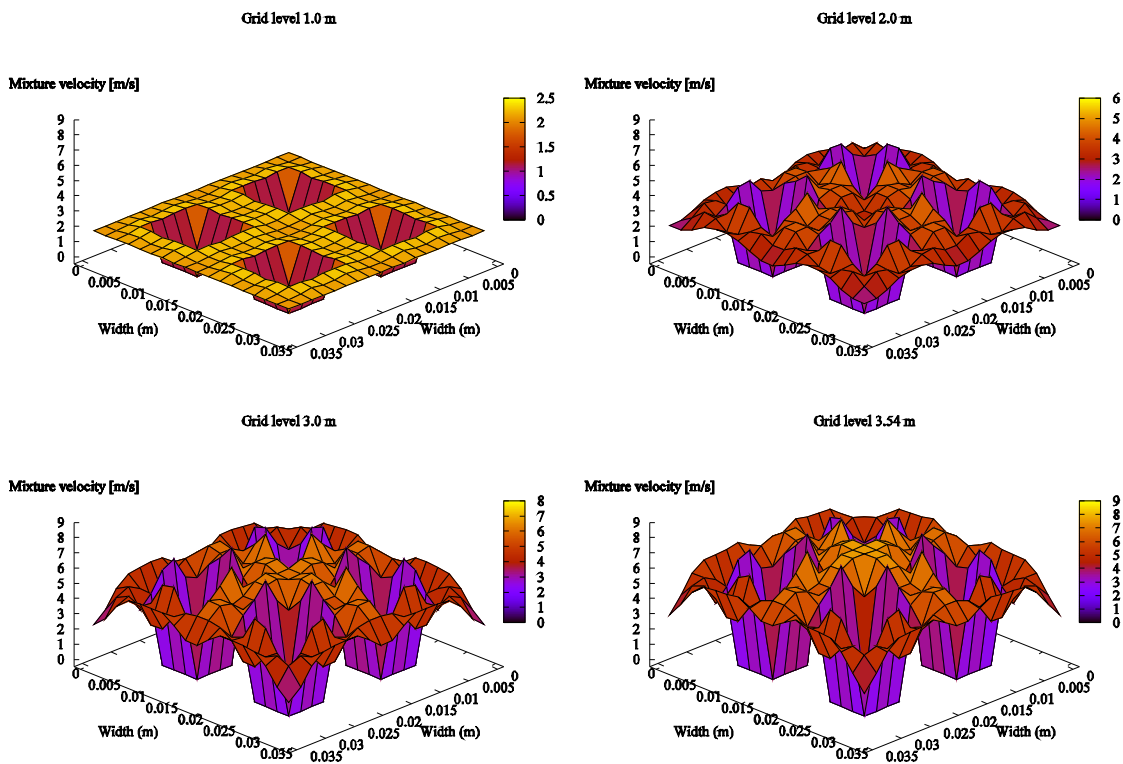


Figure 10.9: Mixture velocity distributions at 1.0 m, 2.0 m, 3.0 m and 3.54 m elevations.

11 DISCUSSION OF SIMULATION RESULTS

The results of the under-relaxation factor variations are pretty much what was to be expected; the cumulative number of iterations, using both SIMPLE and SIMPLEC, was strongly dependent on the under-relaxation factor for pressure, while the influence of the velocity under-relaxation was virtually negligible compared to pressure under-relaxation. Increase in either the under-relaxation factor for pressure or velocities decreased the cumulative number of iterations at the end of the preset transient. In all of the parameter variations, both SIMPLE and SIMPLEC alike, the number of iterations needed to reach a converged state at the end of the time step increased towards the end of the simulation, which indicates a slight dependence on either void fraction or mixture velocity.

A bit surprisingly, divergence of the solution was not encountered in any of the test cases, despite the fact that quite aggressive combinations of the under-relaxation factors were tested, the last SIMPLEC variation, $\alpha_p = 0.99$ and $\alpha_u = 0.80$, in particular. The reason for the steady convergence might be that the whole solution procedure used in PORFLO was non-iterative, meaning that the pressure-velocity solution had no feedback from the changes in fluid properties and heat transfer during the SIMPLE or SIMPLEC-iterations. In addition, the pressure-velocity solution probably benefited from the use of such short time steps, 2 ms which is in compliance with the Courant's criterion for velocity of the flow, since the inertia terms in the mixture momentum equations are increased compared to the convective terms.

In light of the results of the under-relaxation factor variations, the use of SIMPLEC with aggressive under-relaxation factors, such as $\alpha_p = 0.99$ and $\alpha_u = 0.80$, is suggested when using non-iterative solution mode with short time-steps (below the CFL limit), since no effect on convergence was witnessed, and since the savings in CPU-time compared to the SIMPLE algorithm are substantial: 14 – 30 percent in all of the SIMPLEC variations compared to the most aggressive combination of under-relaxation factors using SIMPLE, $\alpha_p = 0.70$ and $\alpha_u = 0.70$. When longer time steps or iterative solution mode is used, these results may no longer apply and further testing might be necessary.

Though no sign of divergent behavior was encountered in the under-relaxation factor variations, some oscillations are visible in the results of the transient simulation performed on the $(18 \times 18 \times 90)$ nodalization. The maximum void fraction, and maximum mixture velocity in particular, experienced oscillations as the mixture flow rate was increased due to fully developed boiling. The amplitude of the oscillations might be somewhat distorted, since it is the maximum values that were plotted. Nevertheless, the oscillations are real, since the fact that the location of the maximum value might change during the transient does not mean that local oscillations do not exist; in fact, local oscillations might be even larger. These minor oscillations are not too critical regarding the stability of the code, after all the oscillations seemed to dampen towards the end of the simulation, but the cause of the oscillations should be studied further.

Excluding the minor oscillations in maximum void fraction and maximum mixture velocity, the rest of the parameters plotted in Figures 10.2 through 10.5 display promising behaviour; the changes during the power transient are smooth and the maximum values settle down to a certain level shortly after the maximum power has been reached. Figure 10.5, maximum pressure, in particular, is interesting, since the result of the incompressible formulation is clearly visible. During the acceleration of the inflow rate (0 – 0.4 s), the maximum pressure, which is essentially the pressure difference measured over the length of the fuel bundle, is gradually increasing due to the increase in flow resistance. But as soon as the mass flux at inlet reaches the desired level and after which the flow rate is kept constant, the maximum pressure instantly drops down to a constant value. The difference in the maximum pressures between the two instants is the pressure difference needed to accelerate the fluid particles along the whole length of the fuel bundle.

The rapid increase in boiling, from approximately 2.5 to 4.5 s, increases the volumetric flow rate of the mixture, and temporarily the mass flow rate in the upper parts of the fuel bundle as well, which causes an increase in the pressure difference between inflow and outflow. The temporary increase in the mass flow rate at the upper parts of the fuel bundle is caused by the increase in creation of void fraction, which decreases the total mass inventory of the fuel bundle. By continuity: if the mass flow rate at inlet remains constant, the mass flow rate at outlet must increase for the total mass inventory to be decreased. After the boiling rate has converged, the pressure difference between inflow and outflow

settles down to a value which is defined by the sum of pressure loss due to friction and the hydrostatic pressure of the fluid column.

There is much to say about the steady-state results obtained at the end of the transient simulation. The void fraction distribution, Figure 10.6, is smooth along most of the length of the fuel bundle, which indicates that the phase separation is modeled correctly. However, if the horizontal resolution could be increased, the functioning of the drift-flux model would become more visible. The only concern is the area in the middle of the flow channel, which has lower void fractions than the area near the fuel rods; it seems possible that the proportions of the calculation grid could affect the propagation of void fraction in the horizontal direction. In addition to the void fraction distribution, the distribution of the velocity difference between the phases, Figure 10.7, is smooth as well, and follows the shape of the void fraction distribution quite nicely, which is to be expected, since the velocity difference is essentially a function of the local void fraction.

The temperature profiles, Figure 10.8, are otherwise quite satisfactory, but there seems to be a negative temperature gradient in the radial direction in few locations right next to the fuel rods where the grid lines are perpendicular to the surface of the fuel rods. This might be due to an error in the heat transfer calculations, but the possibility of this being caused by an error in the recording of the data has to be excluded first.

The mixture velocity profiles, Figure 10.9, are the least convincing of the results. Large differences in the local velocity gradients in the radial direction exist throughout the length of the fuel bundle, and there are significant spikes in the nodes that contact the fuel rods, but again especially in those nodes that contact the fuel rods perpendicular to the grid lines. As can be seen in Figure 10.1, these are the nodes that have the smallest fluid fractions.

The pressure distribution, which is the other part of the pressure-velocity solution, is not presented as a figure, since it is completely flat in the radial direction. This in turn indicates, contrary to the jagged velocity profile, that the solution procedure is working. It seems that the mixture velocity distribution, most of all, is affected by the compromises made in the grid generation; the flow area for horizontal flow is 20 times larger than for vertical flow, in the nodalization used to obtain these results. This means that the

convective terms in the horizontal direction can easily have more effect in the momentum equations than the convective terms in the vertical direction, even though the velocities in the cross-flow direction are significantly smaller than in vertical direction. As was briefly mentioned, there is no turbulence model available in the current version of PORFLO, which undeniably affects the results, again the velocity distribution in particular.

In conclusion to the performance of the code in transient simulations, despite some minor oscillations, quite encouraging results were obtained using non-iterative solution mode and time steps shorter than the CFL limit for flow velocity. As far as the steady-state results are concerned, much needs to be improved: both the horizontal and vertical resolution need to be increased to further validate the results and to facilitate the solution of the full (8×8) fuel bundle.

12 CONCLUSIONS

The most important objectives of this thesis were to develop an iterative method based on the SIMPLE algorithm for pressure velocity solution, and to demonstrate its usefulness in two-phase flow simulations in BWR fuel bundle geometry. Most of the effort was spent on debugging the main program in PORFLO and the subroutine that implements the SIMPLE variants. One of the first tasks, once the code was functioning properly, was to determine a set of under-relaxation factors that provide both stable and fast convergence, and to compare the performance of SIMPLE and SIMPLEC.

According to the results presented in section 10.1, when using a non-iterative solution mode with time-steps below the CFL limit for flow velocity, relatively large values of the under-relaxation factors produced fastest convergence in both SIMPLE and SIMPLEC simulations. The fastest convergence was achieved using $\alpha_p = 0.70$ and $\alpha_u = 0.70$ for the under-relaxation factors in the SIMPLE algorithm, and $\alpha_p = 0.99$ and $\alpha_u = 0.80$ in the SIMPLEC algorithm. In addition to this, SIMPLEC was found to be substantially faster in all of the parameter variations compared to SIMPLE with the fastest set of under-relaxation factors.

Though the results of the simulations are not completely satisfactory, the application of the SIMPLE variants in two-phase flow simulation was successfully demonstrated. No further conclusions, regarding the functioning of the subroutine that implements the SIMPLE variants, can be drawn at this moment, since substantial compromises in the nodalization were made.

The mixture velocity profiles in Figure 10.9, in particular, cause concern about the functioning of PORFLO, since in a situation where the friction factor was set uniform over the entire domain, the mixture velocity profiles should most likely be smoother. Before the cause of such jagged velocity profiles can be determined, the resolution of the calculation grid must be improved in both the horizontal and vertical directions.

First priority in the future development of PORFLO should therefore be given to the development of iterative solution of the linear systems of equations, in order to facilitate

the solution of a larger number of grid points. In addition to the compromises made in nodalization, the absence of a turbulence model is questionable, and may affect the mixture velocities profiles in particular. Hence the development of turbulence modeling should be considered in the future. Once these two improvements, mentioned above, are introduced in PORFLO, the applicability of the solution procedure developed during this thesis, or 5-equation models in a more general sense, in two-phase simulation can be fully assessed.

Nevertheless, the development of PORFLO has been noticeable during the period of this thesis, and several obstacles have been overcome both in the older solution procedure, as well as in the newly developed one. From the perspective of future code development, the subroutine developed during this thesis provides a basis for the implementation of the phase coupled SIMPLE algorithm, if 6-equation models are to be tested in PORFLO.

REFERENCES

- Adams, Robert A. 1999. *Calculus: a Complete Course, Fourth Edition*. Don Mills, Ontario: Addison Wesley Longman Ltd. 1027 p. ISBN 0-201-39607-6
- Blasius, H. 1913. *Das Ähnlichkeitsgesetz bei Reibungsvorgängen in Flüssigkeiten*, Forschungs-Arbeit des Ingenieur-Wesens p. 131. (in German).
- Chexal, B & Lellouche, G. 1986. A Full-Range Drift Flux Correlation for Vertical Flows (Revision 1). EPRI Report NP-3989-SR.
- Collier, John G. & Thome, John R. 1996. *Convective Boiling and Condensation, Third Edition*. New York: Oxford University Press. 596 p. ISBN 0-19-856296-9
- Dittus, F. W. & Boelter, L.M.K. 1930. Heat Transfer in Automobile Radiators of the Tubular Type. University of California Publications on Engineering. Vol. 2. p. 443. Berkeley, CA.
- Griffith, P. & Pearson, J. F. & Lepkowski, R. J. 1977. Critical heat flux during a loss-of-coolant accident. *Nuclear Safety*, Vol. 18, part 3. pp. 298-305.
- Hewitt, G. F. & Delhay, J. M. & Zuber, N. 1986. *Multiphase Science and Technology*, Vol. 2. Hemisphere, 479 p.
- Inoue, Akira & al. 1995. Void Fraction Distribution in BWR Fuel Assembly and Evaluation of Subchannel Code. *Journal of Nuclear Science and Technology*. Vol. 32, part 7. pp. 629-640. (July 1995) ISSN 0022-3131
- Kreyszig, Erwin. 1999. *Advanced Engineering Mathematics, 8th Edition*. New York: John Wiley & Sons. 1156 p. ISBN 0-471-33328-X
- Lahey, R. T. & Moody, F. J. 1993. *The Thermal-Hydraulics of a Boiling Water Nuclear Reactor, Second Edition*. La Grange Park, IL: American Nuclear Society. 631 p. ISBN 0-89448-037-5
- Moran, Michael J. & Shapiro, Howard N. 1998. *Fundamentals of Engineering Thermodynamics, Third Edition (SI Version)*. Chichester: John Wiley & Sons. 799 p. ISBN 0-471-97960-0
- Nuclear Energy Agency, Nuclear Science Committee 2005. *NUPEC BWR Full-size Fine-mesh Bundle Test (BFBT) Benchmark, Volume I: Specifications*. Paris: OECD Publications. 132 p. ISBN 92-64-01088-2
- Patankar, Suhas V. 1980. *Numerical Heat Transfer and Fluid Flow*. New York: Hemisphere Publishing Corporation. 197 p. ISBN 0-89116-522-3

Stewart, G. W. 1998. *Afternotes on Numerical Analysis: Afternotes Goes to Graduate School*. Philadelphia: Society for Industrial and Applied Mathematics. 248 p. ISBN 0-89871-404-4

Stosic, Zoran V. & Stevanovic, Vladimir D. 2002. *Advanced Three-Dimensional Two-Fluid Porous Media Method for Transient Two-Phase Flow Thermal-Hydraulics in Complex Geometries*. *Numerical Heat Transfer, Part B*, Vol. 41. Philadelphia: Taylor & Francis. pp. 263-289. ISSN 1040-7790

Vasquez, S.A. & Ivanov, V.A. 2000. *A phase coupled method for solving multiphase problems in unstructured meshes*. In: *Proceedings of ASME FEDSM'00: ASME 2000 Fluids Engineering Division Summer Meeting*, Boston.

Versteeg, H. K. & Malalasekera, W. 2007. *An Introduction to Computational Fluid Dynamics: The Finite Volume Method, Second Edition*. Harlow: Pearson Education Limited. 503 p. ISBN 978-0-13-127498-3

Wesseling, Pieter 2001. *Principles of Computational Fluid Dynamics*. Berlin: Springer-Verlag. 644 p. ISBN 3-540-67853-0

White, Frank M. 2006. *Viscous fluid flow, Third Edition*. New York: The McGraw-Hill Companies, Inc. 629 p. ISBN 007-124493-X

Zuber, N. & Findlay, J. A. 1965. *Average Volumetric Concentration in Two-phase Flow Systems*. *Journal of Heat Transfer*. Vol. 87. pp. 453-468. ISSN 0022-1481

APPENDIX A DISCUSSION OF VISCOUS FORCES

Viscous forces acting on a fluid element are defined by nine viscous stress components, six of which are independent in isotropic fluids, shown in Figure A.1

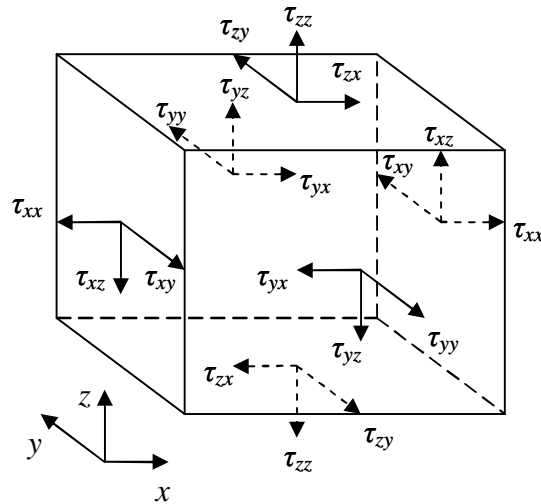


Figure A.1: Stress components on the faces of the control volume.

The force resulting from surface stress is the product of stress component and surface area. The net force in x-direction is the sum of viscous forces acting in x-direction. Stress components in x-direction are shown in Figure A.2

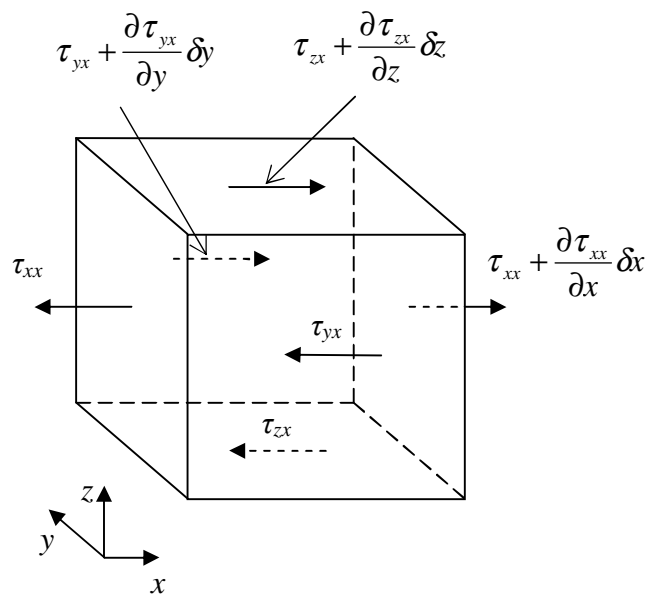


Figure A.2: Stress components in x-direction.

The net force in x-direction:

$$\begin{aligned}
F_{x,\text{vis}} &= \left[\left(\tau_{xx} + \frac{\partial \tau_{xx}}{\partial x} \delta x \right) - \tau_{xx} \right] \delta y \delta z + \left[\left(\tau_{yx} + \frac{\partial \tau_{yx}}{\partial y} \delta y \right) - \tau_{yx} \right] \delta x \delta z \\
&+ \left[\left(\tau_{zx} + \frac{\partial \tau_{zx}}{\partial z} \delta z \right) - \tau_{zx} \right] \delta x \delta y \\
&= \frac{\partial \tau_{xx}}{\partial x} \delta x \delta y \delta z + \frac{\partial \tau_{yx}}{\partial y} \delta x \delta y \delta z + \frac{\partial \tau_{zx}}{\partial z} \delta x \delta y \delta z
\end{aligned} \tag{A.1}$$

The total force per unit volume in x-direction is:

$$\frac{F_{x,\text{vis}}}{V} = \frac{\partial \tau_{xx}}{\partial x} + \frac{\partial \tau_{yx}}{\partial y} + \frac{\partial \tau_{zx}}{\partial z}, \tag{A.2}$$

or equivalently, when the surface stress components are written as a tensor of rank 2, the net force per unit volume in x-direction is simply the divergence of the surface stress components:

$$\nabla \cdot \mathbf{T} = \nabla \cdot \begin{bmatrix} \tau_{xx} & \tau_{yx} & \tau_{zx} \\ \tau_{xy} & \tau_{yy} & \tau_{zy} \\ \tau_{xz} & \tau_{yz} & \tau_{zz} \end{bmatrix} = \begin{bmatrix} \frac{\partial \tau_{xx}}{\partial x} + \frac{\partial \tau_{yx}}{\partial y} + \frac{\partial \tau_{zx}}{\partial z} \\ \frac{\partial \tau_{xy}}{\partial x} + \frac{\partial \tau_{yy}}{\partial y} + \frac{\partial \tau_{zy}}{\partial z} \\ \frac{\partial \tau_{xz}}{\partial x} + \frac{\partial \tau_{yz}}{\partial y} + \frac{\partial \tau_{zz}}{\partial z} \end{bmatrix} \Rightarrow \begin{cases} \frac{F_{x,\text{vis}}}{V} = \frac{\partial \tau_{xx}}{\partial x} + \frac{\partial \tau_{yx}}{\partial y} + \frac{\partial \tau_{zx}}{\partial z} \\ \frac{F_{y,\text{vis}}}{V} = \frac{\partial \tau_{xy}}{\partial x} + \frac{\partial \tau_{yy}}{\partial y} + \frac{\partial \tau_{zy}}{\partial z} \\ \frac{F_{z,\text{vis}}}{V} = \frac{\partial \tau_{xz}}{\partial x} + \frac{\partial \tau_{yz}}{\partial y} + \frac{\partial \tau_{zz}}{\partial z} \end{cases} \tag{A.3}$$

Equations (A.2) and (A.3) contain as unknowns the viscous stress components. A more practical version of these equations can be derived by introducing a suitable model for the viscous stresses. Newton's law of viscosity uses two constants of proportionality, μ and λ , to relate shear stresses to fluid velocities. Dynamic viscosity, μ , is used to relate stresses to linear deformations and the second viscosity, λ , relates the stresses to volumetric deformation. The volumetric deformation is simply:

$$(\nabla \cdot \mathbf{u}) = \frac{\partial u}{\partial x} + \frac{\partial v}{\partial y} + \frac{\partial w}{\partial z} \tag{A.4}$$

According to White (2006, pp. 65-68) the nine viscous stresses are:

$$\begin{aligned}
\tau_{xx} &= 2\mu \frac{\partial u}{\partial x} + \lambda(\nabla \cdot \mathbf{u}) & \tau_{yy} &= 2\mu \frac{\partial v}{\partial y} + \lambda(\nabla \cdot \mathbf{u}) & \tau_{zz} &= 2\mu \frac{\partial w}{\partial z} + \lambda(\nabla \cdot \mathbf{u}) \\
\tau_{xy} = \tau_{yx} &= \mu \left(\frac{\partial u}{\partial x} + \frac{\partial v}{\partial y} \right) & \tau_{xz} = \tau_{zx} &= \mu \left(\frac{\partial u}{\partial z} + \frac{\partial w}{\partial x} \right) & \tau_{yz} = \tau_{zy} &= \mu \left(\frac{\partial v}{\partial z} + \frac{\partial w}{\partial y} \right)
\end{aligned} \tag{A.5}$$

These viscous stresses can be substituted into equation (A.2) to obtain the net force per unit volume in x-direction:

$$\frac{F_{x,\text{vis}}}{V} = \frac{\partial}{\partial x} \left[2\mu \frac{\partial u}{\partial x} + \lambda(\nabla \cdot \mathbf{u}) \right] + \frac{\partial}{\partial y} \left[\mu \left(\frac{\partial u}{\partial x} + \frac{\partial v}{\partial y} \right) \right] + \frac{\partial}{\partial z} \left[\mu \left(\frac{\partial u}{\partial z} + \frac{\partial w}{\partial x} \right) \right] \tag{A.6}$$

The terms are often rearranged so that the less significant ones are moved to the back and combined inside brackets.

$$\begin{aligned}
\frac{F_{x,\text{vis}}}{V} &= \frac{\partial}{\partial x} \left(\mu \frac{\partial u}{\partial x} \right) + \frac{\partial}{\partial y} \left(\mu \frac{\partial u}{\partial y} \right) + \frac{\partial}{\partial z} \left(\mu \frac{\partial u}{\partial z} \right) \\
&+ \left[\frac{\partial}{\partial x} \left(\mu \frac{\partial u}{\partial x} \right) + \frac{\partial}{\partial y} \left(\mu \frac{\partial v}{\partial x} \right) + \frac{\partial}{\partial z} \left(\mu \frac{\partial w}{\partial x} \right) + \frac{\partial}{\partial x} (\lambda(\nabla \cdot \mathbf{u})) \right]
\end{aligned} \tag{A.7}$$

At this point an approximation is made: the terms inside the square brackets can be ignored, since their magnitude is insignificant compared to the first three terms. After this approximation the viscous net force per unit volume in x-direction is reduced to the following form:

$$\Rightarrow \frac{F_{x,\text{vis}}}{V} = \frac{\partial}{\partial x} \left(\mu \frac{\partial u}{\partial x} \right) + \frac{\partial}{\partial y} \left(\mu \frac{\partial u}{\partial y} \right) + \frac{\partial}{\partial z} \left(\mu \frac{\partial u}{\partial z} \right) \tag{A.8}$$

The discretized form of the viscous net force in x-direction is obtained by integrating equation (A.8) over the u-control volume and time step Δt .

$$\iiint_V \int_t^{t+\Delta t} \left[\frac{\partial}{\partial x} \left(\mu \frac{\partial u}{\partial x} \right) + \frac{\partial}{\partial y} \left(\mu \frac{\partial u}{\partial y} \right) + \frac{\partial}{\partial z} \left(\mu \frac{\partial u}{\partial z} \right) \right] dt dV \tag{A.9}$$

Implicit time discretization is selected, hence

$$\begin{aligned}
& \iiint_V \int_t^{t+\Delta t} \left[\frac{\partial}{\partial x} \left(\mu \frac{\partial u}{\partial x} \right) + \frac{\partial}{\partial y} \left(\mu \frac{\partial u}{\partial y} \right) + \frac{\partial}{\partial z} \left(\mu \frac{\partial u}{\partial z} \right) \right] dt dV \\
&= \iiint_V \left[\frac{\partial}{\partial x} \left(\mu \frac{\partial u}{\partial x} \right) + \frac{\partial}{\partial y} \left(\mu \frac{\partial u}{\partial y} \right) + \frac{\partial}{\partial z} \left(\mu \frac{\partial u}{\partial z} \right) \right] dV \Delta t
\end{aligned} \tag{A.10}$$

The divergence theorem can be implemented to transform the volume integrals into surface integrals.

$$\begin{aligned}
& \iiint_V \left[\frac{\partial}{\partial x} \left(\mu \frac{\partial u}{\partial x} \right) + \frac{\partial}{\partial y} \left(\mu \frac{\partial u}{\partial y} \right) + \frac{\partial}{\partial z} \left(\mu \frac{\partial u}{\partial z} \right) \right] dV \Delta t \\
&= \oiint_A \left(\mu \frac{\partial u}{\partial x} \bar{i} + \mu \frac{\partial u}{\partial y} \bar{j} + \mu \frac{\partial u}{\partial z} \bar{k} \right) \cdot \bar{n} dA \\
&= \oiint_{A_e} \left(\mu \frac{\partial u}{\partial x} \bar{i} \right) \cdot \bar{i} dA_e + \oiint_{A_w} \left(\mu \frac{\partial u}{\partial x} \bar{i} \right) \cdot (-\bar{i}) dA_w \\
&+ \oiint_{A_n} \left(\mu \frac{\partial u}{\partial y} \bar{j} \right) \cdot \bar{j} dA_n + \oiint_{A_s} \left(\mu \frac{\partial u}{\partial y} \bar{j} \right) \cdot (-\bar{j}) dA_s \\
&+ \oiint_{A_u} \left(\mu \frac{\partial u}{\partial z} \bar{k} \right) \cdot \bar{k} dA_u + \oiint_{A_d} \left(\mu \frac{\partial u}{\partial z} \bar{k} \right) \cdot (-\bar{k}) dA_d
\end{aligned} \tag{A.11}$$

$$\begin{aligned}
& \Leftrightarrow \iiint_V \left[\frac{\partial}{\partial x} \left(\mu \frac{\partial u}{\partial x} \right) + \frac{\partial}{\partial y} \left(\mu \frac{\partial u}{\partial y} \right) + \frac{\partial}{\partial z} \left(\mu \frac{\partial u}{\partial z} \right) \right] dV \Delta t \\
&= \left(\mu \frac{\partial u}{\partial x} \right)_e (\mathcal{E}A)_e - \left(\mu \frac{\partial u}{\partial x} \right)_w (\mathcal{E}A)_w + \left(\mu \frac{\partial u}{\partial y} \right)_n (\mathcal{E}A)_n - \left(\mu \frac{\partial u}{\partial y} \right)_s (\mathcal{E}A)_s \\
&+ \left(\mu \frac{\partial u}{\partial z} \right)_u (\mathcal{E}A)_u - \left(\mu \frac{\partial u}{\partial z} \right)_d (\mathcal{E}A)_d
\end{aligned} \tag{A.12}$$

where

$$(\mathcal{E}A)_e = \varepsilon_{I,J,K} A_{I,J,K}^i \tag{A.13}$$

$$(\mathcal{E}A)_w = \varepsilon_{I-1,J,K} A_{I-1,J,K}^i \tag{A.14}$$

$$(\mathcal{E}A)_n = \frac{1}{2} \left(\varepsilon_{I-1,J+1,K}^j A_{I-1,J+1,K}^j + \varepsilon_{I,J+1,K}^j A_{I,J+1,K}^j \right) \tag{A.15}$$

$$(\mathcal{E}A)_s = \frac{1}{2} \left(\varepsilon_{I-1,J,K}^j A_{I-1,J,K}^j + \varepsilon_{I,J,K}^j A_{I,J,K}^j \right) \tag{A.16}$$

$$(\varepsilon A)_u = \frac{1}{2} (\varepsilon_{I-1,J,K+1}^k A_{I-1,J,K+1}^k + \varepsilon_{I,J,K+1}^k A_{I,J,K+1}^k) \quad (\text{A.17})$$

$$(\varepsilon A)_d = \frac{1}{2} (\varepsilon_{I-1,J,K}^k A_{I-1,J,K}^k + \varepsilon_{I,J,K}^k A_{I,J,K}^k) \quad (\text{A.18})$$

where the porosities at the pressure node boundaries are defined as presented before:

$$\varepsilon_{I,J,K}^i = \frac{\varepsilon_{I,J,K} \Delta x_{I-1,J,K} + \varepsilon_{I-1,J,K} \Delta x_{I,J,K}}{\Delta x_{I-1,J,K} + \Delta x_{I,J,K}} \quad (\text{A.19})$$

$$\varepsilon_{I,J,K}^j = \frac{\varepsilon_{I,J,K} \Delta y_{I,J-1,K} + \varepsilon_{I,J-1,K} \Delta y_{I,J,K}}{\Delta y_{I,J-1,K} + \Delta y_{I,J,K}} \quad (\text{A.20})$$

$$\varepsilon_{I,J,K}^k = \frac{\varepsilon_{I,J,K} \Delta z_{I,J,K-1} + \varepsilon_{I,J,K-1} \Delta z_{I,J,K}}{\Delta z_{I,J,K-1} + \Delta z_{I,J,K}} \quad (\text{A.21})$$

Similar expressions are used for dynamic viscosities at the u-control volume boundaries:

$$\mu_e = \mu_{I,J,K} \quad (\text{A.22})$$

$$\mu_w = \mu_{I-1,J,K} \quad (\text{A.23})$$

$$\mu_n = \frac{\mu_{I-1,J+1,K}^j \Delta x_{I-1,J+1,K} + \mu_{I,J+1,K}^j \Delta x_{I,J+1,K}}{\Delta x_{I-1,J+1,K} + \Delta x_{I,J+1,K}} \quad (\text{A.24})$$

$$\mu_s = \frac{\mu_{I-1,J,K}^j \Delta x_{I-1,J,K} + \mu_{I,J,K}^j \Delta x_{I,J,K}}{\Delta x_{I-1,J,K} + \Delta x_{I,J,K}} \quad (\text{A.25})$$

$$\mu_u = \frac{\mu_{I-1,J,K+1}^k \Delta x_{I-1,J,K+1} + \mu_{I,J,K+1}^k \Delta x_{I,J,K+1}}{\Delta x_{I-1,J,K+1} + \Delta x_{I,J,K+1}} \quad (\text{A.26})$$

$$\mu_d = \frac{\mu_{I-1,J,K}^k \Delta x_{I-1,J,K} + \mu_{I,J,K}^k \Delta x_{I,J,K+1}}{\Delta x_{I-1,J,K} + \Delta x_{I,J,K}} \quad (\text{A.27})$$

where the dynamic viscosities at the pressure node faces are given through

$$\mu_{I,J,K}^i = \frac{\mu_{I,J,K} \Delta x_{I-1,J,K} + \mu_{I-1,J,K} \Delta x_{I,J,K}}{\Delta x_{I-1,J,K} + \Delta x_{I,J,K}} \quad (\text{A.28})$$

$$\mu_{I,J,K}^j = \frac{\mu_{I,J,K} \Delta y_{I,J-1,K} + \mu_{I,J-1,K} \Delta y_{I,J,K}}{\Delta y_{I,J-1,K} + \Delta y_{I,J,K}} \quad (\text{A.29})$$

$$\mu_{I,J,K}^k = \frac{\mu_{I,J,K} \Delta z_{I,J,K-1} + \mu_{I,J,K-1} \Delta z_{I,J,K}}{\Delta z_{I,J,K-1} + \Delta z_{I,J,K}} \quad (\text{A.30})$$

Using these expressions for the dynamic viscosities and porosities the discretized equation (A.12) is shortened significantly. In addition, the porosities, equations (A.19) through (A.21), need to be calculated only once during the whole simulation and the dynamic viscosities, equations (A.22) through (A.30), only once during each time step, hence the computational time is reduced when using these abbreviations.

Discretized viscous force in x-direction:

$$\left(\mu \frac{\partial u}{\partial x} \right)_e (\mathcal{E}A)_e - \left(\mu \frac{\partial u}{\partial x} \right)_w (\mathcal{E}A)_w = \mu_e \frac{(u_{i+1,J,K} - u_{i,J,K})}{\Delta x_{I,J,K}} (\mathcal{E}A)_e - \mu_w \frac{(u_{i,J,K} - u_{i-1,J,K})}{\Delta x_{I-1,J,K}} (\mathcal{E}A)_w \quad (\text{A.31})$$

$$= \frac{\mu_e (\mathcal{E}A)_e}{\Delta x_{I,J,K}} u_{i+1,J,K} + \frac{\mu_w (\mathcal{E}A)_w}{\Delta x_{I-1,J,K}} u_{i-1,J,K} - \left[\frac{\mu_e (\mathcal{E}A)_e}{\Delta x_{I,J,K}} + \frac{\mu_w (\mathcal{E}A)_w}{\Delta x_{I-1,J,K}} \right] u_{i,J,K}$$

$$\left(\mu \frac{\partial u}{\partial y} \right)_n (\mathcal{E}A)_n - \left(\mu \frac{\partial u}{\partial y} \right)_s (\mathcal{E}A)_s = \mu_n \frac{(u_{i,J+1,K} - u_{i,J,K})}{\frac{1}{2}(\Delta y_{I,J,K} + \Delta y_{I,J+1,K})} (\mathcal{E}A)_n - \mu_s \frac{(u_{i,J,K} - u_{i,J-1,K})}{\frac{1}{2}(\Delta y_{I,J-1,K} + \Delta y_{I,J,K})} (\mathcal{E}A)_s \quad (\text{A.32})$$

$$= \frac{\mu_n (\mathcal{E}A)_n}{\frac{1}{2}(\Delta y_{I,J,K} + \Delta y_{I,J+1,K})} u_{i,J+1,K} + \frac{\mu_s (\mathcal{E}A)_s}{\frac{1}{2}(\Delta y_{I,J-1,K} + \Delta y_{I,J,K})} u_{i,J-1,K} - \left[\frac{\mu_n (\mathcal{E}A)_n}{\frac{1}{2}(\Delta y_{I,J,K} + \Delta y_{I,J+1,K})} + \frac{\mu_s (\mathcal{E}A)_s}{\frac{1}{2}(\Delta y_{I,J-1,K} + \Delta y_{I,J,K})} \right] u_{i,J,K}$$

$$\begin{aligned}
& \left(\mu \frac{\partial u}{\partial z} \right)_u (\mathcal{E}A)_u - \left(\mu \frac{\partial u}{\partial z} \right)_d (\mathcal{E}A)_d = \\
& \mu_u \frac{(u_{i,J,K+1} - u_{i,J,K})}{\frac{1}{2}(\Delta z_{I,J,K} + \Delta z_{I,J,K+1})} (\mathcal{E}A)_u - \mu_d \frac{(u_{i,J,K} - u_{i,J,K-1})}{\frac{1}{2}(\Delta z_{I,J,K-1} + \Delta z_{I,J,K})} (\mathcal{E}A)_d
\end{aligned} \tag{A.33}$$

$$\begin{aligned}
& = \frac{\mu_u (\mathcal{E}A)_u}{\frac{1}{2}(\Delta z_{I,J,K} + \Delta z_{I,J,K+1})} u_{i,J,K+1} + \frac{\mu_d (\mathcal{E}A)_d}{\frac{1}{2}(\Delta z_{I,J,K-1} + \Delta z_{I,J,K})} u_{i,J,K-1} \\
& - \left[\frac{\mu_u (\mathcal{E}A)_u}{\frac{1}{2}(\Delta z_{I,J,K} + \Delta z_{I,J,K+1})} + \frac{\mu_d (\mathcal{E}A)_d}{\frac{1}{2}(\Delta z_{I,J,K-1} + \Delta z_{I,J,K})} \right] u_{i,J,K}
\end{aligned}$$

$$\begin{aligned}
& \Rightarrow \frac{F_{x,\text{vis}}}{V} \\
& = \frac{\mu_e (\mathcal{E}A)_e}{\Delta x_{I,J,K}} u_{i+1,J,K} + \frac{\mu_w (\mathcal{E}A)_w}{\Delta x_{I-1,J,K}} u_{i-1,J,K} \\
& + \frac{\mu_n (\mathcal{E}A)_n}{\frac{1}{2}(\Delta y_{I,J,K} + \Delta y_{I,J+1,K})} u_{i,J+1,K} + \frac{\mu_s (\mathcal{E}A)_s}{\frac{1}{2}(\Delta y_{I,J-1,K} + \Delta y_{I,J,K})} u_{i,J-1,K} \\
& + \frac{\mu_u (\mathcal{E}A)_u}{\frac{1}{2}(\Delta z_{I,J,K} + \Delta z_{I,J,K+1})} u_{i,J,K+1} + \frac{\mu_d (\mathcal{E}A)_d}{\frac{1}{2}(\Delta z_{I,J,K-1} + \Delta z_{I,J,K})} u_{i,J,K-1} \\
& - \left[\frac{\mu_e (\mathcal{E}A)_e}{\Delta x_{I,J,K}} + \frac{\mu_w (\mathcal{E}A)_w}{\Delta x_{I-1,J,K}} \right. \\
& + \frac{\mu_n (\mathcal{E}A)_n}{\frac{1}{2}(\Delta y_{I,J,K} + \Delta y_{I,J+1,K})} + \frac{\mu_s (\mathcal{E}A)_s}{\frac{1}{2}(\Delta y_{I,J-1,K} + \Delta y_{I,J,K})} \\
& \left. + \frac{\mu_u (\mathcal{E}A)_u}{\frac{1}{2}(\Delta z_{I,J,K} + \Delta z_{I,J,K+1})} + \frac{\mu_d (\mathcal{E}A)_d}{\frac{1}{2}(\Delta z_{I,J,K-1} + \Delta z_{I,J,K})} \right] u_{i,J,K}
\end{aligned} \tag{A.34}$$

Since the analogy is quite obvious, the discretized viscous net forces per unit volume are merely presented for y and z-directions.

The viscous net force per unit volume in y-direction is given through

$$\begin{aligned}
\frac{F_{y,\text{vis}}}{V} &= \iiint_V \frac{\partial}{\partial x} \left(\mu \frac{\partial v}{\partial x} \right) + \frac{\partial}{\partial y} \left(\mu \frac{\partial v}{\partial y} \right) + \frac{\partial}{\partial z} \left(\mu \frac{\partial v}{\partial z} \right) dV \\
&= \frac{\mu_e(\varepsilon A)_e}{\frac{1}{2}(\Delta x_{I,J,K} + \Delta x_{I+1,J,K})} v_{I+1,j,K} + \frac{\mu_w(\varepsilon A)_w}{\frac{1}{2}(\Delta x_{I-1,J,K} + \Delta x_{I,J,K})} v_{I-1,j,K} \\
&+ \frac{\mu_n(\varepsilon A)_n}{\Delta y_{I,J,K}} v_{I,j+1,K} + \frac{\mu_s(\varepsilon A)_s}{\Delta y_{I,J-1,K}} v_{I,j-1,K} \\
&+ \frac{\mu_u(\varepsilon A)_u}{\frac{1}{2}(\Delta z_{I,J,K} + \Delta z_{I,J,K+1})} v_{I,j,K+1} + \frac{\mu_d(\varepsilon A)_d}{\frac{1}{2}(\Delta z_{I,J,K-1} + \Delta z_{I,J,K})} v_{I,j,K-1} \\
&- \left[\frac{\mu_e(\varepsilon A)_e}{\frac{1}{2}(\Delta x_{I,J,K} + \Delta x_{I+1,J,K})} + \frac{\mu_w(\varepsilon A)_w}{\frac{1}{2}(\Delta x_{I-1,J,K} + \Delta x_{I,J,K})} \Delta x_{I,J,K} \right. \\
&+ \frac{\mu_n(\varepsilon A)_n}{\Delta y_{I,J,K}} + \frac{\mu_s(\varepsilon A)_s}{\Delta y_{I,J-1,K}} \\
&\left. + \frac{\mu_u(\varepsilon A)_u}{\frac{1}{2}(\Delta z_{I,J,K} + \Delta z_{I,J,K+1})} + \frac{\mu_d(\varepsilon A)_d}{\frac{1}{2}(\Delta z_{I,J,K-1} + \Delta z_{I,J,K})} \right] v_{I,j,K}
\end{aligned} \tag{A.35}$$

where

$$(\varepsilon A)_e = \frac{1}{2} (\varepsilon_{I+1,J-1,K}^i A_{I+1,J-1,K}^i + \varepsilon_{I+1,J,K}^i A_{I+1,J,K}^i) \tag{A.36}$$

$$(\varepsilon A)_w = \frac{1}{2} (\varepsilon_{I,J-1,K}^i A_{I,J-1,K}^i + \varepsilon_{I,J,K}^i A_{I,J,K}^i) \tag{A.37}$$

$$(\varepsilon A)_n = \varepsilon_{I,J,K}^j A_{I,J,K}^j \tag{A.38}$$

$$(\varepsilon A)_s = \varepsilon_{I,J-1,K}^j A_{I,J-1,K}^j \tag{A.39}$$

$$(\varepsilon A)_u = \frac{1}{2} (\varepsilon_{I,J-1,K+1}^k A_{I,J-1,K+1}^k + \varepsilon_{I,J,K+1}^k A_{I,J,K+1}^k) \tag{A.40}$$

$$(\varepsilon A)_d = \frac{1}{2} (\varepsilon_{I,J-1,K}^k A_{I,J-1,K}^k + \varepsilon_{I,J,K}^k A_{I,J,K}^k) \tag{A.41}$$

and the dynamic viscosities at the v-control volume faces can be expressed through

$$\mu_e = \frac{\mu_{I+1,J-1,K}^i \Delta y_{I+1,J-1,K} + \mu_{I+1,J,K}^i \Delta y_{I+1,J,K}}{\Delta y_{I+1,J-1,K} + \Delta y_{I+1,J,K}} \quad (\text{A.42})$$

$$\mu_w = \frac{\mu_{I,J-1,K}^i \Delta y_{I,J-1,K} + \mu_{I,J,K}^i \Delta y_{I,J,K}}{\Delta y_{I,J-1,K} + \Delta y_{I,J,K}} \quad (\text{A.43})$$

$$\mu_n = \mu_{I,J,K} \quad (\text{A.44})$$

$$\mu_s = \mu_{I,J-1,K} \quad (\text{A.45})$$

$$\mu_u = \frac{\mu_{I,J-1,K+1}^k \Delta y_{I,J-1,K+1} + \mu_{I,J,K+1}^k \Delta y_{I,J,K+1}}{\Delta y_{I,J-1,K+1} + \Delta y_{I,J,K+1}} \quad (\text{A.46})$$

$$\mu_d = \frac{\mu_{I,J-1,K}^k \Delta y_{I,J-1,K} + \mu_{I,J,K}^k \Delta y_{I,J,K}}{\Delta y_{I,J-1,K} + \Delta y_{I,J,K}} \quad (\text{A.47})$$

The viscous net force per unit volume in z-direction is given through

$$\begin{aligned} \frac{F_{z,\text{vis}}}{V} &= \iiint_V \frac{\partial}{\partial x} \left(\mu \frac{\partial w}{\partial x} \right) + \frac{\partial}{\partial y} \left(\mu \frac{\partial w}{\partial y} \right) + \frac{\partial}{\partial z} \left(\mu \frac{\partial w}{\partial z} \right) dV \\ &= \frac{\mu_e(\varepsilon A)_e}{\frac{1}{2}(\Delta x_{I,J,K} + \Delta x_{I+1,J,K})} w_{I+1,J,k} + \frac{\mu_w(\varepsilon A)_w}{\frac{1}{2}(\Delta x_{I-1,J,K} + \Delta x_{I,J,K})} w_{I-1,J,k} \\ &\quad + \frac{\mu_n(\varepsilon A)_n}{\frac{1}{2}(\Delta y_{I,J,K} + \Delta y_{I,J+1,K})} w_{I,J+1,k} + \frac{\mu_s(\varepsilon A)_s}{\frac{1}{2}(\Delta y_{I,J-1,K} + \Delta y_{I,J,K})} w_{I,J-1,k} \\ &\quad + \frac{\mu_u(\varepsilon A)_u}{\Delta z_{I,J,K}} w_{I,J,k+1} + \frac{\mu_d(\varepsilon A)_d}{\Delta z_{I,J,K-1}} w_{I,J,k-1} \\ &\quad - \left[\frac{\mu_e(\varepsilon A)_e}{\frac{1}{2}(\Delta x_{I,J,K} + \Delta x_{I+1,J,K})} + \frac{\mu_w(\varepsilon A)_w}{\frac{1}{2}(\Delta x_{I-1,J,K} + \Delta x_{I,J,K})} \right. \\ &\quad \left. + \frac{\mu_n(\varepsilon A)_n}{\frac{1}{2}(\Delta y_{I,J,K} + \Delta y_{I,J+1,K})} + \frac{\mu_s(\varepsilon A)_s}{\frac{1}{2}(\Delta y_{I,J-1,K} + \Delta y_{I,J,K})} \right. \\ &\quad \left. + \frac{\mu_u(\varepsilon A)_u}{\Delta z_{I,J,K}} + \frac{\mu_d(\varepsilon A)_d}{\Delta z_{I,J,K-1}} \right] w_{I,J,k} \end{aligned} \quad (\text{A.48})$$

where

$$(\varepsilon A)_e = \frac{1}{2}(\varepsilon_{I+1,J,K-1}^i A_{I+1,J,K-1}^i + \varepsilon_{I+1,J,K}^i A_{I+1,J,K}^i) \quad (\text{A.49})$$

$$(\varepsilon A)_w = \frac{1}{2}(\varepsilon_{I,J,K-1}^i A_{I,J,K-1}^i + \varepsilon_{I,J,K}^i A_{I,J,K}^i) \quad (\text{A.50})$$

$$(\varepsilon A)_n = \frac{1}{2}(\varepsilon_{I,J+1,K-1}^j A_{I,J+1,K-1}^j + \varepsilon_{I,J+1,K}^j A_{I,J+1,K}^j) \quad (\text{A.51})$$

$$(\varepsilon A)_s = \frac{1}{2}(\varepsilon_{I,J,K-1}^j A_{I,J,K-1}^j + \varepsilon_{I,J,K}^j A_{I,J,K}^j) \quad (\text{A.52})$$

$$(\varepsilon A)_u = \varepsilon_{I,J,K} A_{I,J,K}^k \quad (\text{A.53})$$

$$(\varepsilon A)_d = \varepsilon_{I,J,K-1} A_{I,J,K-1}^k \quad (\text{A.54})$$

and the dynamic viscosities at the v-control volume faces can be expressed through

$$\mu_e = \frac{\mu_{I+1,J,K-1}^i \Delta z_{I+1,J,K-1} + \mu_{I+1,J,K}^i \Delta z_{I+1,J,K}}{\Delta z_{I+1,J,K-1} + \Delta z_{I+1,J,K}} \quad (\text{A.55})$$

$$\mu_w = \frac{\mu_{I,J,K-1}^i \Delta z_{I,J,K-1} + \mu_{I,J,K}^i \Delta z_{I,J,K}}{\Delta z_{I,J,K-1} + \Delta z_{I,J,K}} \quad (\text{A.56})$$

$$\mu_n = \frac{\mu_{I,J+1,K-1}^j \Delta z_{I,J+1,K-1} + \mu_{I,J+1,K}^j \Delta z_{I,J+1,K}}{\Delta z_{I,J+1,K-1} + \Delta z_{I,J+1,K}} \quad (\text{A.57})$$

$$\mu_s = \frac{\mu_{I,J,K-1}^j \Delta z_{I,J,K-1} + \mu_{I,J,K}^j \Delta z_{I,J,K}}{\Delta z_{I,J,K-1} + \Delta z_{I,J,K}} \quad (\text{A.58})$$

$$\mu_u = \mu_{I,J,K} \quad (\text{A.59})$$

$$\mu_d = \mu_{I,J,K-1} \quad (\text{A.60})$$

APPENDIX B DISCRETIZED FORMS OF THE MOMENTUM EQUATIONS FOR SIMPLE

The discretized momentum equation in y-direction (v-momentum):

$$\begin{aligned} & \frac{1}{2}(V_{I,J-1,K} + V_{I,J,K}) \mathcal{E}_{I,J,K}^j \frac{[\rho_{I,J,K}^j v_{I,J,K} - (\rho_{I,J,K}^j)^\circ v_{I,J,K}^\circ]}{\Delta t} \\ & + [\langle F_w \rangle + \langle F_s \rangle + \langle F_d \rangle + \langle -F_e \rangle + \langle -F_n \rangle + \langle -F_u \rangle + (F_e - F_w) + (F_n - F_s) + (F_u - F_d)] v_{I,j,K} \quad (\text{B.1}) \\ & = \langle F_w \rangle v_{I-1,j,K} + \langle F_s \rangle v_{I,j-1,K} + \langle F_d \rangle v_{I,j,K-1} + \langle -F_e \rangle v_{I+1,j,K} + \langle -F_n \rangle v_{I,j+1,K} + \langle -F_u \rangle v_{I,j,K+1} \\ & - \frac{1}{2} \frac{f}{d_e} \rho_{I,J,K}^j \mathcal{E}_{I,J,K}^j \frac{1}{2} (V_{I,J-1,K} + V_{I,J,K}) v_{I,j,K} |v_{I,j,K}^*| - (p_{I,J,K} - p_{I,J-1,K}) \mathcal{E}_{I,J,K}^j A_{I,J,K}^j \end{aligned}$$

$$\begin{aligned} & [\langle F_w \rangle + \langle F_s \rangle + \langle F_d \rangle + \langle -F_e \rangle + \langle -F_n \rangle + \langle -F_u \rangle + (F_e - F_w) + (F_n - F_s) \\ & + (F_u - F_d) + \frac{1}{2} (V_{I,J-1,K} + V_{I,J,K}) \mathcal{E}_{I,J,K}^j \rho_{I,J,K}^j \left(\frac{1}{\Delta t} + \frac{1}{2} \frac{f}{d_e} |v_{I,j,K}^*| \right)] v_{I,j,K} \quad (\text{B.2}) \\ & = \langle F_w \rangle v_{I-1,j,K} + \langle F_s \rangle v_{I,j-1,K} + \langle F_d \rangle v_{I,j,K-1} + \langle -F_e \rangle v_{I+1,j,K} + \langle -F_n \rangle v_{I,j+1,K} + \langle -F_u \rangle v_{I,j,K+1} \\ & - (p_{I,J,K} - p_{I,J-1,K}) \mathcal{E}_{I,J,K}^j A_{I,J,K}^j + \frac{1}{2} (V_{I,J-1,K} + V_{I,J,K}) \mathcal{E}_{I,J,K}^j (\rho_{I,J,K}^j)^\circ \frac{v_{I,j,K}^\circ}{\Delta t} \end{aligned}$$

where

$$\begin{aligned} F_w & = \frac{1}{2} \mathcal{E}_{I,J-1,K}^i A_{I,J-1,K}^i [\langle u_{i,J-1,K} \rangle \rho_{I-1,J-1,K} - \langle -u_{i,J-1,K} \rangle \rho_{I,J-1,K}] \\ & + \frac{1}{2} \mathcal{E}_{I,J,K}^i A_{I,J,K}^i [\langle u_{i,J,K} \rangle \rho_{I-1,J,K} - \langle -u_{i,J,K} \rangle \rho_{I,J,K}] \quad (\text{B.3}) \end{aligned}$$

$$\begin{aligned} F_e & = \frac{1}{2} \mathcal{E}_{I+1,J-1,K}^i A_{I+1,J-1,K}^i [\langle u_{i+1,J-1,K} \rangle \rho_{I,J-1,K} - \langle -u_{i+1,J-1,K} \rangle \rho_{I+1,J-1,K}] \\ & + \frac{1}{2} \mathcal{E}_{I+1,J,K}^i A_{I+1,J,K}^i [\langle u_{i+1,J,K} \rangle \rho_{I,J,K} - \langle -u_{i+1,J,K} \rangle \rho_{I+1,J,K}] \quad (\text{B.4}) \end{aligned}$$

$$F_s = \frac{1}{2} \rho_{I,J-1,K} \mathcal{E}_{I,J-1,K}^j A_{I,J-1,K}^j (v_{I,j-1,K} + v_{I,j,K}), \quad (\text{B.5})$$

$$F_n = \frac{1}{2} \rho_{I,J,K} \mathcal{E}_{I,J,K}^j A_{I,J,K}^j (v_{I,j,K} + v_{I,j+1,K}), \quad (\text{B.6})$$

$$\begin{aligned} F_d & = \frac{1}{2} \mathcal{E}_{I,J-1,K}^k A_{I,J-1,K}^k [\langle w_{I,J-1,k} \rangle \rho_{I,J-1,K-1} - \langle -w_{I,J-1,k} \rangle \rho_{I,J-1,K}] \\ & + \frac{1}{2} \mathcal{E}_{I,J,K}^k A_{I,J,K}^k [\langle w_{I,J,k} \rangle \rho_{I,J,K-1} - \langle -w_{I,J,k} \rangle \rho_{I,J,K}] \quad \text{and} \quad (\text{B.7}) \end{aligned}$$

$$\begin{aligned} F_u & = \frac{1}{2} \mathcal{E}_{I,J-1,K+1}^k A_{I+1,J-1,K+1}^k [\langle w_{I,J-1,k+1} \rangle \rho_{I,J-1,K} - \langle -w_{I,J-1,k+1} \rangle \rho_{I,J-1,K+1}] \\ & + \frac{1}{2} \mathcal{E}_{I,J,K+1}^k A_{I,J,K+1}^k [\langle w_{I,J,k+1} \rangle \rho_{I,J,K} - \langle -w_{I,J,k+1} \rangle \rho_{I,J,K+1}] \quad (\text{B.8}) \end{aligned}$$

The discretized momentum equation in z-direction (w-momentum):

$$\begin{aligned}
& \frac{1}{2}(V_{I,J,K-1} + V_{I,J,K}) \boldsymbol{\varepsilon}_{I,J,K}^k \frac{\left[\rho_{I,J,K}^k w_{I,J,k} - (\rho_{I,J,K}^k)^\circ w_{I,J,k}^\circ \right]}{\Delta t} \\
& + \left[\langle F_w \rangle + \langle F_s \rangle + \langle F_d \rangle + \langle -F_e \rangle + \langle -F_n \rangle + \langle -F_u \rangle + (F_e - F_w) + (F_n - F_s) + (F_u - F_d) \right] w_{I,J,k} \quad (\text{B.9}) \\
& = \langle F_w \rangle w_{I-1,J,k} + \langle F_s \rangle w_{I,J-1,k} + \langle F_d \rangle w_{I,J,k-1} + \langle -F_e \rangle w_{I+1,J,k} + \langle -F_n \rangle w_{I,J+1,k} + \langle -F_u \rangle w_{I,J,k+1} \\
& - \frac{1}{2} \frac{f}{d_e} \rho_{I,J,K}^k \boldsymbol{\varepsilon}_{I,J,K}^k \frac{1}{2} (V_{I,J,K-1} + V_{I,J,K}) w_{I,J,k} |w_{I,J,k}^*| - (p_{I,J,K} - p_{I,J,K-1}) \boldsymbol{\varepsilon}_{I,J,K}^k A_{I,J,K}^k
\end{aligned}$$

$$\begin{aligned}
& \left[\langle F_w \rangle + \langle F_s \rangle + \langle F_d \rangle + \langle -F_e \rangle + \langle -F_n \rangle + \langle -F_u \rangle + (F_e - F_w) + (F_n - F_s) \right. \\
& \left. + (F_u - F_d) + \frac{1}{2} (V_{I,J,K-1} + V_{I,J,K}) \boldsymbol{\varepsilon}_{I,J,K}^k \rho_{I,J,K}^k \left(\frac{1}{\Delta t} + \frac{1}{2} \frac{f}{d_e} |w_{I,J,k}^*| \right) \right] w_{I,J,k} \quad (\text{B.10}) \\
& = \langle F_w \rangle w_{I-1,J,k} + \langle F_s \rangle w_{I,J-1,k} + \langle F_d \rangle w_{I,J,k-1} + \langle -F_e \rangle w_{I+1,J,k} + \langle -F_n \rangle w_{I,J+1,k} + \langle -F_u \rangle w_{I,J,k+1} \\
& - (p_{I,J,K} - p_{I,J,K-1}) \boldsymbol{\varepsilon}_{I,J,K}^k A_{I,J,K}^k + \frac{1}{2} (V_{I,J,K-1} + V_{I,J,K}) \boldsymbol{\varepsilon}_{I,J,K}^k (\rho_{I,J,K}^k)^\circ \frac{w_{I,J,k}^\circ}{\Delta t} \\
& - \frac{1}{2} (V_{I,J,K-1} + V_{I,J,K}) \boldsymbol{\varepsilon}_{I,J,K}^k \rho_{I,J,K}^k g
\end{aligned}$$

where

$$\begin{aligned}
F_w & = \frac{1}{2} \boldsymbol{\varepsilon}_{I,J,K-1}^i A_{I,J,K-1}^i \left[\langle u_{i,J,K-1} \rangle \rho_{I-1,J,K-1} - \langle -u_{i,J,K-1} \rangle \rho_{I,J,K-1} \right] \\
& \quad + \frac{1}{2} \boldsymbol{\varepsilon}_{I,J,K}^i A_{I,J,K}^i \left[\langle u_{i,J,K} \rangle \rho_{I-1,J,K} - \langle -u_{i,J,K} \rangle \rho_{I,J,K} \right] \quad , \quad (\text{B.11})
\end{aligned}$$

$$\begin{aligned}
F_e & = \frac{1}{2} \boldsymbol{\varepsilon}_{I+1,J,K-1}^i A_{I+1,J,K-1}^i \left[\langle u_{i+1,J,K-1} \rangle \rho_{I,J,K-1} - \langle -u_{i+1,J,K-1} \rangle \rho_{I+1,J,K-1} \right] \\
& \quad + \frac{1}{2} \boldsymbol{\varepsilon}_{I+1,J,K}^i A_{I+1,J,K}^i \left[\langle u_{i+1,J,K} \rangle \rho_{I,J,K} - \langle -u_{i+1,J,K} \rangle \rho_{I+1,J,K} \right] \quad , \quad (\text{B.12})
\end{aligned}$$

$$\begin{aligned}
F_s & = \frac{1}{2} \boldsymbol{\varepsilon}_{I,J,K-1}^j A_{I,J,K-1}^j \left[\langle v_{I,j,K-1} \rangle \rho_{I,J-1,K-1} - \langle -v_{I,j,K-1} \rangle \rho_{I,J,K-1} \right] \\
& \quad + \frac{1}{2} \boldsymbol{\varepsilon}_{I,J,K}^j A_{I,J,K}^j \left[\langle v_{I,j,K} \rangle \rho_{I,J-1,K} - \langle -v_{I,j,K} \rangle \rho_{I,J,K} \right] \quad , \quad (\text{B.13})
\end{aligned}$$

$$\begin{aligned}
F_n & = \frac{1}{2} \boldsymbol{\varepsilon}_{I,J+1,K-1}^j A_{I,J+1,K-1}^j \left[\langle v_{I,j+1,K-1} \rangle \rho_{I,J,K-1} - \langle -v_{I,j+1,K-1} \rangle \rho_{I,J+1,K-1} \right] \\
& \quad + \frac{1}{2} \boldsymbol{\varepsilon}_{I,J+1,K}^j A_{I,J+1,K}^j \left[\langle v_{I,j+1,K} \rangle \rho_{I,J,K} - \langle -v_{I,j+1,K} \rangle \rho_{I,J+1,K} \right] \quad , \quad (\text{B.14})
\end{aligned}$$

$$F_d = \frac{1}{2} \rho_{I,J,K-1} \boldsymbol{\varepsilon}_{I,J,K-1}^k A_{I,J,K-1}^k (w_{I,J,k-1} + w_{I,J,k}) \quad \text{and} \quad (\text{B.15})$$

$$F_u = \frac{1}{2} \rho_{I,J,K} \boldsymbol{\varepsilon}_{I,J,K}^k A_{I,J,K}^k (w_{I,J,k} + w_{I,J,k+1}). \quad (\text{B.16})$$